JOURNAL OF MECHANICAL ENGINEERING

STROJNIŠKI VESTNIK

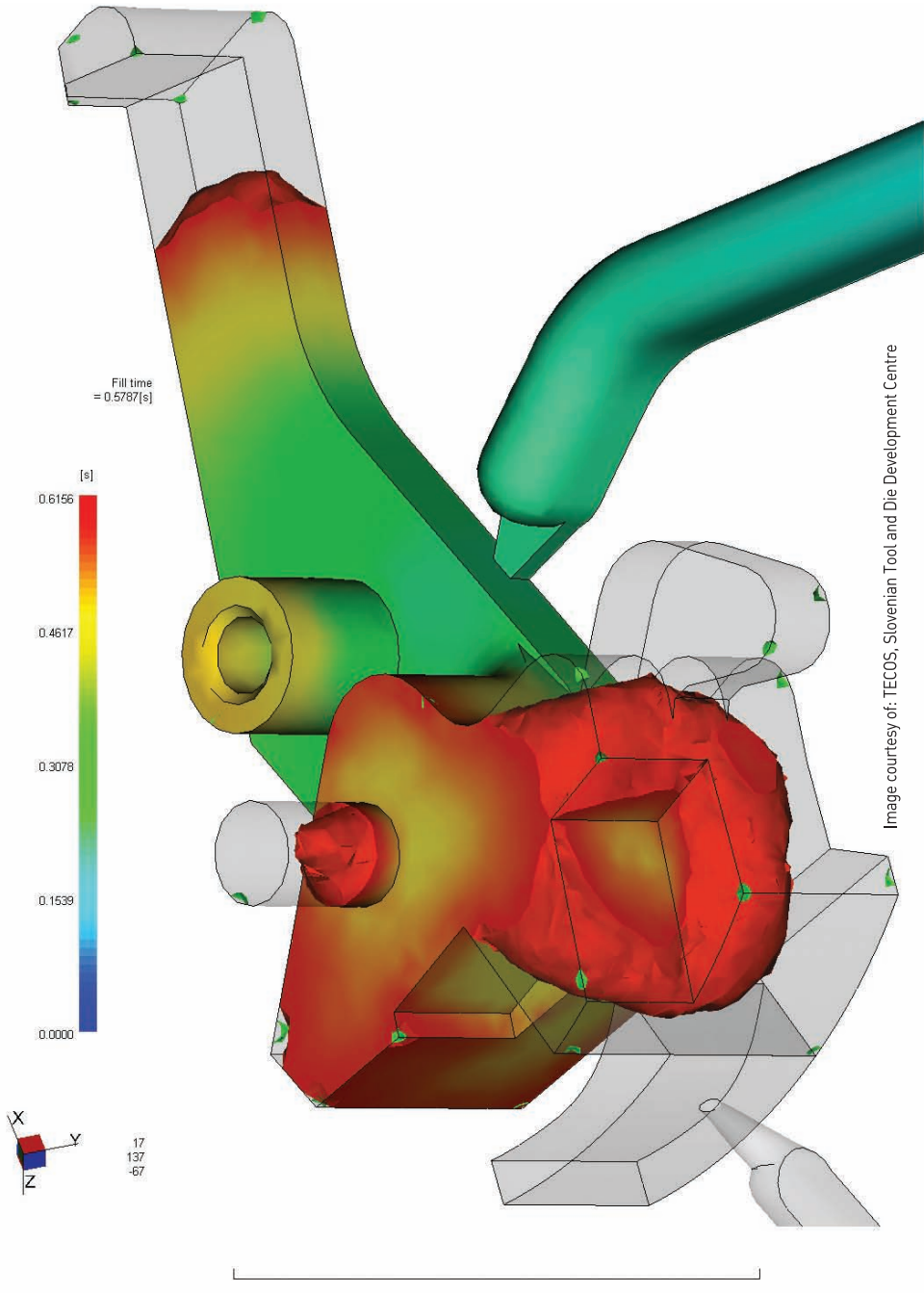

Image courtesy of: TECOS, Slovenian Tool and Die Development Centre

no. 4
year 2008
volume 54

Contents

Strojniški vestnik - Journal of Mechanical Engineering
volume 54, (2008), number 4
Ljubljana, April 2008
ISSN 0039-2480

Published monthly

Editorial
Gantar, G. 248

Papers
Gantar, G., Sterzing, A.: Robust Design of Forming Processes 249
Fernandez, A., Mercado, D., Javierre, C., Muniesa, M.: Large Thermoplastic Parts Quality Improvements Using Monitorized Nozzle 258
Petek, A., Podgornik, B., Kuzman, K., Čekada, M., Waldhauser, W., Vižintin, J.: The Analysis of Complex Tribological System of Single Point Incremental Sheet Metal Forming - SPIF 266
Kocańda, A., Czyżewski, P.: Experimental and Numerical Analysis of Side Forces in a Forging Die 274
Kopač, J., Kržič, P.: CAM Algorithm as Important Element by Achieving of Good Machined Surface Quality 280
Vrh, M., Halilovič, M., Štok, B.: Impact of Young's Modulus Degradation on Springback Calculation in Steel Sheet Drawing 288

Instructions for Authors 297

Editorial

Only few are aware how important is the role of production process engineers and tool manufacturing experts in the product development cycle. They are strategically a very important part of the product-development-chain in all industrial sectors due to the following reasons:

1. New forming technologies must be developed and new tools produced for every new product.
2. Properties and quality of forming tools have major influence on the properties and costs of final products.
3. Development of production technologies and manufacturing of forming tools step forward in the final, usually critical stage of product development cycle. Each mistake at this stage is therefore significant for time-to-market.

Production process planning and tool manufacturing companies are one of the driving forces of technological development and have a multiplying effect on the economic situation of the environment (country, region or company) where they operate. Despite the fact that the GDP share of these companies is less than 1%, 42% of the manufacturing industry depends on their support. There are many examples in the fields of medicine, mechatronic systems, electronics, where new products are developed and tested successfully by prototypes. But to implement these new products into serial production, reliable production processes development department and tool manufacturing partners are needed. For example, it is not a problem to design a mobile phone with 50% smaller dimensions of the existing ones, but only company which is capable of implementing the technologies for production of all micro components, needed for such phone can succeed on the market. Similarly, the most attractive designs by the renowned industrial designers are not easy to manufacture with acceptable costs.

This thematic issue presents some very interesting papers dealing with technology development and tools by a number of authors. All the papers are collected from the international conference ICIT&MPT 2007 which was organized by Slovenian Tool and Die Development Centre TECOS with the aim to transfer the research results into industrial environment. While they were presented in the proceedings as short papers here they have been extended especially for this issue.

Assist. Prof. Dr. Gašper Gantar
Director of TECOS

Strojniški vestnik - Journal of Mechanical Engineering 54(2008)4, 249-257
UDC 621.9
Paper received: 23.2.2008
Paper accepted: 15.5.2008

Robust Design of Forming Processes

Gašper Gantar*,[1] - Andreas Sterzing[2]
[1]TECOS - Slovenian Tool and Die Development Centre, Celje, Slovenia
[2]Fraunhofer Institut für Werkzeugmaschinen und Umformtechnik, Chemnitz, Germany

Properties of raw materials (sheet metal, bars, etc.) used in forming processes are not constant. Other input parameters of forming system (friction conditions, machine settings, temperature, etc.) also scatter considerably during production. Improvement of production processes has always been an important goal in metal forming industry. The aim is to develop cost effective and stabile forming processes where the number of non-conforming products (scrap) is reduced to the minimum. In the first part of the paper an approach is described which enables the user to predict how the scatter of input parameters would influence the final properties of the products. In the second part of the paper the developed approach is used for optimization of forming process with respect to uncontrollable scatter of input parameters with the aim of minimizing scrap ratio. Optimization is based on the use of numerical simulations, response surface methodology and stochastic optimization. It can be performed in the early stage of the production process development cycle. The presented approach was successfully applied in industrial environment during development of technology for forming of various work pieces.

Keywords: forming processes, robust design, numerical simulation, optimization

0 INTRODUCTION

Improvement of production processes has always been an important goal in metal forming industry. The aim is to develop cost effective and stabile forming processes where the number of non-conforming products (scrap) is reduced to the minimum. Numerical simulations are used daily for validation and optimization of forming processes [1] and [2]. They replace physical experiments for reducing costs and speeding up product development. But numerical models are based on the exactly defined constant set of the input parameters (material properties, friction conditions, machine settings etc.), which in reality scatter considerably during production. Technological solutions are therefore achieved without actually understanding exactly how stabile they are. This results in product loss which can be as high as a few percentage of the production volume [3].

Many authors are dealing with the problem of predicting stability of forming processes [3] to [9] but in many cases the approach is too complex and too time consuming for industrial use. The aim of presented research is to develop the simplest possible optimization approach which gives reliable results is the shortest time possible. In practice this means with minimum possible number of numerical simulations. The proposed methodology which consists of numerical simulations, response surface methodology and stochastic optimization is described in Section 1. It was successfully applied during the development of forming procedures for forming of automotive parts. In section 2 it is shown how it is possible to predict scatter of final properties of the product based on scatter in input parameters. In section 3 it is used for optimization of forming process with respect to uncontrollable scatter of input parameters with the aim to avoid high scrap ratio. In the end the results are commented upon and the conclusions are given in Section 4.

1 PROPOSED METHODOLOGY FOR PREDICTION AND INCREASING THE STABILITY OF FORMING PROCESSES

In general metal forming process, the input can be categorized as energy (for powering the press), information (contained by CAD models) and unreformed material (sheet metal, bars, etc.). The response is the deformed product or actually the selected properties of product (e.g. the geometry,

*Corr. Author's Address: TECOS - Slovenian Tool and Die Development Centre, Kidričeva 25, SI-3000 Celje, Slovenia, gasper.gantar@tecos.si

thinning, final material properties due to hardening of input material, etc.). Also entering the process are control input variables (the variables that can be controlled by the process engineer – for example shape of the forming tool, setting on the forming press) and noise input variables (the variables that cannot be controlled by industrial settings (temperature for example). The control variables, the noise variables and also some of the input variables are stochastic variables.

The presence of stochastic input variables will cause variations of the response - the properties of the products. If the response deviates too much from the intended properties of the products the products may not be acceptable. A stable process is a process which is insensitive to the variations of the stochastic variables influencing the process, i.e. when the expected scatter of the input parameters (material properties and position, machine settings, friction conditions, etc.) do not cause unacceptable properties of the final products [10].

In our research the following approach (integrating numerical simulations, the response surface methodology and stochastic optimization based on Monte Carlo method) was used to study and optimize the stability of the considered stamping process.

1. Numerical models were developed and used for the prediction of the forming processes. Only the critical forming stages were modelled. PAM-STAMP 2G V2004.0 software was used for numerical simulations of stamping processes and DEFORM 2D Ver. 8.2 software was used for numerical simulations of bulk metal forming processes.
2. According to the selected design of experiments numerical simulations were run. Different designs of experiments can be used. In our research a three level Box-Behnken Design of experiments was used. Based on results an empirical model (termed a response function) was developed which approximated the relationship between the response of a system and input variables of the system that affect the response [11]. It is expected that the behaviour of forming system is non-linear therefore a second-order polynomial was used.
3. Based on empirical models, the Monte Carlo simulations were run to find the variation of the studied product properties due to scatter of input parameters [12]. It was assumed that all input variables form a normal distribution.
4. The probabilistic sensitivity of studied output product properties variations to each input parameter scatter was calculated in order to determine the relative magnitude of the effect caused by each input parameter on scatter of final properties. Based on these results a designer is able to select critical input parameters, which have major influence variation of output parameters and can suggest changes in input parameter scatter in a way that the value of studied product properties does not exceed specified tolerances.

2 PREDICTION OF SCATTER OF OUTPUT PARAMETERS

The developed approach was firstly used to predict the scatter of output parameters. Forging of a magnetic core, presented in Figure 1 has been studied as an example. The part had to be forged to the required final shape and it was expected that it would be difficult to keep the scatter of the thickness of the flange h within the required tolerance field. Therefore the thickness h was selected as the only studied product property.

The studied product was planned to be produced by a multi step forging procedure in 2 presses. Only the forming steps performed in the second mechanical press with nominal force $F_i = 8000$ kN and stiffness of k = 2.2 MN/mm were studied without final piercing and cutting steps (see Fig. 2). The material Qst-32-3 was used. The preforms were phosphated and lubricated with Na soap.

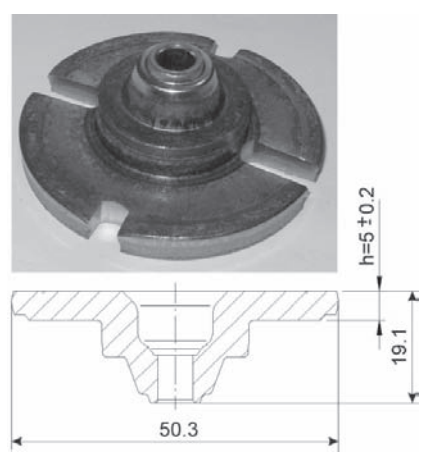

Fig. 1. *Magnetic core*

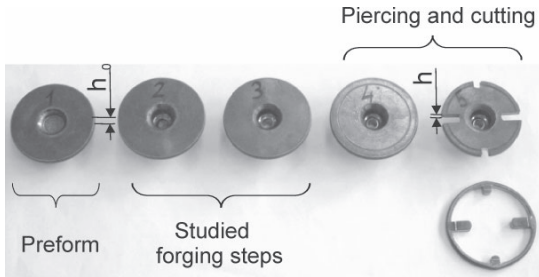

Fig. 2. *Studied forming sequence*

In Table 1 the most important input parameters, their nominal values and expected scatter of values are presented, on the basis of the data previously gathered in the ISKRA Avtoelektrika Ltd. plant [13].

The numerical results, calculated with mean values of input parameters, are presented in Figure 3. The surfaces of the tool parts were defined as rigid. The billet was discretized by elements, representing the material with a plastic constitutive law. The friction between the billet and the tool parts was modelled by the constant shear law. The friction coefficient $m = 0.09$ was used on the basis of previous experience.

An empirical model was developed which approximated the relationship between the response of a system (height of the flange h) and input variables of the system that affect the response (h_o, R_p, C, n, m). A three level Box-Behnken Design of experiments was used. A part of the design matrix (6 out of 42 runs) can be seen in Table 2. The advantage of this design is that fewer runs are required to obtain quadratic response function in comparison with other designs.

Heights of the flange h, which can also be seen in the left column of Tab. 2, were estimated by taking into account the forming forces, predicted by numerical simulations and measured stiffness of the press. Then a quadratic response function presented by equations (1) was calculated. The response function coefficients had been determined by a standard method of least squares, which minimizes the sum of the squared deviations of fitted values:

$$\begin{aligned} h = & -2.57736 + 3.14615 \cdot h_0 - 2.75319 \cdot 10^{-3} \cdot R_p \\ & - 5.35512 \cdot 10^{-3} \cdot C - 1.63355 \cdot n - 10.77242 \cdot m \\ & - 0.32937 \cdot h_0^2 + 1.71602 \cdot 10^{-6} \cdot R_p^2 + 2.29794 \cdot 10^{-7} \cdot C^2 \\ & - 1.84732 \cdot n^2 + 13.4623 \cdot m^2 + 3.6378 \cdot 10^{-4} \cdot h_0 \cdot R_p \\ & + 1.06929 \cdot 10^{-3} \cdot h_0 \cdot C + 0.81315 \cdot h_0 \cdot n \\ & + 0.062976 \cdot h_0 \cdot m - 4.04583 \cdot 10^{-7} \cdot R_p \cdot C \\ & - 9.0494 \cdot 10^{-3} \cdot R_p \cdot n + 0.010795 \cdot R_p \cdot m \\ & - 1.15119 \cdot 10^{-3} \cdot C \cdot n + 5.65905 \cdot 10^{-3} \cdot C \cdot m \\ & + 8.05595 \cdot n \cdot m \end{aligned} \quad (1).$$

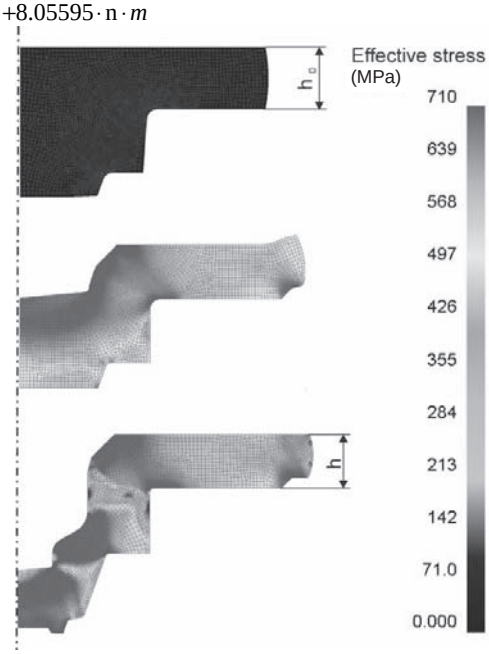

Fig. 3. *Numerical simulation of forging process*

Table 1. *Expected scatter of input parameters*

Input parameter	Mean value and expected scatter
Height out of 1st press [mm]	$h_0 = 6.1 \pm 0.1$
Yield stress [MPa]	$R_p = 400 \pm 40$
Hardening coefficient [MPa]	$C = 676 \pm 50$
Hardening exponent	$n = 0.165 \pm 0.02$
Coefficient of friction for constant shear law	$m = 0.09 \pm 0.01$

where C and n are coefficients used in hardening law $\sigma_f = C \cdot \varphi^n$

Table 2. *Experimental design matrix and results of numerical simulations*

Run						h
	h_0	R_p	C	n	m	
1	6.1	440	726	0.1685	0.09	5.080
2	6.2	400	676	0.1685	0.1	5.020
3	6.2	400	676	0.1885	0.09	4.985
4	6	400	676	0.1885	0.09	4.959
5	6.1	400	676	0.1685	0.09	5.002
42	6	400	726	0.1685	0.09	5.071

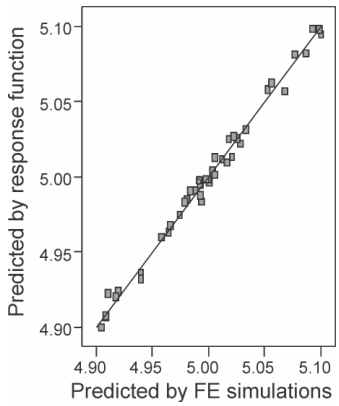

Fig. 4. *Predicted versus actual response*

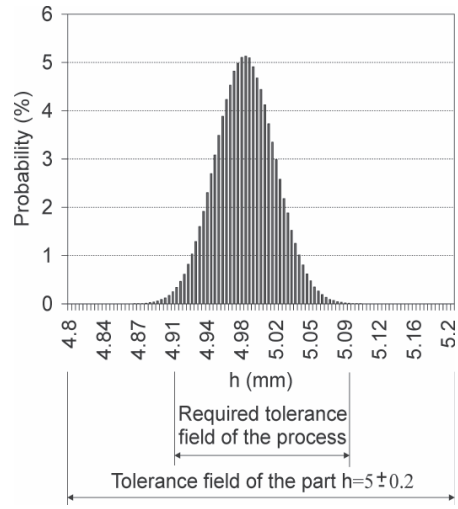

Fig. 5. *Probability chart for predicted h*

In Figure 4 the response of the system predicted by numerical simulations is compared to the one predicted by equation (1). It can be seen that equation (1) predicts the response of the system with good reliability.

Once the response function was obtained, the Monte Carlo techniques were used to extract the statistical distribution of the studied response for a specific set of statistical variations of input parameters. It was assumed that the variations of all input parameters are normally distributed with a mean value and standard deviation σ equal to 1/6 of the expected scatter specified in Table 1. Figure 5 shows the predicted probability chart for the scatter of the studied flange dimension *h*.

The required tolerance of the height of the flange *h* is ±0.2 mm. On the basis of the results of stochastic modelling it is predicted that practically 100% of the parts produced would be within the required tolerance. But in real production the whole tolerance field cannot be used only to compensate for the scatter of input parameters (dimensions, material properties and friction) listed in Table 2. The forging tools wear out during the production. Therefore they are produced with dimensions that allow maximum possible tool life and production is not carried out in the middle of the tolerance fields. Another reason is that customers of the forged products expect that only with a small percent of forged products the dimensions will be close to the limits of the requested tolerance fields. In industrial practice for the parts similar to the one presented in the paper, the scatter of dimension *h* during the test production process must be lower than ±0.1 mm in order to assure a stable large batch production over the time. For such requirement it is predicted in Figure 5 that the scatter of dimension *h* could be critical. During the trial production flange dimensions *h* of all test pieces were between 4.955 and 5.052 mm.

Figure 6 shows the sensitivity chart for the part attribute h, which was calculated based on the contribution of each input parameter to variance. The purpose of this is to determine, which input parameters significantly affect the studied part dimension. It provides us the ability to quickly judge the influence of the scatter of each input parameter on the studied part dimension.

From the Figure 6 the following conclusions can be extracted:

1. Studied dimension h is most sensitive to variations of the hardening properties of the material *C* and *n*.

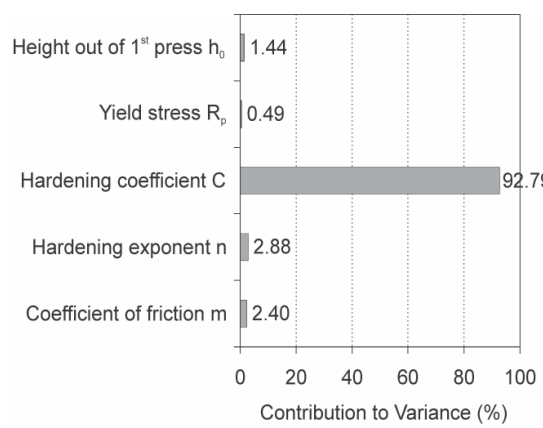

Fig. 6. *Sensitivity chart for predicted h*

2. Variations of coefficient of friction m and flange height after the first pass h_0 are of minor importance.
3. The scattering of Yield stress R_p is not very important.

In order to reduce the amount of rejected parts after the forging process it is reasonable to reduce the scatter of hardening properties of the material C and n. If this is too costly to achieve it is also possible to use the mechanical press with higher stiffness to produce the performance in the first pass. By this the scatter of flange height after first pass h_0 can be reduced.

3 OPTIMIZATION OF FORMING PROCESS AIMING AT MAXIMUM ROBUSTNESS

In some cases it is not enough only to predict the scatter of final properties of product, but it is also necessary to optimize the production process. Stamping process for production of part, whose geometry and approximate dimensions are presented in the upper part of Figure 7, was studied. In this case the object of study was prediction of reject rate and optimisation of stamping procedure. The selected stamping procedure is presented in the lower part of Figure 7. Drawbead was planned in stage 2 to prevent wrinkling in the walls of the part. The two main input parameters which could be optimized during development of forming procedure were: the initial shape of the blank (size of the cut-out produced in stage 1, defined by parameter *a*), and properties of drawbead (defined by restraining force F_{db}). If the cut-out is big and restraining force F_{db} is low then material flow into the die cavity is less constrained and only minor sheet thinning but higher wrinkling is expected. On the other hand if the cut-out is small and restraining force F_{db} is high, then material flow into the die cavity is more constrained and lower wrinkling but danger of excessive sheet thinning and localization is expected.

Table 3. *Expected scatter of input parameters*

Input parameter	Mean value and expected scatter
Initial sheet thickness (mm)	$s_0 = 0.7 \pm 0.05$
Yield stress (MPa)	$R_p = 152 \pm 45$
Hardening coefficient (MPa)	$C = 373 \pm 50$
Hardening exponent (1)	$n = 0.218 \pm 0.036$
Coefficient of anisotropy	$r = 2.12 \pm 0.2$
Coulomb's coefficient of friction (1)	$\mu = 0.1 \pm 0.015$

In Table 3 the most important input parameters, their nominal values and expected scatter of values are presented, based on of the data previously gathered [10] and on industrial experience.

The optimum solution was searched for within the following search space: cut-out a = 0 to 90 mm and restraining force F_{db} = 0.02 to 0.08 kN/mm. If a equals 0, no cut-out is produced at all and a should not be greater than 90 mm, otherwise there is not enough material in the blank to form the product with the required dimensions. Restraining force F_{db} = 0.02 kN/mm can be ensured by a modest drawbead and restraining force F_{db} = 0.08 kN/mm can be ensured by strong drawbead.

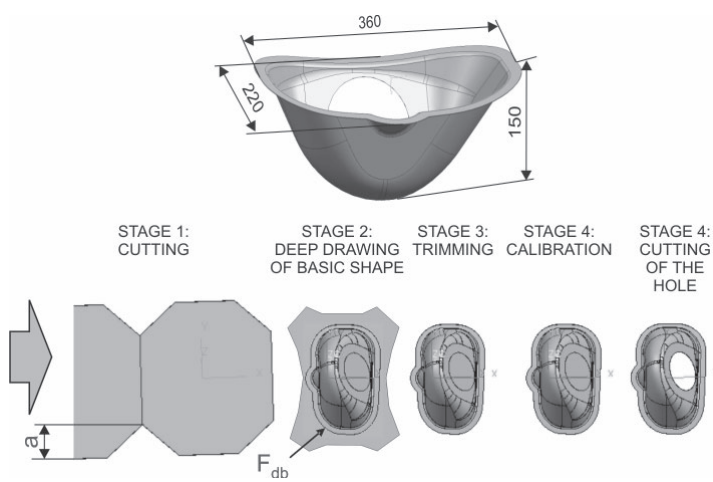

Fig. 7. *CAD model of the studied part and selected forming procedure*

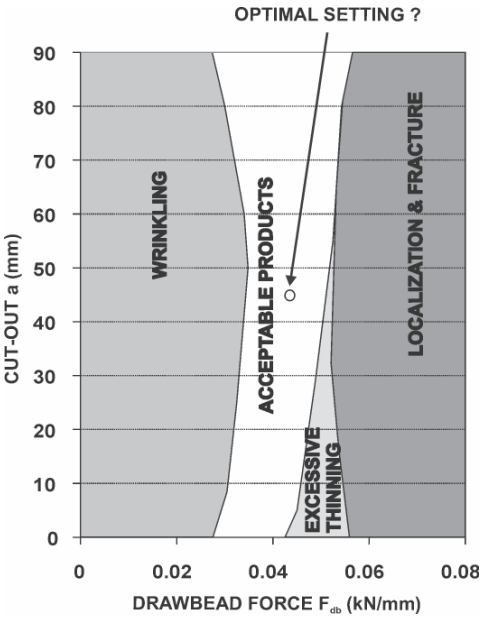

Fig. 8. *Technological window for the studied stamping process*

In metal forming, the combination of input parameters leading to a successful forming operation and acceptable products is defined as a technological window of the process. For the studied example, where the only two input parameters that could be varied were the following: the size of the cut-out a and the drawbead force F_{db}, therefore the technological window can be easily determined by several numerical simulations or experimental trials (see Fig. 8).

The questions arose how to evaluate and how to maximize the stability of the forming process. What is the optimum size of the cut-out and what is the optimum setting of the drawbead force F_{db} for the maximum stability? Intuitively, it would be reasonable to set parameters exactly in the middle of the technological window. But is this really the best solution?

The following approach was used to answer this question. A numerical model and the results calculated with average input parameters are presented in Figure 9. The surfaces of the tool parts were defined as rigid. The blank sheet was discretized by quadrangle elements, representing the material with an elasto-plastic constitutive law. For the material hardening determination the Krupkowski law was used. The friction between the blank and the tool parts was modelled by the Coulomb's Law. Prediction of localization was done by comparing the strain states to the Forming Limit Curve (FLC) that was determined as described in [14]. Prediction of wrinkling was done by comparing the heights of the wrinkles to the selected critical value. The allowed thinning was selected to be 20% for the studied example in compliance with the requirements of the customers from automotive industry.

For better understanding of the results it is reasonable to define the response of the system by Equation (2), which evaluates the danger of the unwanted output properties:

$$D(a, F_{db}) = \max(D_L, D_T, D_W)$$
$$D_L = \frac{\varepsilon}{\varepsilon_{FLD}}\ ; D_T = \frac{s_0 - s}{s_0 - s_{\min}}; D_W = \frac{h_w}{h_{w\max}} \quad (2).$$

D_L is defined as the danger of localization, D_T is defined as the danger of extensive thinning, D_W is defined as the danger of wrinkling, ε is the critical actual strain path (shown in Fig. 9), ε_{FLD} the allowed

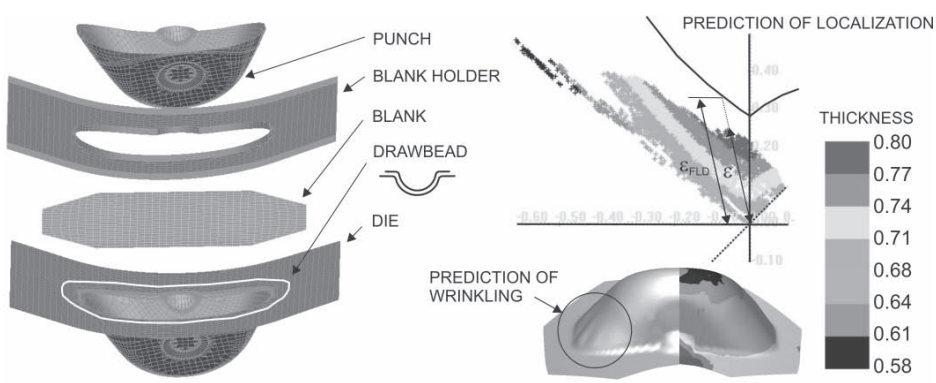

Fig. 9. *Numerical model and results*

strain path (shown in Fig. 9), s_0 the initial sheet thickness, s sheet thickness at the product, s_{min} allowed minimum final sheet thickness, h_w the height of the wrinkles detected on the product and $h_{w\,max}$ allowed height of the wrinkles. Finally D is defined as the parameter predicting the danger that any of the unwanted output properties will occur. If the value D is low, the technological safety is high. In the case of $D>1$ the product is unacceptable (at least one of the unwanted output properties occurs). In our research a three level Box-Behnken Design of experiments was used. Later the empirical models (termed the response functions) were developed, which approximated the relationship between the response of a system (danger of localization, excessive thinning and wrinkling) and input variables of the system affecting the response. Response functions are given by:

$$\begin{aligned}\text{Ln } D_L &= -32.064+111.136\cdot F_{db}-0.240\cdot a-79.673\cdot s-0.301\cdot R_p\\ &+0.147\cdot C-334.126\cdot n+76.087\cdot r+215.998\cdot\mu+942.625\cdot F_{db}^2\\ &-5.203\cdot10^{-5}\cdot a^2-14.662\cdot s^2+2.306\cdot10^{-5}\cdot R_p^2+3.185\cdot10^{-6}\cdot C^2\\ &+28.484\cdot n^2-0.209\cdot r^2-148.556\cdot\mu^2-0.230\cdot F_{db}\cdot a+123.445\\ &\cdot F_{db}\cdot s-0.338\cdot F_{db}\cdot R_p-0.049\cdot F_{db}\cdot C+115.446\cdot F_{db}\cdot n-\\ &82.454\cdot F_{db}\cdot r-186.487\cdot F_{db}\cdot\mu+0.160\cdot a\cdot s+1.645\cdot10^{-4}\cdot a\cdot R_p\\ &-1.967\cdot10^{-4}\cdot a\cdot C\end{aligned} \quad (3)$$

$$\begin{aligned}\text{Ln } D_T &= -86.568-30.745\cdot F_{db}-0.207\cdot a+1.609\cdot s+0.061\cdot R_p\\ &+0.270\cdot C-39.125\cdot n+39.849\cdot r+2.893\cdot\mu+755.905\cdot F_{db}^2\\ &+1.906\cdot10^{-6}\cdot a^2+17.309\cdot s^2+8.397\cdot10^{-5}\cdot R_p^2-2.879\cdot10^{-4}\cdot C^2\\ &+63.085\cdot n^2+1.690\cdot r^2+636.884\cdot\mu^2-0.092\cdot F_{db}\cdot a+119.264\cdot F_{db}\cdot s\\ &-0.254\cdot F_{db}\cdot R_p+0.039\cdot F_{db}\cdot C-62.648\cdot F_{db}\cdot n-2.614\cdot F_{db}\cdot r\\ &-462.911\cdot F_{db}\cdot\mu+0.132\cdot a\cdot s-1.275\cdot10^{-4}\cdot a\cdot R_p+5.629\cdot10^{-5}\cdot a\cdot C\end{aligned} \quad (4)$$

$$\begin{aligned}\text{Ln } D_W &= +16.052+50.031\cdot F_{db}-0.125\cdot a+43.156\cdot s-1.163\cdot10^{-3}R_p\\ &+0.039\cdot C-71.520\cdot n+8.190\cdot r-642.077\cdot\mu+251.456\cdot F_{db}^2\\ &-1.304\cdot10^{-4}\cdot a^2-84.569\cdot s^2+2.619\cdot10^{-5}\cdot R_p^2-7.516\cdot10^{-5}\cdot C^2\\ &-133.624\cdot n^2-1.079\cdot r^2-1870.281\cdot\mu^2-0.030\cdot F_{db}\cdot a+45.461\cdot F_{db}\cdot s\\ &+0.248\cdot F_{db}\cdot R_p+0.177\cdot F_{db}\cdot C-485.248\cdot F_{db}\cdot n+13.555\cdot F_{db}\cdot r\\ &-1545.954\cdot F_{db}\cdot\mu-0.010\cdot a\cdot s+1.712\cdot10^{-4}\cdot a\cdot R_p+4.355\cdot10^{-5}\cdot a\cdot C\end{aligned} \quad (5).$$

Once the response functions were obtained, the Monte Carlo techniques were used for the determination of the optimal setting of input parameters a_{opt} and $F_{db\,opt}$.

The results of the optimization procedure are presented on the left hand side of Figure 10. It is predicted that maximum stability (minimum reject rate) can be achieved when the forming procedure is performed with the settings a_{opt} = 70 mm and $F_{db\,opt}$ = 0.04 kN/mm. The forming tool was produced with regards to the results given above. It is presented on the right hand side of Figure 10. After the preliminary testing in the tool manufacturing company it was decided that the geometry of the drawbead, which provides restraining force F_{db} = 0.04 kN/mm, would be selected appropriately, but the cut-out produced in stage 1 would be 20 mm higher that the theoretically calculated optimum choice.

Finally Figure 11 shows the sensitivity chart for the danger of the unwanted output properties D which was calculated based on the contribution of each input parameter to variance. It provides us with the ability to quickly judge the influence of the scatter of each input parameter to the studied process stability.

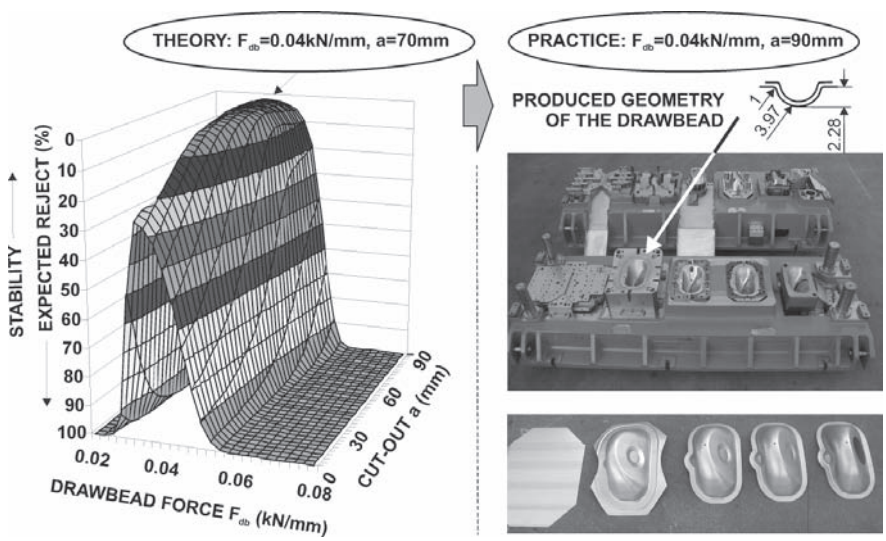

Fig. 10. *Results of the optimization procedure*

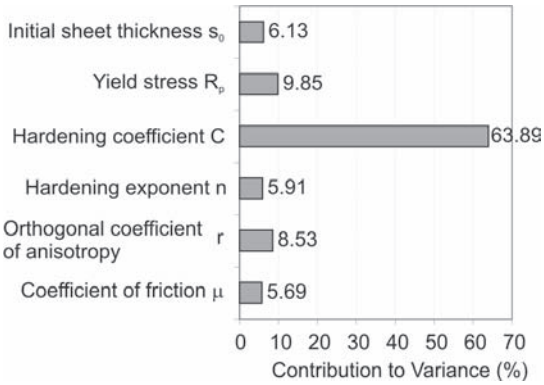

Fig. 11. *Sensitivity chart for the predicted stability*

From the Fig. 11 the following conclusions can be extracted:

1. Process stability is most sensitive to variations of the hardening properties of the material (especially hardening coefficient *C*).
2. Variations of other input parameters (initial sheet thickness, yield stress, orthogonal coefficient of anisotropy and coefficient of friction) are of minor importance.

4 DISCUSSION AND CONCLUSIONS

Manufacturing processes consist of variability which can deteriorate product quality and increase costs. The process of generating experimental data in the early stage of production process development is quite difficult. For such cases numerical simulation can be directly applied for generating the experimental data. In the paper the approach that can help to predict and optimize the forming processes from the stability point of view is presented. It gives feedback and direction for design improvement.

Using this approach the optimization process can be performed with the minimum number of time-consuming numerical simulations. The method is simple, appropriate for industrial use. It is especially appropriate for cases where the number of input parameters taken into account is relatively low (lower that 10). In such cases it gives excellent results with low number of required (and for complex industrial examples many times quite time consuming) numerical simulations. For solving the cases where the number of input parameters is higher the number of numerical simulations required becomes large no matter which design of experiments is used. In such cases other optimization approaches give results faster. Only the so called "technological reject" is evaluated. The reject resulting from other reasons (failure of the tool, wrong setting of the machine, etc.) is not the subject of the presented paper.

In order to confirm the presented results of optimization, the mass production with different settings of input parameters should be observed. In industrial practice this is impossible to achieve since companies are unwilling to perform changes on the tool and run the production with undesirable settings just to measure the increase of the reject rate. But the experts from the production floor were satisfied with the presented calculations and results.

In future the cost function must be integrated into the optimization procedure in order to correctly optimize the studied production processes from the economical point of view. For example, in some cases it is reasonable to use cheaper raw material with higher scatter of properties although the production is performed with higher scrap ratio.

5 REFERENCES

[1] Barišić, B., Cukor, G., Math, M. Estimate of consumed energy at backward extrusion process by means of modeling approach. *Journal of Materials Processing Technology*, vol. 153-154, 2004, p. 907-912.

[2] Petek, A., Pepelnjak, T., Kuzman, K. An improved method for determining a forming limit diagram in the digital environment. *Journal of Mechanical Engineering*, vol. 51, 2005, p. 330-345.

[3] Kini, S., Shivpuri, R. A Response surface based FEM approach for improving quality of forging processes. *Proc. of 8th ICTP 2005, International Conference on Technology of Plasticity*, Verona, 9-13 October, 2005.

[4] Kuzman, K. Comments on the cold metal forming processes stability control. *Journal of Materials Processing Technology*, vol. 185, 2007, p. 132-138.

[5] Herron, J.C., Hodgson, P.D., Cardew-Hall , M.J. Defining the operating window for an automotive sheet pressing operation. *Journal of Materials Processing Technology*, vol. 80-81, 1998, p. 68-75.

[6] Hu, J., Peng, Y., Li, D., Yin, J. Robust optimization based on knowledge discovery from metal forming simulation. *Journal of Materials Processing Technology*, vol. 187-188, 2007, p. 698-701.

[7] Chen, D.C., Chen, C.F. Use of Taguchi method to develop a robust design for the shape rolling of porous sectioned sheet. *Journal of Materials Processing Technology*, vol. 177, 2006, p. 104-108.

[8] Zhang, Y., Zhu, P., Chen, G. Lightweight design of automotive front side rail based on robust optimization. *Thin-Walled Structures*, vol. 45, 2006, p. 670-676.

[9] Krušič, V., Mašera, S., Pepelnjak, T., Kuzman, K., Rodič, T. The impact of the forming system parameters on tool service life and product accuracy in cold forging. *Proceedings of the 6th JSTP International Seminar on Industrial tools*, Bled, 11-14 September, 2007.

[10] Gantar, G., Kuzman, K. Sensitivity and stability evaluation of the deep drawing process. *Journal of Materials Processing Technology*, vol. 125-126, 2002, p. 302-308.

[11] Myres, R.H., Montgomery, D.C. *Response surface methodology, process and product optimization using designed experiments*. New York: John Wiley & Sons, 2002.

[12] Rubinstein, R.Y. *Simulation and Monte Carlo methods*. New York: John Wiley & Sons, 1981.

[13] Gantar G., Mašera, S., Krušič, V. Increasing the stability of forging processes. *Proceedings of the 4th JSTP International Seminar on Precision Forging*, Nara, 21-25, March 2006.

[14] Forming limit diagrams are now available for higher strength steels. *National Steel Automotive Technical Bulletin FO-2A9*.

Strojniški vestnik - Journal of Mechanical Engineering 54(2008)4, 258-265
UDC 678-1
Paper received: 6.12.2007
Paper accepted: 15.5.2008

Large Thermoplastic Parts Quality Improvements Using Monitorized Nozzle

Angel Fernandez* - Daniel Mercado - Carlos Javierre - Manuel Muniesa
University of Zaragoza, Faculty of Mechanical Engineering, Spain

Rheological behaviour control of thermoplastic material is critical to achieve reliable production series free of defects such us flashes or short shots. Defects are especially critical when injecting large parts if stability of processing parameters cannot be achieved. Viscosity variation during production depends specially of lot of raw material and programmed parameters concerning temperature. Understanding rheological behaviour of molten material in injection nozzle is critical to obtain repetitive series of large parts free of defects. In this paper apparent viscosity was obtained using monitorized nozzle and used as an input to MoldFlow analysis to predict defects. The Simulation model included a two different cavities mould for washing machine tubs made of talc filled polypropylene, hot runner manifold and the machine nozzle. To validate analysis several complete series of parts were injected using a nozzle with two pressure and temperature sensors in a heated thick cylindrical channel, and a screw displacement sensor. Previously the nozzle was validated testing the effect of pressure losses with shear rate variation; apparent viscosity with pressure variations; and others such as viscous heating of polymer. Part defects were characterized using statistical analysis of registered parameters during filling and packing phase of the mould. Simulations of identical experimental parameters for correct and failed parts were used to validate results and characterized the defects.

Keywords: nozzles, polyolefins, viscosity, injection moulding, pressure measurement, temperature measurement

0 INTRODUCTION

This paper summarizes the research work developed by the Mechanical Engineering Area of the University of Zaragoza in cooperation with Foundation AITIIP technological center.

The results are focussed to determine apparent viscosity values of talc filled polyolefins in the nozzle of the injection moulding machine and to register operational parameters during injection of large parts such us bumpers and washing machine tubs in order to establish relationships with typical defects like flashes or short shots.

There are different methods for viscosity measurement of molten polymers [8] to [10]. The capillary rheometer determines the relathionships between viscosity and shear rate, temperature and pressure variations. For this reason this is the most used way to fully characterizate the rheological behaviour of a thermoplastic grade in order to develope further calculations such us injection moulding simulations.

One of the goals of this research work is to determine apparent viscosity in an injection moulding machine during operation [10]. Some advantages can be gained with this technology. First is a real-time viscosity calculation of the raw material used for producing injected parts which is highly dependent of the lot of supplied material. Second is the monitorization of the variations in viscosity values on-line to advance potential fails in injected parts. Third is the influence of scale effects that differ from measurements made through a capillar channel less than 1mm diameter and those made through mould and machine channels from 2 to 20 mm thickness. Other is the information obtained about the injection moulding processing parameters on-line, the possiblity to establish relationships with part defects and the additional option to determine the properties of materials that cannot be tested in the laboratory such us recycled materials and re-used scrap material.

The injection moulding of large parts through very large series over than 1,000 cycles per day is critical because very small defects like

*Corr. Author's Address: University of Zaragoza, Faculty of Mechanical Engineering, C.P.S Torres Quevedo, María de Luna, 3, 50018 Zaragoza, Spain, afernan@unizar.es

short shots and flashes are highly dependent on the viscosity of the material and it can vary depending the lot of raw material. This complex process can be improved using especial sensors for pressure and temperature measurement in the nozzle of the machine. They will be usefull for apparent viscosity determination and also for small variations detection in processing parameters that could induce these defects that affect to less than 1% of the part but force to reject heavy parts and even stop the production lines.

1 APPARENT VISCOSITY MEASUREMENT

1.1 Equipment - Monitorized Nozzle

A customized nozzle (Fig. 1) has been developed with an internal channel of 12 mm diameter and 300 mm length. It has been installed in an Italtech 3000T/WP19800 machine, suitable for large parts injection such us car bumpers, containers and washing machine tubs. The nozzle is equipped with three chain heaters controled by thermocouples to control the temperature of the molten material, and two kistler 4083A sensors for melt pressure and temperature measurement. These transducers are assemblied to their charge amplifiers. The plastication unit is equipped with a wire potenciometer and hydraulic pressure sensor. A complete system of computer, software, acquisition card, signal conditioning, etc. complete the measure chain.

Another nozzle has been simultaneously developed with an internal channel of 3mm thickness, 20 mm width and 100 mm lenght. It has been intalled at a JSW 85EL II machine.

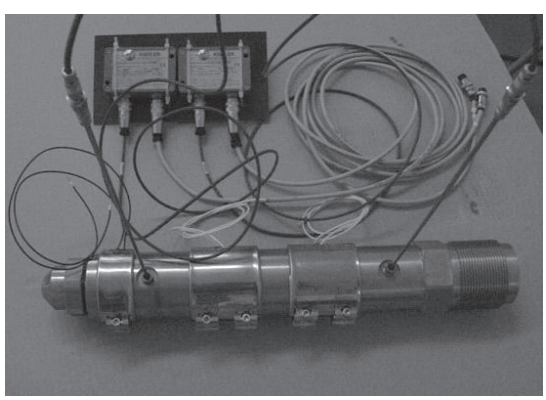

Fig. 1. *Nozzle with sensors for 3000T Machine*

1.2 Apparent Viscosity Measurement - Theory

One of the crytical problems when injecting large parts is to maintain production parameters inside a process window if using large amounts of raw material whose viscous properties can vary between different lots. For this reason it is necessary the use of an apparatus that allows to determine viscous properties during production machine operation [10] to [13] and [15]. In this case the monitorized nozzle is assembled between the plasticating cylinder and the mould the measure the properties of the molten plastic.

The procedure the measure the apparent viscosity consists in make free purges of the cylinder through this nozzle with constant screw speed. Pressure losses and temperatures are measured with the sensors, also screw position is measured with the wire potenciometer. Actual temperature of the molten plastic is also measured with a contact phyrometer placed in the injected mass after each purge. Graph curves like showed in figure 2, and time dependent data were stored in the computer.

The screw speed is a calculation by derivating screw displacement and the flow rate (Q) by multiplying the speed and the cross section of the channel.

Wall shear rate (γ_w), wall shear stress (τ_w) and apparent viscosity (η_{app}) are calculated using this formulae (8), (9) and (14):

$$\dot{\gamma}_w \cong \left(-\frac{dv}{dt} \right)_{r=R} = \frac{4 \cdot Q}{\pi \cdot R^3} \tag{1}$$

$$\tau_w \cong \tau_{rz}(r = R) = \frac{-\Delta P \cdot R}{2 \cdot L} \tag{2}$$

$$\eta_{app} = \frac{\tau_w}{\dot{\gamma}_w} \tag{3}.$$

Where, Q is the channel flow rate, R is the radius of the nozzle channel, ΔP is the difference of measured pressure values in the transducers and L is the distance between transducers.

1.3 Experimental Viscosity Calculation

Six different screw speeds and three different temperatures were programmed and each trial was repeated five times. This calculations are made each purge cycle to obtain one value of apparent viscosity associated to a shear rate and temperature value.

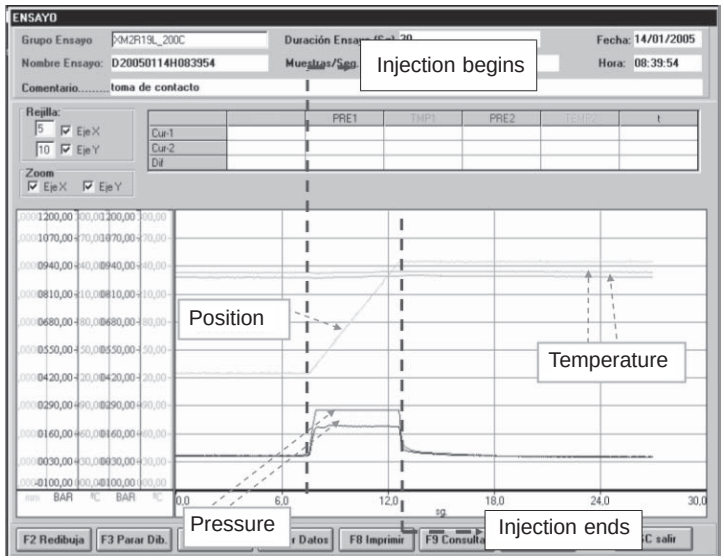

Fig. 2. *Air purge data acquisition*

After a complete test up to 90 results have to be fitted to construct a viscous model.

The results obtained for a 20% Talc filled Polypropilene, Hostacom XM2 R19L, were compared with those found in Moldflow material database and the raw material supplier, Basell, database. Also, the actual lot of material has been characterizated in a Gottfert 1,500 capillary rheometer. The fifth source of material data has been the results obtained from a similar procedure with a sensored nozzle with rectangular cross section operated in a 85Ton electrical machine.

Resultant data have been fitted using Visdat application to calculate Klein model constants for viscosity calculation accordingly to this equation:

$$\ln(\eta) = a_1 + a_2 \ln(\dot{\gamma}) + a_3 T + a_4 [\ln(\dot{\gamma})]^2 + a_5 \ln(\dot{\gamma}) T + a_6 T^2$$

where:

η [Pa·s] represents apparent viscosity,

γ [s^{-1}] represents shear rate,

T [ºC] represents mass temperature,

a_1 ... a_6 are model constants.

The result of data fitting has been complex because of the origin of the measured points that differs roughly from a conventional capillary rheometer. Table 1 shows the selected values at 3 different temperatures (column 1), wide range of calculated shear rate (column 2), measured viscosity (column 3) and calculated viscosity with Klein model after data fitting and six constants a_i calculation (column 4). It has been necessary to filter some information further 6% error from fitted data (column 6) so it can be concluded, the precision of this way of viscosity measurement is less precise than capillary rheometry.

Table 2 summarizes a comparison between calculated constants for Klein model (column 1) from different sources. The coefficients in the

Table 1. *Comparison between measured and fitted data*

Temp. [ºC]	Shear rate [s^{-1}]	Meas. V [Pa·s]	Calc. V [Pa·s]	% error
200	315.97	244.81	244.50	-0.127
200	1014.73	133.00	129.96	-2.338
200	4137.13	47.68	48.40	1.497
200	8174.26	28.93	27.44	-5.452
220	315.27	211.06	211.06	0.000
220	4164.88	45.23	48.15	6.047
240	300.60	208.91	212.19	1.548
240	2037.58	59.10	55.82	-5.881
240	4181.90	28.80	30.02	4.069

Table 2. *Comparison of Klein model constants*

Klein coeff.	Capillar rheometer	Rectangular nozzle	Circular nozzle
a1	7.3077	11.556	11.196
a2	-0.47197	-0.64547	0.83060
a3	1.67471E-02	-1.48095E-02	-5.68294E-02
a4	-2.16310E-02	-2.20278E-02	-6.26514E-02
a5	8.47880E-04	1.0327E-03	-2.88984E-03
a6	-7.08439E-05	6.78162E-06	-1.57621E-04
Standar dev.	6.36E-03	8.5E-03	1.32E-02

second column result after fitting the measured viscosity values obtained for the same lot of raw material using a capillary rheometer.

The third column shows the coefficients obtained using the same raw material and the monitorized nozzle with rectangular cross section. The fourth column shows the coefficients obtained using the nozzle with sensors described in this paper. Tha last row evidences the accuracy of the fitted coeffients in terms of standard deviation below 1.32%. With all this coefficients a complete plot for apparent viscosity can be drawn, and all necesary values of viscosity as a function of shear rate and temperature can be determined for injection moulding simulation.

Different curves representing shear rate influence in viscosity calculation at a temperature of 240ºC are plotted in Figure 3. Calculated Klein models are used for this plots. The differences in the curves are similar at different temperatures (200ºC, 220ºC, 240ºC) and the qualitative tendency is quite similar. The differences are caused mainly for the use of Newtonian model for vicosity calculation that is suitable for capillary rheology but not for thick sections as in the nozzle. This phenomenon has been introduced in previous studies [1] to [7].

The results show how the differences in viscosity values increase with the cross section thickness of the measurement apparatus. In this case, the prediction on viscosity with the 3x20 mm section nozzle is no more than 9.5% higher than with the reometer. The differences measured with the 12 mm section nozzle grow up to 30% higher that with the nozzle at the highest shear rates (> 4.000 s^{-1}). The values coming from the material supplier database are coincident with the rectangular nozzle and evidence differences with those measured in the rheometer that depend on the lot of raw material, quite different from that one tested in the laboratory prior this research work.

2 SHORT SHOT CHARACTERIZATION

2.1 Experimental Work

Short shots are one of the most common defects when injecting large plastic parts. These

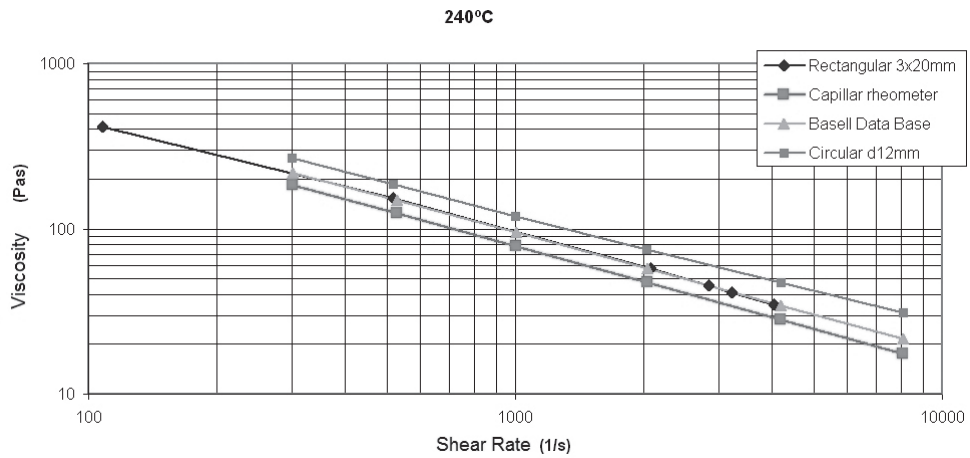

Fig. 3. *Comparison of plots from differen Klein models at 240ºC temperature*

kind of defects are extremely severe because they prove that processing conditions are unstable or unsteady. The result of a short shot implies the refuse of a heavy part of several kilograms weight because of a very small defect of just a few grams. The visual inspection in-line of the produced parts is needed to prevent failed parts are delivered involving additional costs.

A complete parameter registration has been developed up to 2.37 cycles during a test of a mould for washing machine tubs. The monitorized nozzle has been used in combination with the hydraulic pressure transducer of the injection machine and the Statistic Process Control (SPC) of the machine.

It has been proved the productive parameters follow different patterns depending on a raw material lot. For this reason injection parameters must be readjusted periodically because of the viscosity variations, specifically those related to injection and packing phase. The different lots of raw material are certified for production of parts between a range of values of Melt Flow Index so that variations in rheological behaviour of the molden plastics must be assumed in the production lines. It influences the thermal response of the material in terms of heat generated during plastification process by means of viscous heating of the melt. Melt temperature variations induce fails such us short shots as shown in Figure 4. For this reason, the monitorized nozzle is used to check temperature evolution and to control the plastic viscosity monitoring pressure losses between transducers.

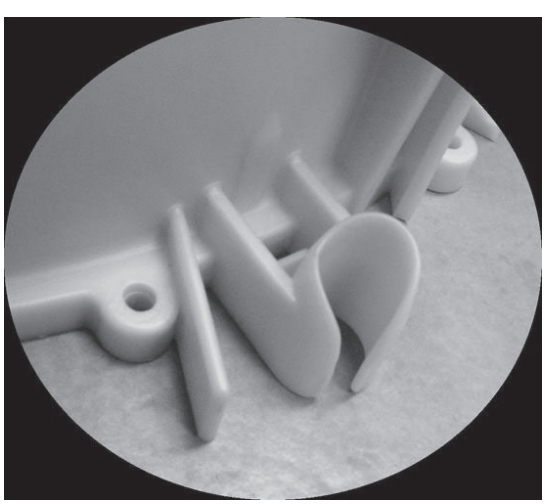

Fig. 4. *Short shot at the end of filled cavity*

Table 2. *Operation parameters and deviations*

Parameter	Part OK	Part NOK	Abs. diff	Rel. diff
Inj. time	6.672	8.188	1.52	22.72
St. dev.	0.033	0.073		
Pack. time	10.424	10.312	0.11	-1.07
St. dev.	0.159	0.082		
Hydr. pres.	176.046	200	23.95	13.6
St. dev.	0.487	0		
Sensor 1 pres.	512	531.7	19.7	3.85
St. dev.	1.225	1.059		
Sensor 2 pres.	863.814	884.627	20.81	2.41
St. dev.	2.455	2.133		
Av. pack. pres.	116.032	115.057	-0.98	-0.84
St. dev.	0.227	1.174		
Nozzle temp	281.661	271.693	-9.968	-3.54
St. dev.	0.071	0.142		
Screw. displ.	353.22	332.17	-21.05	-5.96
St. dev.	0.446	0.819		

Table 2 shows the most relevant parameters when producing these parts. Results for 1.940 parts completely filled (column 2) demonstrate they are produced under stable parameters. The standard deviations are 0.033 for injection time, 0.487 for hydraulic pressure, 0.071 for nozzle temperature and 0.446 for screw displacement. Also measured hydraulic pressure, pressure in both sensors in the nozzle and average hydraulic pressure during packing are quite stable. Results for 430 short shots (column 3) show the effect of viscosity increment with lower mass temperature. The reduction of mass temperature of 9.968 ºC is due to a reduction of viscosity of raw material that reduces roughly the contribution of viscous friction to plastic heating.

Two plots of the registered parameters of correct and failed parts are shown in Figures 5 and 6. These plots show the evolution of several properties through the cycle time. The optimum process shown in Figure 5 is developed under high hydraulic pressure conditions over 190 bar (*PH*). Total volume injected is nearly proportional to screw displacement (*Carr*). Temperature variations in the nozzle during a cycle are neglectable (*T_1* and *T_2*). In Figure 6 it can be observed that melt temperature decreases 3.54% and consecuently nozzle pressure increases. Defects occur when the hydraulic pressure reaches the injection pressure limit (200 bar). From this moment the end of filling phase is delayed (22.72%) because of the reduction of screw speed and a total screw displacement is reduced (5.96%) inducing short shot.

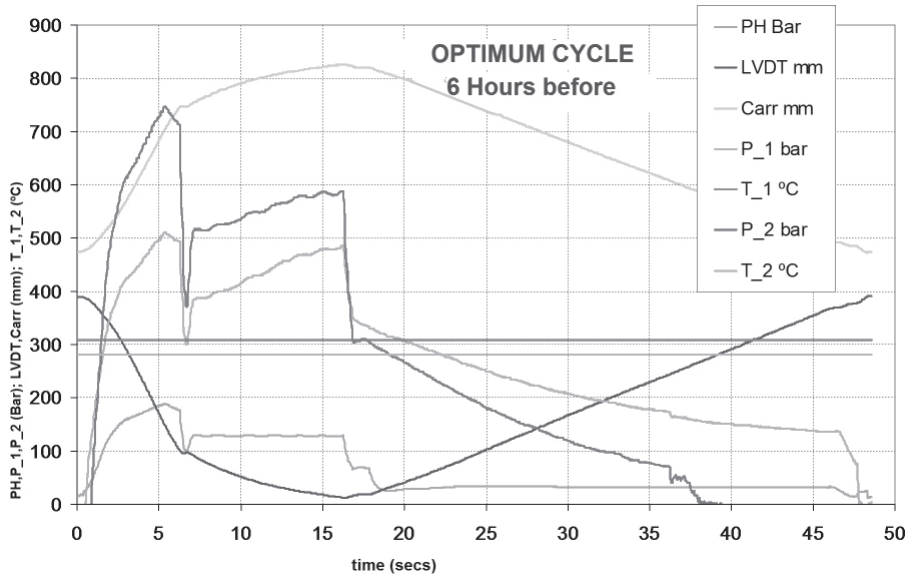

Fig. 5. *Optimum cycle parameters*

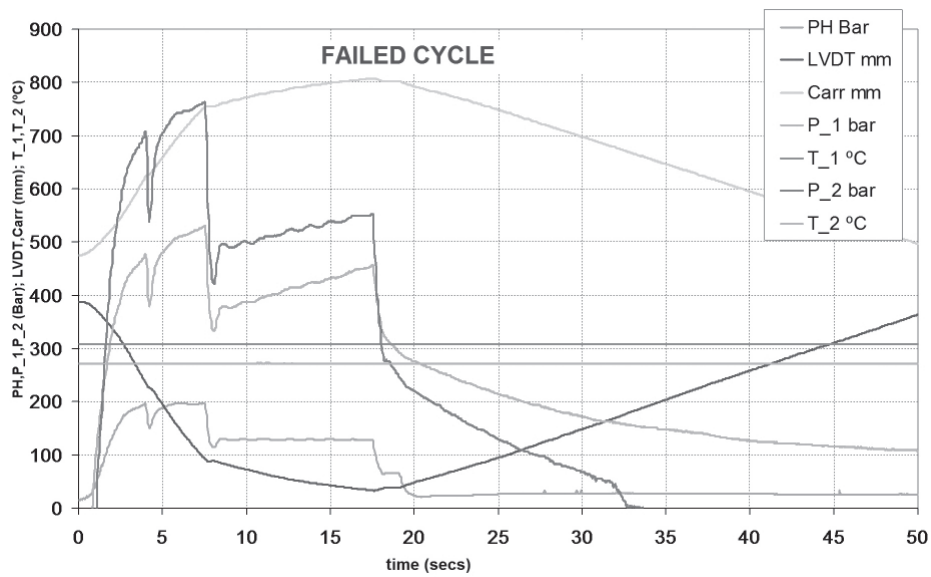

Fig. 6. *Parameters when short shot appears*

2.2 Simulation Work

A complete simulation has been done with Moldflow 5.0 software. Simulations have been developed using measured material viscosity data and measured processing conditions as inputs. A limit of 200 bar in injection pressure has been introduced so, as this limit has been reached the programed injection time has extended up to 18.08 s that fits with the measured time in the machine of 18.5 s.

Results have demonstrated that operation under these conditions increases roughly injection pressure and short shot appears because the slower displacement of the injection screw that stand the flow front to freeze. Figure 7 shows the results of the simulation regarding mould filling. Comparing this image with Figure 4 it can be predicted the exact location of the short shot.

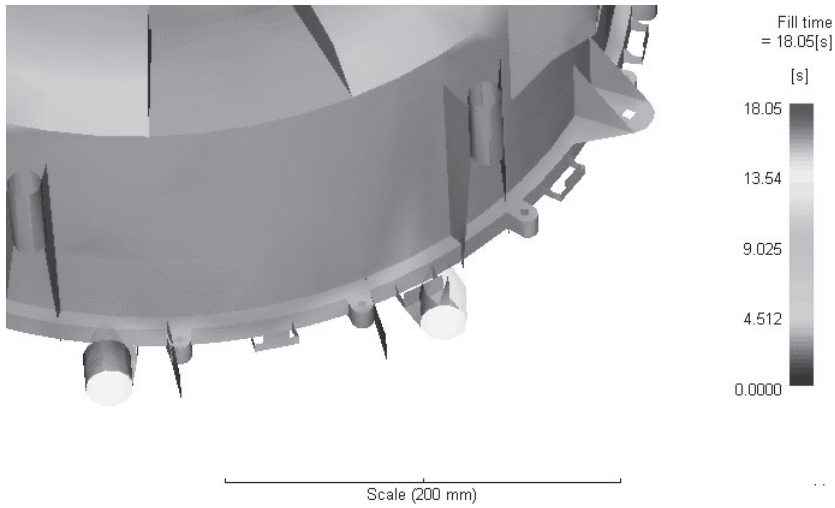

Fig.7. *Short shot simulation*

3 DISCUSION

The use of monitorized nozzle to determine apparent viscosity of molten polymers in an injection moulding machine has been accurate enough to compare results with those obtained from differen sources. But data fitting and construction of Klein model has demonstrated less accuracy than capillary rheometry. This unaccuray grows at high shear rate values due to divergences between the fully developed flow pattern through a capillar and the flow pattern through a thick channel.

Comparisons between results from different sources have demonstrated that as thicker is the cross section greater are the differences between viscosity predictions. Also the calculation of pressure losses when filling thick cavities or runners is less accurate as they are thicker because of the assumptions made for polymer flow modellisation.

The experimental work with large parts evidences that small variations in raw material properties influence process parameters such us pressure and temperature without varying processing conditions, so that, monitoring those parameters with a nozzle with sensors fits to suitable process control.

Graph plots of processing parameters show that short shots could be prevented because they appear as a consecuence of gradual degradation in processing conditions as slow decrease of melt temperature and increment of pressure needed for complete mould filling. This incident occurs after several cycles as different lots of raw materials are still mixed so that an alarm could be installed attached to the monitorized nozzle or temperature conditions could be automatically readjusted.

Concordance between actual filed parts and simulated ones allows to manage the inspection activities of the produced parts easily, revealing the risk zones of them. The results of the simulation have fitted the defects obtained in the experimental work when using the material data generated with the monitorized nozzle better that those available in the database.

A similar work has been developed to prevents fails like flashes (Fig. 8), but results have not been succesful. All these defects have appeared suddenly, without oriented variation in processing parameters. The main reason for this defects has been the temporal obstruction of some of the gate points or hot runners.

Fig. 8. *Flashes in large parts*

4 CONCLUSIONS

A monitorized nozzle has been used to measure apparent viscosity and calculate Klein model for a talc filled polypropylene. Estimated error increases with the dameter or thickness fo the cross section through the nozzle due to differences in the flow behaviour with capillary rheometer mainly. Several phenomena have been also detected like increments of viscosity up to 20% with higher level of pressure downstream, and viscous heating through the nozzle at high shear rates.

A monitorized nozzle has been used to register injection moulding parameters of thousands of washing machine tubs. Also sets of patterns of operation parameters have been compared in free of defects parts and failed ones. Short shot defect has been characterizated.

The progressive evolution of parameters from good to failed parts allow to establish knowledge based criteria to predict fails such us short sort.

5 REFERENCES

[1] Lee, B.L., White, J.L. *Trans. Soc. Rheol.*, 18, 467 (1974).

[2] Shertzer, C.R., Metzner, A.B. *Trans. Plast. Inst.*, 31, 148 (1963).

[3] Han, C.D. *J. Appl. Polym. Sci*. 14, 1775 (1970).

[4] Ferry, J.D. *Viscoelastic properties of polymers*, 2nd Ed. New York: Wiley, 1970.

[5] Sekiguchi, M. *Chem. High Polym.*, 26(295), 721 (1969).

[6] Mendelson, R.A., Finger, F.L. *J. Appl. Polm. Sci.*, 17, 797 (1973).

[7] Bagley, E.B., Duffey, H.J. *Trans. Soc. Rheol*., 14, 454 (1970).

[8] Han, C.D. *Rheology in polymer processing*. London: Academia Press, 1976.

[9] Cogswell, F.N. *Polymer melt reology*. London: George Goodwin Limited, 1981.

[10] Mercado, D. *Comparison of different methodologies to determine rheological curves of polypropylene*, Ph.D. thesis. University of Zaragoza, 2003. (In Spanish).

[11] Fernandez, A., et al. Criteria on feeding system design: convencional and sequential injection moulding. *Journal of materials processing technology*, 171 (2006), p. 373-384.

[12] Fernandez, A., et al. Influence of ther recycled material percentage on the rheological behaviour of thermoplastic material in injection moulding process. *Waste Management*, 27 (2007), p. 656-663.

[13] Serraller, F. *Collection and analysis of filling parameters of an spiral mould with ABS to be applied on industrial molded parts*, Ph.D. thesis. University of Zaragoza, 1995. (In Spanish).

[14] Javierre, C., Claveria, I., Ponz, L. Method for generation of rheological model to characterize non-conventional injection molding by means of spiral mould. *Journal of Materials Processing Technology*, 162-163 (2005), p. 477-483.

[15] Javierre, C., Aisa, J., de la Serna, J.A. An example of simulation tools use for large injection moulds desing: The Contenur 2400 l. solid waste container. *Journal of Materials Processing Technology*, 175 (2006), p. 15-19.

Strojniški vestnik - Journal of Mechanical Engineering 54(2008)4, 266-273
UDC 621.9
Paper received: 7.2.2008
Paper accepted: 15.5.2008

The Analysis of Complex Tribological System of Single Point Incremental Sheet Metal Forming - SPIF

Aleš Petek*[,1] - Bojan Podgornik[1] - Karl Kuzman[1] - Miha Čekada[2] -
Wolfgang Waldhauser[3] - Jožef Vižintin[1]
[1]University of Ljubljana, Faculty of Mechanical Engineering, Slovenia
[2]Institute ″Jozef Stefan″, Slovenia
[3]Joanneum Research, Leoben Laser Centre, Austria

In contemporary industrial production the ecological aspects have increasingly important role in selection of sheet metal forming process. To produce sheet metal parts with minimum environmental burdening the shortening of forming processes including the procedures for production of appurtenant forming tools as well as decrease use of lubricant is prerequisite. In general, majority of the sheet metal forming processes demand use of lubricants with oils involving additives, which are hazardous for several reasons. Therefore, the paper is focused towards the analysis of different manners of lubrication (dry contact, liquid lubricant and hard coatings) and to investigate tribological properties during a single point incremental forming (SPIF) technology, which is nowadays very attractive and manly used for small and medium batch production. The first phase of the evaluation was performed on a model test rig by simulating single point incremental forming process, where the coefficient of friction was recorded and compared as a function of lubrication method used. In addition, the paper presents the forming tool temperature measurements for three different manners of lubrication, arising from friction during the single point incremental forming of the pyramid-shaped part.

Keywords: incremental sheet metal forming, friction, DLC coatings

0 INTRODUCTION

The modern industrial praxis is oriented towards the environmental friendly production consisting of low lubricant use, optimum set-up of forming operations as well as development of new innovative forming processes. One of the most attractive forming processes at the moment applied for small batch production and prototype production of very complex components and parts is single point incremental sheet metal forming. The technology is very flexible, has ability to quickly response to part geometry modifications with minimum expense and on the other hand requires essential longer forming time per part in comparison to conventional forming processes, like deep drawing, bulging, etc. [1] and [2]. Some products performed with SPIF are presented in Figure 1. However, majority sheet metal forming operations require by more pretending forming operations the use of lubricants involving additives, like phosphorus, sulphur, zinc, etc., which are unsafe for several reasons. In order to avoid any unsafe influences the special airing systems, electrostatic filters and protective clothes are needed. Beside all, the intensive application of lubricants and use of inappropriate ones demand cleaning of the workpieces after forming and before their assembly into the final product or before additional procedures of surface treatment (colouring, galvanizing, welding, etc.). Generally, the cleaning costs may reach up to 10 % of product price [3].

All above mentioned are the reasons why the liquid lubricants in forming operations have to be minimized or even replaced with thin hard

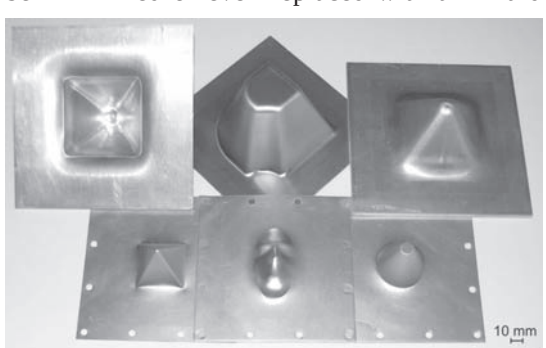

Fig. 1. *Products performed with SPIF*

*Corr. Author's Address: University of Ljubljana, Faculty of Mechanical Engineering, Aškerčeva 6, SI-1000 Ljubljana, Slovenia, ales.petek@fs.uni-lj.si

coatings. In the production companies the hard coatings (like TiN, TiCN, TiAlN, CrN, etc.) are frequently used at least twenty years to protect and enhance the lifetimes of tools by dry machining in metal cutting applications. In contrast to cutting tools, the majority of forming tools is still uncoated. This is due to the large size and complex shape of most conventional forming tools, which makes it difficult to apply a coating and to obtain good adhesion between the coating and the substrate material [4]. Furthermore, in the case that coating fails on the forming tool because of poor adhesion, coating fragments could become a source of abrasive particles within the system. This could lead to poor surface quality of the product and even to the destruction of a very expensive tool. There are also many other reasons why the hard coatings are not frequently used in forming applications. One of the most important is the relatively high coefficient of friction generated by most of the commercial ceramic coatings [5], which leads to a high temperature between the tool and the workpiece and consequently to a sticking of the formed material on the forming tool surface. However, in recent years remarkable progress has been done in the field of hard coatings deposition as well as on the development of coatings on the basis of hard carbon (e.g. diamond like carbon - DLC). These coatings with the major portion of the graphite bonds have in contrast to conventional bonds excellent frictional properties whereat they are still very hard. Because of low friction coefficient and high hardness the DLC coatings could be one of the most appropriate for the movable machine parts protection and also for the forming operations, especially for the incremental forming where only small hemispherical tool head has to be coated.

However, the aim of this research was to investigate the possibilities of using hard coatings on the forming tool by single point incremental forming technology from the frictional properties and temperature between the workpiece and forming tool point of view.

1 SPIF – PROCES DESCRIPTION

Single point incremental forming, also known as dieless forming, is nowadays well known sheet metal forming method. The sheet metal could be formed to a complicated shape without a dedicated die (Fig. 2).

The rod-shaped forming tool with a smooth hemispherical head is clamped into the spindle of the forming machine. The forming tool is usually made of hard material like cemented carbide. The sheet metal is positioned and clamped with the upper blank holder. It is pressed towards the lower blank holder in which the simple die is placed. The whole support tool is inserted and fixed on the worktable of the forming machine. While the forming tool presses and locally deforms the workpiece directly under the tool head with a very small value of deformation, the blank holder and die remained fixed during the entire forming process. As the forming tool follows the predetermined tool path and gradually forms the workpiece in a series of incremental steps until it reaches the final depth it is also spinning at a certain number of revolutions per minute. The steps and process parameters of single point incremental sheet metal forming are shown in Figure 2.

2 DEPOSITION OF THE USED COATINGS

In this investigation three different coatings (CrN, DLC and TiAlN + DLC) were used. The coatings were prepared by different PVD procedures at JOANNEUM RESEARCH, Leoben Laser Centre and Institute “Jozef Stefan” in Ljubljana, respectively. The investigated coatings were deposited on a hemispherical tool head made from cemented carbide and/or ball bearing steel (100Cr6). Before deposition the coatings were grounded and sputter-cleaned in order to obtain optimum adhesion between coating and substrate. The CrN coating was deposited in a Balzers BAI 730 thermionic arc ion plating apparatus. DC ion etching was performed using Ar ions. During deposition Cr targets were evaporated by electrons

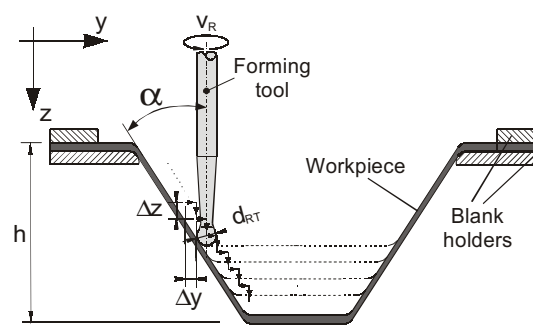

Fig. 2. *Principles and steps of SPIF*

using Ar as the working gas, while N_2 was used as the reactive gas. Other deposition parameters are: base pressure below 2 mPa, working gas pressure 200 mPa, deposition temperature 450 °C and film thickness 3 µm. The CrN coating was chosen for its antiadhesive properties.

The DLC coatings were prepared in a semiindustrial apparatus. The ion etching was performed by the anode layer source using Ar ions. The films were deposited by pulsed laser deposition using four Nd:YAG lasers ablating the carbon targets. As source for hydrogen and nitrogen, C_2H_2 and N_2 were used, respectively. The deposition temperature was below 100 °C. The film thickness was around 1 µm. For this purpose a multilayer coating was deposited, which was achieved by introducing the reactive gases. The structure was a-C / a-C:N. In this case the individual layers have a different ratio of sp3 bonds, hardness and toughness. In this way the multilayer structure was high sp3/ low sp3/ high sp3/ low sp3 etc.

In order to obtain optimum adhesion a composite coating (a hard base coating - TiAlN and a relatively soft topcoat – multilayer DLC) was prepared. However, prior to the DLC coating deposition a TiAlN intermediate layer was deposited. The TiAlN coating was deposited by sputtering in a commercial CemeCon CC 800 apparatus, which is equipped by four unbalanced magnetron sources, while the substrates are mounted on planetary holders. Ion etching is performed in RF mode using Ar ions. For deposition, N_2 is used as reactive gas and a mixture of Ar+Kr as working gas, yielding a film thickness of about 3 µm. The working pressure was around 700 mPa, while the base pressure was below 2 mPa. The deposition temperature is around 450 °C. The TiAlN coating was chosen as being a proven protective coating with high hardness (3500 HV).

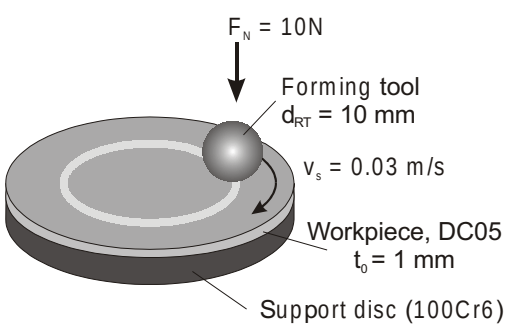

Fig. 3. *Pin-on-disc test*

After TiAlN intermediate layer the DLC coating was deposited in the same way described in previous paragraph.

3 EXPERIMENTAL WORK AND RESULTS

3.1 Tribological Test

Since the friction coefficient can not be measured during single point incremental forming the tribological tests were performed on a pin-on-disc test machine, which presents in the initial testing stage the most reliable method to describe the actual conditions during SPIF. It is worth pointing out that in case of pin-on-disc test the tool contacts the workpiece over the same rounded loop repeatedly whereas in case of SPIF the forming tool never exactly touches the same workpiece area.

However, tribological tests were carried out under dry and oil lubricated sliding conditions. The upper specimens were the forming tools with the diameter of 10 mm made of cemented carbide and coated 10 mm bearing steel balls, respectively. Bearing steel balls (100Cr6) were included in the investigation in order to investigate the possibility of replacing cemented carbide with cheaper substrate. Coated and uncoated forming tools were loaded against rotating 1 mm thick steel sheet plates made from cold-rolled DC05 steel mounted on a hardened 100Cr6 discs, used as a load support (Fig. 3). The normal load applied was 10 N, which corresponds to a maximum Hertzian contact pressure of 1 GPa and sliding speed set to 0.03 m/s. Sixty minute tests corresponding to a total sliding distance of ~100 m were performed at a relative humidity of 50% and a room temperature of 20°C. Oil lubricated tests for uncoated cemented carbide forming tools serving as a reference point were performed with a standard forming oil SYLAC80-05, which does not contain chlorine and steel plate being submerged in lubricant. Prior to testing all test samples were ultrasonically cleaned in ethanol.

During testing coefficient of friction was monitored continuously as a function of time, while contact surfaces were analyzed after the test by means of Optical Microscopy (OM) and Scanning Electron Microscopy (SEM).

Figure 4 shows coefficient of friction curves for different coatings tested on Pin-Disc machine against DC05 steel plates. In the case of cemented carbide forming tool - pin, which was used as a

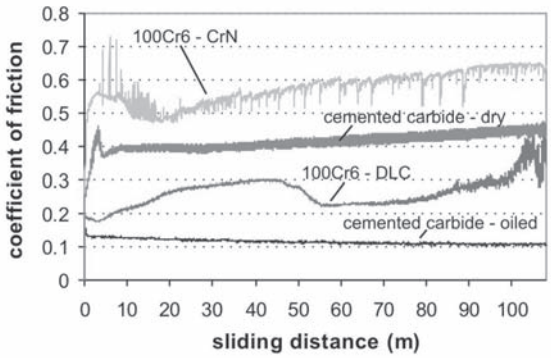

Fig. 4. *Coefficient of friction curves for cemented carbide forming tools and 100Cr6 coated balls*

reference material, coefficient of friction reached steady-state values of about 0.1 if running with forming oil and between 0.4 and 0.45 when running dry (Fig. 4). Relatively high friction under dry sliding conditions indicates adhesion of DC05 steel to the cemented carbide forming tool surface.

CrN coating deposited on bearing steel ball and tested dry showed even higher initial friction of over 0.5, which dropped during first 20 m of sliding as contact surfaces accommodate to each other and smoothening takes place. However, as sliding proceeds coefficient of friction starts to increase and after 100 m of sliding reaches values of about 0.65. Steady friction increase and its abruptions indicate adhesion of DC05 steel to the CrN surface (Fig. 5), followed by adhered material removal. As sliding proceeds contact temperature will increase, thus intensifying the process of DC05 steel adhesion and friction increase (Fig. 4).

On the other hand, DLC coating deposited on the 100Cr6 balls showed low initial friction against DC05 steel even under dry sliding conditions, with the coefficient of friction being in the range of 0.15 to 0.18. As shown in Figure 6 no adhesion of the DC05 steel could be detected in the early stages of sliding. However, as sliding proceeds DLC coating gets removed, either by spallation or wear causing adhesion of DC05 steel to the steel substrate (Fig. 6) and friction increase (Fig. 4).

When deposited on cemented carbide forming tools DLC coatings showed immediate failure, as indicated by high friction recorded at the very beginning of sliding (Fig. 7), and

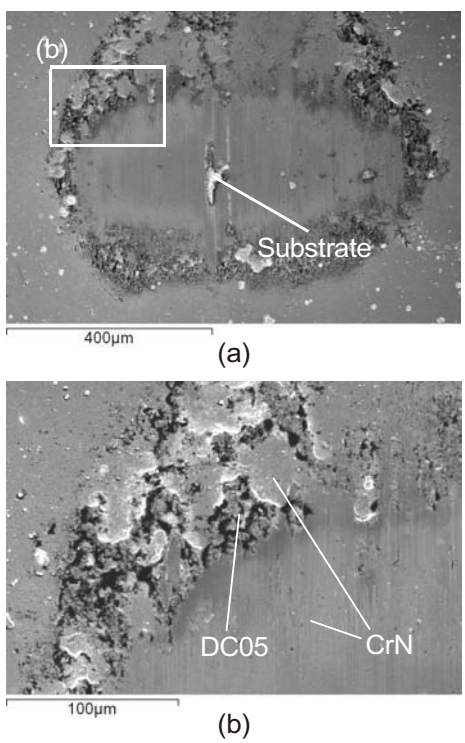

Fig. 5. *SEM micrograph of CrN coated ball tested against DC05 steel after 100m of sliding*

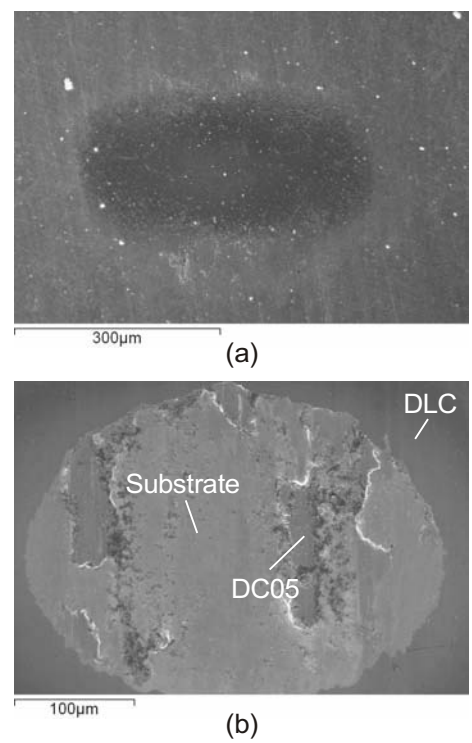

Fig. 6. *SEM micrographs of DLC coated 100Cr6 ball tested against DC05 steel after (a) 10 m of sliding and (b) 100 m of sliding*

confirmed by surface analysis. Further sliding showed similar friction as recorded for uncoated cemented carbide forming tools, indicating adhesion or transfer of DC05 steel material to the cemented carbide substrate. Surface analysis confirmed DLC coating spallation, which is probably caused by unsuitable coating adhesion to the cemented carbide substrate, followed by transfer of steel sheet material to the cemented carbide substrate.

Use of TiAlN support layer considerably improved tribological behaviour of DLC coating when deposited on cemented carbide forming tools, with the DLC coating preventing DC05 steel material transfer for about 20 m of sliding (Fig. 7). However, even with the TiAlN support layer DLC coating eventually failed, leading to cemented carbide/steel contact conditions and material transfer, as shown in Figure 8.

3.2 The Temperature Measurements

The increase of the forming tool temperature usually has a positive influence on the formability but sometimes when the temperature is too high it could cause the sticking of the workpiece material on the forming tool, what leads to the fracture of the workpiece. Beside this, high temperature could also have negative influence on some hard tool coatings. For example, in the case of the tools coated with DLC coating high temperature causes coating spallation because of its poor thermal stability, which beside high internal stresses is one of the greatest weaknesses of the DLC coatings. All above mentioned is the reason why the temperature between the forming tool and workpiece material play so important role in order to assure perfection of the single point incremental formed parts.

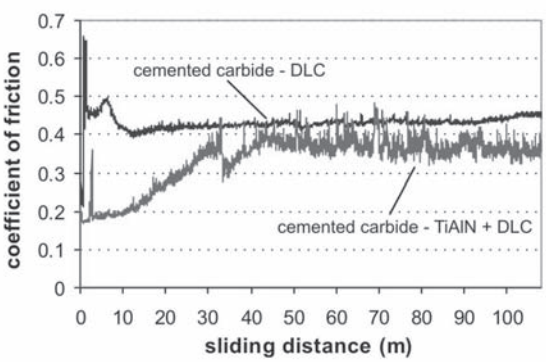

Fig. 7. *Coefficient of friction curves for DLC coatings when deposited on cemented carbide pins*

In order to define real forming tool temperature arising from friction between forming tool and workpiece during SPIF the production of pyramid-shaped part was used as a case study (Fig. 9).

The SPIF experiments were carried out on the CNC milling machine Mori Seiki with the FANUC MSC-521 control system. Due to its frequent use in sheet metal forming production, the same material (DC05) selected for tribological tests was used. Material properties for cold-rolled DC05 steel were obtained by a uniaxial tensile test and are shown in Table 1.

Table 2 shows the selected process parameters for SPIF, which are based on preliminary tests [6].

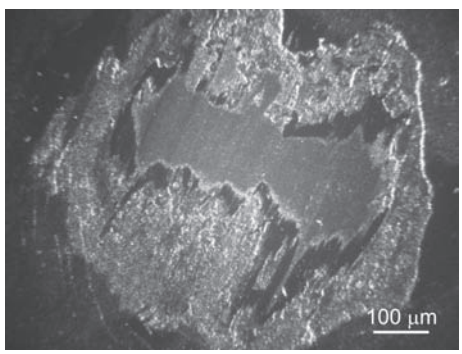

Fig. 8. *OM micrograph of TiAlN+DLC coated cemented carbide forming tool after 100 m of sliding against DC05 steel*

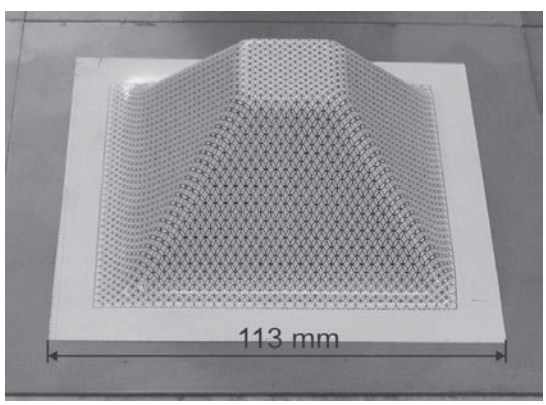

Fig. 9. *Pyramid-shaped part used as a case study and its approximate dimension*

Table 1. *Material properties of DC05 steel*

C = 531.5	strength coefficient [MPa]
n = 0.23	strain hardening exponent
r_0 = 1.59	material anisotropy
r_{45} = 1.06	
r_{90} = 1.76	
E = 210	Young's modulus of elasticity [GPa]
ρ = 7850	density [kg/m^3]
ν = 0.3	Poisson's ratio
t_0 = 1	initial specimen thickness [mm]

Table 2. *Applied SPIF process parameters*

Wall angle α	60°
Forming depth h	38 mm
Rotation speed v_R	60 r.p.m.
Punch diameter d_{RT}	10 mm
Tool path	by steps - CCW
Feed rate f	1700 mm/min
Vertical step size Δz	0.5 mm
Lubricant	SYLAC80-05

The contact temperature was measured on the forming tool for three different contact conditions: liquid lubricant, dry contact and hard coating, respectively. The results of the contact temperature were obtained using special IR thermography camera ThermaCAM™ S60 with the accuracy of ± 2°C [7].

In the first case the workpiece surface was oiled and the contact temperature was measured at the end of the uncoated cemented carbide forming tool rotating in natural direction (NTR). The results in (Fig. 10) show slight increase of the temperature during whole forming process. At the end of the process the maximum temperature of 48.7°C could be observed. In case of additional forming procedure the essential increase of tool temperature could not be expected because of the oil presence.

In the second case TiAlN+DLC coated cemented carbide forming tools rotating in natural direction was analyzed. The TiAlN+DLC coating was selected because it shows the best results by tribological tests. However, the temperature measurement results of such coating system shows similar trend of the temperature curve like the curve obtained by liquid lubrication system, whereas the former lies a little higher (Fig. 10). The reasons could be found in higher friction coefficient (Fig. 7), the absence of cooling/oiling system and very unsuitable coating adhesion and coating spallation in the contact zone during SPIF as presented in Figure 11. Similar results were obtained also by the tribological test (Fig. 8).

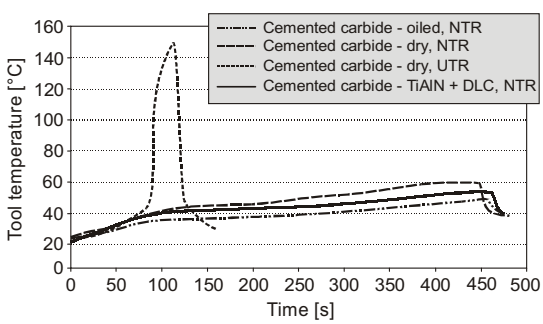

Fig. 10. *The tool temperature in dependence of time during SPIF by various lubrication methods*

When dry contact is taken into account two various tests involving different cemented carbide forming tool rotation strategy were analyzed. Two reasons for concern over the tool rotation strategy, relative to the tool motion, are the heating that occurs and consequentially the quality of the SPIF formed product [6]. The most obvious origin of heating due to the tool rotation strategy are sliding and rolling friction. As the tool travels over the workpiece surface it could rotates in natural or unnatural directions relative to the tool motion. In the case of natural tool rotation (NTR) with the optimum rotation speed relative to the feed rate according to preliminary tests [6] the tool rolls over the workpiece surface during whole forming process. Therefore, excessive heating could not be observed. The results of the thermography analysis during whole SPIF process is evident from the diagram in the Figure 10, whereas the temperature distribution of dry contact between the cemented carbide forming tool and workpiece rotating in NTR after the forming time of 6 min presents Figure 12.

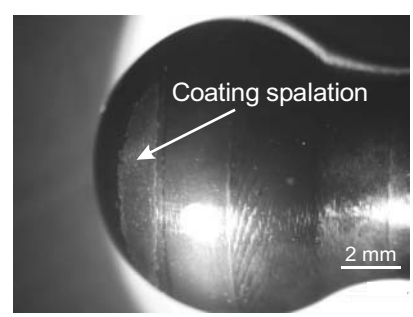

Fig. 11. *OM micrograph of TiAlN+DLC coated cemented carbide forming tool already after first SPIF formed part*

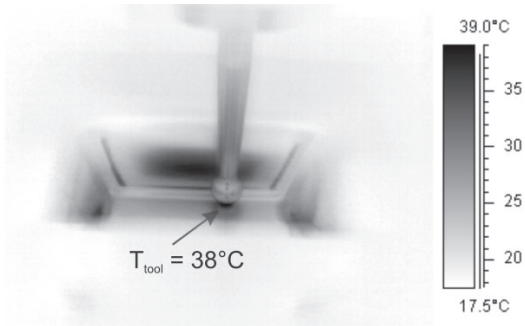

Fig. 12. *The temperature distribution of dry contact, NTR, forming time 382s*

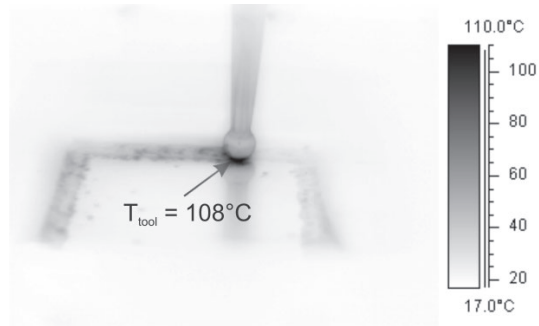

Fig. 14. *The temperature distribution of dry contact, UTR, forming time 117s*

In contrast to NTR the forming tool in the case of unnatural tool rotation (UTR) slides along the workpiece surface, kneading the base material (Fig. 13b), whereat extreme heating due to the large value of sliding friction could be observed. After a few number of revolutions the temperature reaches an extremely higher value (T_{max} = 150°C) than in the other three cases (Fig. 10). Beside this, the sticking of the workpiece material on the forming tool appears (Fig. 13b), while in the case of NTR no base material sticking and excellent surface quality could be observed (Fig.13a).

The temperature distribution of dry contact condition using UTR after the forming time of 117 secs. presents Figure 14.

4 CONCLUSIONS

In the case of incremental sheet metal forming with a hemispherical rigid tool the coating ability to prevent the adhesion of the workpiece is as important as its wear resistance, because of the long forming tool path in order to achieved final product. Usually, the coatings with high wear resistance have besides high friction coefficient also high tendency to sticking of formed material what does not represent the best solution for improving tool lubrication properties by SPIF. Furthermore, the poor adhesion of the coating may lead to the coating crumbling and consequently to the forming tool damaging. On the other hand the coatings with low friction coefficient and anti sticking condition do not reach high wear resistance.

However, from the investigation could be concluded, that CrN coating shows good load-carrying capacity when tested against DC05 steel, while high friction and high tendency for the DC05 steel to adhere to CrN surface does not make CrN coating a good candidate for dry forming of used steel. On the other hand, DLC coating shows low friction against DC05 steel even under dry sliding conditions, but adhesion is relatively poor. Using multilayer DLC coating with TiAlN support layer the adhesion and the tribological properties of DLC coating can be improved, but the adhesion is still not good enough because of long forming tool path in order to achieved final product. Furthermore, the thermography analyses shows that the low temperature appeared by the hard coating system does not have influence on the adhesion of the DLC coating. It has been found that is the tool temperature directly connected with the friction condition for particular SPIF parameters used. The increase in the tool temperature appears with the increase in the friction coefficient.

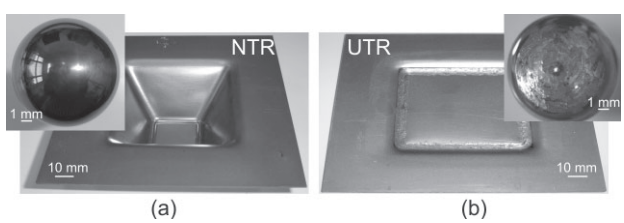

Fig. 13. *The uncoated cemented carbide forming tools and workpieces after SPIF: (a) natural tool rotation – NTR and (b) unnatural tool rotation - UTR*

However, if appropriate adhesion between the forming tool and coatings could be achieved the coatings on the basis of carbon (DLC) seem to be the best solution for improving the tribological properties by incremental sheet metal forming processes, because they may restrict or even eliminate the usage of commonly used lubricating oils, which for great pretending forming operations usually involve unhealthy additives.

In the future the investigations will be oriented to improve DLCs long-term stability for SPIF contact condition, either by increasing its load-carrying capacity, improving its adhesion, making it thicker or changing the substrate material.

5 REFERENCES

[1] Petek, A., Gantar, G., Pepelnjak, T., Kuzman, K. Economical and ecological aspects of single point incremental forming versus deep drawing technology. *Key Engineering Materials*, vol. 344 (2007), p. 931-938.

[2] Allwood, J.M., Utsunomiya, H. A survey of flexible forming processes in Japan. *International Journal of Machine Tools & Manufacture*, 46 (2006), p. 1939-1960.

[3] Panjan, P., Čekada, M. *Tools protection using hard PVD coatings*. Ljubljana: Inštitut Jožef Štefan, 2005, ISBN 961-6303-73-2. (in Slovenian).

[4] Podgornik, B., Hogmark, S., Sandberg, O. Wear and friction properties of hard coatings for forming tools. *Journal of Mechanical Engineering*, vol. 50, no.3 (2004), p. 146-156.

[5] Bhushan, B. *Modern tribology handbook*. NY: CRC Press, 2000.

[6] Petek, A., Kuzman, K., Kopač, J. Forces and deformations analysis of incremental sheet metal forming. *CAM3S*, 2005, paper 1.85.

[7] Golobič, I., Bašelj, M., Papež, A., Petkovšek, J., Kenning, D.B.R. Bubble coalescence in pool boiling on a thin foil investigated by high-speed IR thermography. *13th International Heat Transfer Conference*, Sydney, Australia, 13-18 August, 2006.

Strojniški vestnik - Journal of Mechanical Engineering 54(2008)4, 274-279
UDC 621.73
Paper received: 16.11.2007
Paper accepted: 15.5.2008

Experimental and Numerical Analysis of Side Forces in a Forging Die

Andrzej Kocańda* - Piotr Czyżewski
Warsaw University of Technology, Faculty of Production Engineering, Poland

Though hot forging dies are subject mostly to forces acting in the direction of moving tool/slider, some side forces are also developed in the die cavity according to the flow of material in various directions. These forces would be relatively high especially in the cases of non-axisymmetrical or extended forgings what could result in an offset of upper and lower dies causing geometrical inaccuracy of the forging. This paper presents two ways of determining side forces by means of numerical and physical modeling. Two industrial forging processes for the bracket lever and the valve lever were chosen for the analysis. As the result, values and directions of side forces from the beginning up to the end of deformation stage were obtained. Hence some changes in die design or process stages which would minimize the influence of side forces on geometrical inaccuracy of forgings could be introduced. As an example, some ways to minimize the side forces by changing the inclination of parting surface (bracket lever forging) or changing the positioning of perform (valve lever forging) were shown.

Keywords: forging, forging dies, geometrical inaccuracies, numerical modeling, physical modeling

0 INTRODUCTION

Hot forging has been regarded as one of the main processing techniques due to high productivity and possibility of getting high deformation combined with very good mechanical properties of products. However, a competition from the other techniques has been quite severe and new developments in hot forging are still very crucial. In spite of organizational changes and automatization of processes, further developments in hot forging have been connected mainly with an increase of geometrical accuracy of forgings and with approaching at least a near-net shape in the as-forged condition [1] to [4]. The savings obtained by the reduction of machining allowances and machining operations can be quite substantial. What more, mechanical properties of a precision forging are usually superior to those of a forging subjected to extensive machining. This is because the forged microstructure is preserved intact in the precision forging and the fibre orientation is not disrupted.

Geometrical inaccuracies of forging may be affected by the design of the as-forged product, the process planning and practice of the operational sequence, the properties of the stock material and billet, the lubricant and control of lubrication, the tool and machine, precision of the set-up, control of working temperature, the finish machining and heat treatment. Precision forging is the closed die or fleshless forging. Relatively high geometrical accuracy of forgings could be obtained also by means of hot forging with a flesh. However, it requires an optimization of tool design and tool loading. In this paper some tooling design considerations will be taken into account in order to minimize side movement of the different parts of die and hence to minimize geometrical inaccuracy of forging.

Fast development of computer methods and computer software has been very important in realistic modelling of forging processes. Many features of the forging process have already been covered. There are still some of them, such as inter-stage heat treatment or post-process thermal behaviour, which have received little attention [5]. However, detailed modelling of the forging process sequences and deformation conditions would provide a possibility to control heat exchange and changes in mechanical and physical properties of deformed material as well as to control exactly a flow of metal and tool loading conditions. This leads, for example, to exact determination of deformation force components including side (or

*Corr. Author's Address: Warsaw University of Technology, Faculty of Production Engineering, Department of Metal Forming, Narbutta 85, 02-524 Warsaw, Poland, akocanda@wip.pw.edu.pl

lateral) forces in the forging die [6] and [7]. Side forces are relatively high in production of non-axisymmetrical or extended forgings what results in an offset of the upper and lower dies. This offset introduces geometrical inaccuracies into forgings or increased wear of some parts of die cavity.

There are many well known ways to prevent sideways movement of the different parts of die caused by side components of force [8] and [9]:

- If possible, the parting line should be in the same plane as the forging plane, at a right angle to the direction of deformation; this simple way works well mainly for axisymmetrical impressions.
- The impression must be cut in the die block in such a way that the parting line takes into account local differences in slope angle to the forging plane in order to compensate side component of force.
- Forging of components in pairs in order to achieve symmetry.
- Side lock – step to counterbalance side forces.
- Guiding of forging dies, common in close-die forging, with cylindrical guideways, guide pins and lateral or corner guides.

Most of the above mentioned methods complicate the design of forging tools and increase cost of the tools. For that reason application of any method must be carefully considered. So far, special experience and know-how have usually been crucial for such a tool designing. Generally, determination of directions and values of the side forces would be very helpful in the design procedure. This paper presents two ways of determining side forces by means of numerical and physical modeling. Two industrial forging processes for the bracket lever and the valve lever were chosen for the analysis.

1 FORGING OF BRACKET LEVER

1.1 Numerical Modeling

MSC/SuperForge software based on finite volume method has been used in numerical modeling of the processes. Geometrical models were prepared by means of Solid Works software. The dies were assumed as stiff bodies. Combined thermo-mechanical numerical analysis has taken into account all stages and blows of the forging processes. Geometrical changes, residual stress and temperature fields have been imported for all subsequent stages.

The forging of the bracket lever, shown in Figure 1, was performed on a crank forging press. The lever was made of medium carbon dispersion hardening ferritic-pearlitic steel. In industrial practice, this bracket has been forged in several steps from a round bar of 20 mm in diameter.

In this paper, only the operation in the final impression has been examined. The inclination α of parting surface of lower and upper dies corresponding to 0, 10, 20, 30 an 40 degrees was a variable for the analysis of forging in the final impression (Fig. 2). Initial temperature of the workpiece was 1100 °C and the dies were preheated to 300 °C. Friction conditions were defined by Coulomb's law with friction coefficient 0.1.

A change in the inclination α of the main part of parting surface from 0 to 40 degrees resulted in changes in the maximum side force X (direction x – Fig.2) as shown in Figure 3. Calculated force components were presented as relative values, i.e. the maximum values of side force X and forging force Z found for the inclination α=20 degrees were assumed as 100%. It should be pointed out that the

Fig. 1. *Bracket lever*

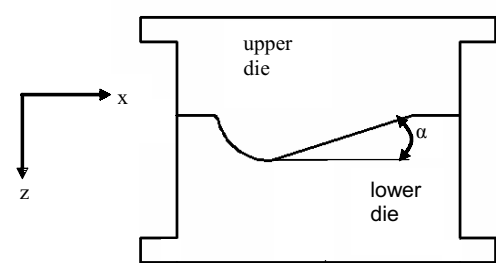

Fig. 2. *Schematic presentation of bracket lever forging dies; α - the inclination of parting surface*

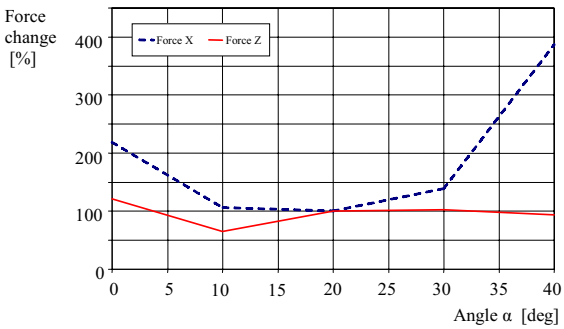

Fig. 3. *Influence of parting surface inclination on changes (%) in maximum values of side X and vertical Z forces (forging of bracket lever)*

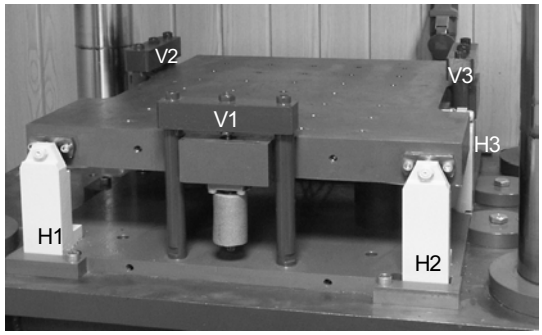

Fig. 4. *6-axis force transducer with vertical and horizontal supporting elements*

smallest side force X has been just for this angle. Values of the angle α lower or higher than 20 degrees caused considerable increase of X. On the other hand, the forging force Z was the smallest for α=10 degrees. Generally, the values of side force X were equal to about 10% of the values of forging force Z. These calculated data open the possibility to design tools in a proper way. For example, if a side force X should be as small as possible then the inclination of parting surface would be about 20 degrees. If both forces X and Z should be as small as possible than α=10 degrees would be the best solution.

1.2 Physical Modeling

It has been essential to validate the results of numerical simulations and to get greater confidence in the application of side forces analysis.

As for hot forging, physical modeling has been a valuable alternative to numerical modeling [10] to [14]. Physical modeling based on wax is faster, easier and less expensive than a subscale production process. To take all the advantages of using physical modeling, the modeling press and 6-axis force transducer have been used. The modeling press is very stiff in both lateral and angular directions. Its elastic deflections do not influence the material flow. The 6-axis force transducer consists of the upper and lower plates (Fig. 4). The transducer is mounted to the base plate of the press and the modeling tool is located on the upper plate of transducer (Fig. 5). The upper plate of the transducer is supported vertically by three carrying elements V1, V2, V3 and the other three elements support the plate horizontally – H1, H2, H3. Hence, the vertical force Z loads mainly the vertical carrying elements whereas the side forces X and Y

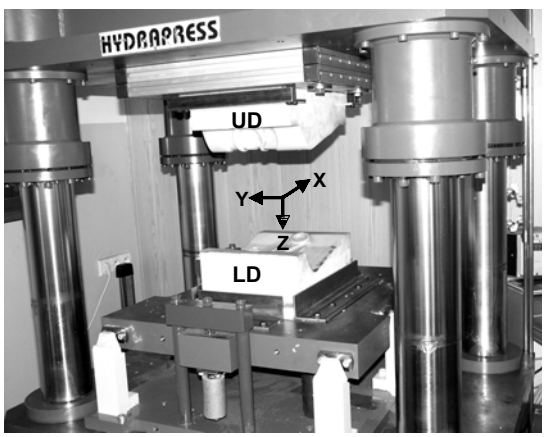

Fig. 5. *Upper die (UD) and lower die (LD) arrangements on the modeling press*

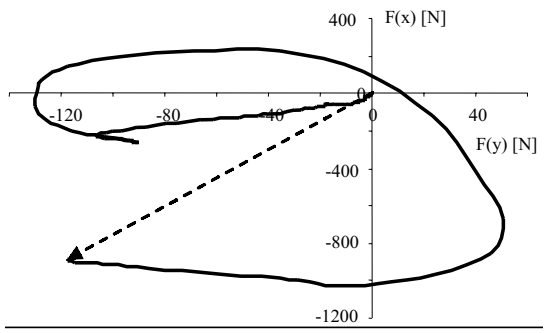

Fig.6. *History of changes in side forces X and Y as a result of physical modeling; parting surface inclination 20 degrees*

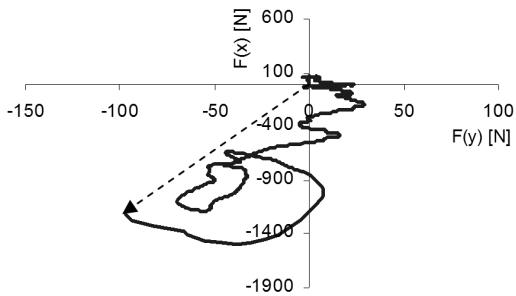

Fig. 7. *History of changes in side forces X and Y as a result of numerical modeling; parting surface inclination 20 degrees, material for physical modeling*

load the horizontal carrying elements. Upper and lower dies for physical modeling of bracket lever forging were made of tool resin. Preforms were made of wax composition for which a shape of stress-strain curve was in a reasonable agreement with the curve for the real material. During deformation of preform between upper and lower dies, vertical Z as well as side X and Y forces were measured. Side force X has been much higher than side force Y.

The history of changes in side forces X and Y is shown in Figure 6. It is presented in a form of changes in resulting side force in order to point out the direction and value of the force from the beginning up to the end of deformation. Broken line shows the resulting side force just at the end of forging. It has changed the direction over 300 degrees during the whole forging process. Hence, the side lock design in the die should counterbalance the side force from different directions. The results shown in Figure 6 were in a quite good agreement with the results of numerical simulation carried out for modeling material (Fig. 7). The direction of the final resulting side force is almost the same as in physical

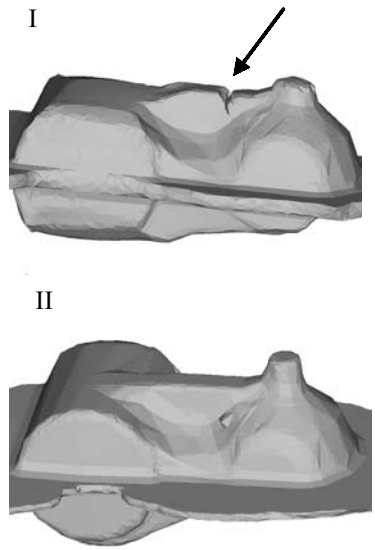

Fig. 9. *A forging with overlapping (case I) and a forging without any defect (case II)*

modeling. There are some differences between these two curves in the initial stage of deformation when the forces are relatively small. It could be caused by slight differences in placement of preforms and friction conditions.

2 FORGING OF VALVE LEVER

Forging process of valve lever was analysed by means of results of numerical modeling. The process was performed on a forging hammer. Initial temperature of preform was 1100 °C and the dies were preheated to 250 °C.

The upper and the lower dies were designed as to have fuller, blocker and finisher impressions (Fig.8). The full process consisted of the following stages:

- Initial upsetting (1 blow),
- Fullering (2 blows),

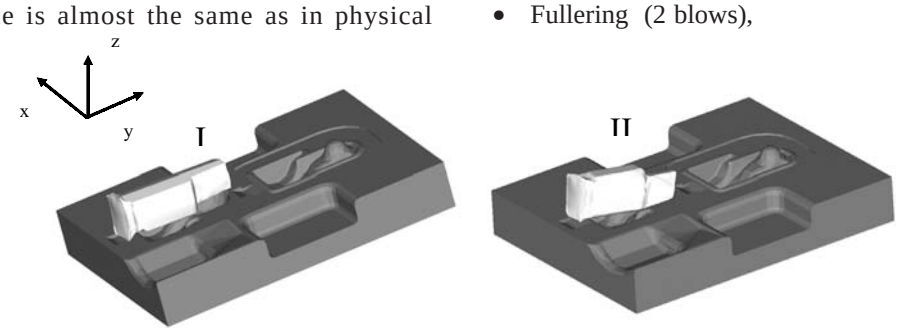

Fig. 8. *Pre-forms placed in the blocker impressions of the lower dies for forging of valve levers (case I and II)*

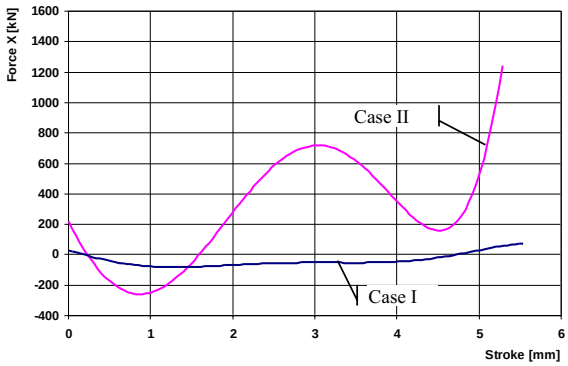

Fig.10. *Changes of the lateral force in X direction for two cases of preform orientation*

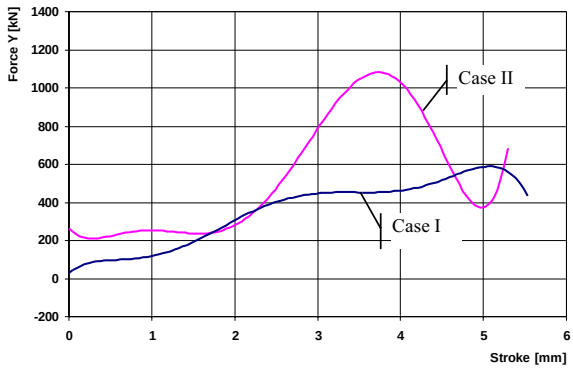

Fig.11. *Changes of the lateral force in Y direction for two cases of preform orientation*

- 90^0 counter-clockwise (case I) or clockwise (case II) rotation of preform and additional fullering (2 blows),
- Forging in the blocker impression to get the general final shape (3 blows),
- Forging in finisher impression to get the final overall shape (1 blow).

As an example, forging in the blocker impression has been chosen for analysis [7]. As in the case of bracket lever modeling, all of the previous stages and number of blows were taken into account during numerical simulation. Geometrical changes and temperature fields have been imported for all subsequent stages. The forging obtained after deformation of preform characterized by case I showed a forging defect in the form of overlapping (Fig. 9). As for the case II, the forging did not show any defect. Figures 10 and 11 present changes in lateral forces X and Y as a function of upper die stroke (third blow). The lateral forces have been much smaller for the case I than for the case II. It means that the necessity to change the preform positioning for getting the forging without overlapping lead to a considerable increase in values of lateral forces (case II). What more, the directions of the highest resulting side forces were different during the course of the process as shown in Figure 12 for the finisher impression (case II). It means that the guiding of the upper and lower dies is necessary in the analysed forging process for getting a high geometrical accuracy of forgings.

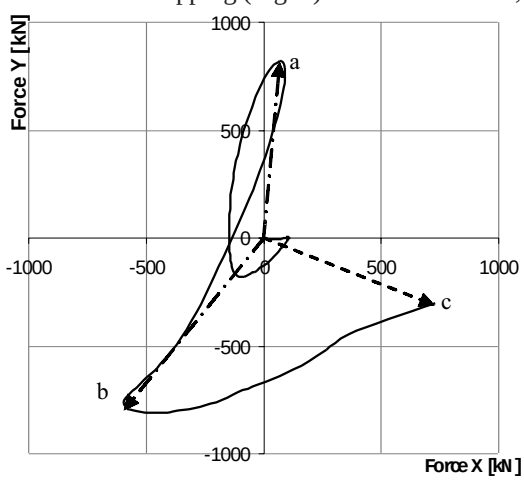

Fig.12. *History of changes in side forces X and Y in finisher impression of die (case II); a,b,c – high values of the resultant side forces at different stages of the forging process*

3 CONCLUSIONS

- There are many ways to prevent sideways movement of upper and lower dies caused by side forces. Choice of the way would be supported by the results of numerical modeling.
- Numerical modeling of the bracket lever forging for various inclinations of the parting surface has been helpful in minimizing the lateral force. The lowest values of lateral force and forging forces have been found for the inclination angle of about 10 degrees.
- The results of bracket lever numerical modeling have been in a good agreement with the results of physical modeling. Hence, a method of numerical modeling with taking into account all stages of forging process and changes in physical and mechanical properties of deformed bodies has been a valuable tool for finding force components, including side ones.

- Necessity to avoid the overlapping defects in valve lever forging resulted in a considerable increase in values of lateral forces.
- The ratio of lateral to vertical forces was up to about 10% in the two forging processes analyzed in this paper.

Acknowledgement

This research work has been financially supported by the Ministry of Science and Higher Education, grant no. 4 T07D 037 29. The authors also wish to thank graduate students M. Andrzejewski, D. Lukasiewicz and R. Warmiak for their assistance in physical modeling.

4 REFERENCES

[1] Kudo, H. Towards net-shape forming. Journal of Materials Processing Technology, vol. 22, no. 3, 1990, p. 307-342.

[2] Douglas, R., Kuhlmann, D. Guidelines for precision hot forging with applications. *Journal of Materials Processing Technology*, vol. 98, no. 2, 2000, p. 182-188.

[3] Balendra, R. Net-shape forming: state of art. *Journal of Materials Processing Technology*, vol. 115, no. 2, 2001, p. 172-179.

[4] Behrens, B.-A., Doege, E., Reinsch, S., Telkamp K., Daehndel H., Specker A. Precision forging process for high-duty automotive components. *Journal of Materials Processing Technology*, vol. 185, 2007, p. 139-146.

[5] Hartley, P., Pillinger, I. Numerical simulation of the forging process. *Computer Methods in Applied Mechanics and Engineering*, vol. 195, no. 48-49, 2006, p. 6676-6690 .

[6] Kocanda, A., Czyzewski, P., Krzyszkowski, P. Some developments in analysis of lateral forces and cyclic loading with relation to forging dies. *Proceedings of the 8th ICTP "Advanced Technology of Plasticity"*, Verona, 2005, p. 171.

[7] Kocanda, A., Czyzewski, P. An influence of some process parameters on lateral forces in forging dies. *Computer Methods in Materials Science*, vol.7, 2007, p. 208-211 .

[8] Wasiunyk, P. *Hot Forging*. WNT, Warszawa, 1975. (in Polish).

[9] Lange, K. *Handbook on metal forming*. McGraw-Hill, 1985.

[10] Wanheim, T., Maegaard, V., Danckert, J. The physical modelling of plastic working processes. *Advanced Technology of Plasticity, Proc. 1st Int. Conf. on Technology of Plasticity*, vol. II, Kyoto, 1984, p. 984-996.

[11] Wanheim, T., Danckert, J. Combined physical and numerical modelling of metal forming processes. *Advanced Technology of Plasticity, Proc. 2nd Int. Conf. on Technology of Plasticity*, vol. II, Stuttgard, 1987, p. 29-36.

[12] *Metals handbook*, 9th Ed., vol. 14, Forming and Forging, ASM Int., 1988.

[13] Hengan, O. *Finite element analysis and experimental investigation of stiffness characteristics of forming presses and forging of turbine aerofoil components.* PhD Thesis, University of Strathclyde, 2001.

[14] Zhan, M., Liu, Y., Yang, H. Physical modeling of the forging of a blade with a damper platform using plasticine. *Journal of Materials Processing Technology*, vol. 117, 2001, p.62-65.

[15] Chodnikiewicz, K., Kocanda, A., Prejs, T. Hydraulic press and force transducer for physical modelling of bulk metal forming. *Proceedings of the "Baltic Sea Metal Forming and Cutting Seminar BAMFAC '98"*, Vilnius, 1998, p. 12-18.

Strojniški vestnik - Journal of Mechanical Engineering 54(2008)4, 280-287
UDC 621.9
Paper received: 7.1.2008
Paper accepted: 15.5.2008

CAM Algorithm as Important Element by Achieving of Good Machined Surface Quality

Janez Kopač* - Primož Kržič
University of Ljubljana, Faculty of Mechanical Engineering, Slovenia

The paper deals with test of four different NC programs created by 4 different CAM algorithms using identical settings. The subsequent experimental verification has resulted in a conclusion that arrangement of the points on the tool path does have influence on the machining time and finish surface quality.

Keywords: CAM systems, toolpath optimization, NC programs, surface quality, machining time

0 INTRODUCTION

CNC toolpaths are based on NC programs which are created using CAM systems. These systems utilize different methods and mathematical algorithms for calculating or optimization of toolpaths, which can givevery different results with the same parameter settings [8] and [9]. In our past work we have noticed that arrangement of the points along the toolpath can have a substantial influence on the machining time and finished surface of the part.

1 EXPERIMENT PREPARATION

With the presented experiment we wanted to prove that the toolpath point arrangement could influence on machining time and a quality of the finished surface. We tested four different toolpaths, which were calculated with four different CAM algorithms using same settings.

The geometry of the part was presented by a half-sphere with a diameter of a 24 mm. On a bottom it transforms to a 3 mm radius (Fig. 1). The stock was a cylinder with a 30 mm diameter. The stock material was AlMgSi0.5.

All the experiments were made on a Sodick MC430L milling machine (Fig. 2 and Table 1).

The test tool had the following features:

- Tool manufacturer and type: OSG WXS-LN-EBD,
- Tool type: ball mill,
- Tool Diameter: 2 mm,
- Tool Radius: 1 mm.

The test toolpath had the following common parameters:

Toolpath strategy: all the tested toolpaths had identical programmed toolpath strategy – cutting the surface with the helical moves from top to bottom (Fig. 3).

Toolpath tolerance: 0.002 mm (Fig. 4)

Feed rate: we tested the toolpaths with two feed

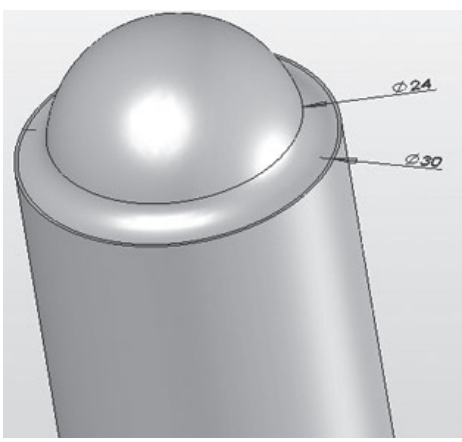

Fig.1. *Part CAD model*

Fig.2. *Sodick MC430L milling machine*

*Corr. Author's Address: University of Ljubljana, Faculty of Mechanical Engineering, Aškerčeva 6, SI-1000 Ljubljana, Slovenia, janez.kopac@fs.uni-lj.si

Table 1. *Machine data*

Working area X × Y × Z	420 mm × 350 mm × 200 mm
Table size X × Y	600 mm × 400 mm
Spindle speed	6,000 – 40,000 min^{-1}
Max acceleration	1.0 G
Fast feed rate	36 m/min
Max tool diameter	Ø6 mm

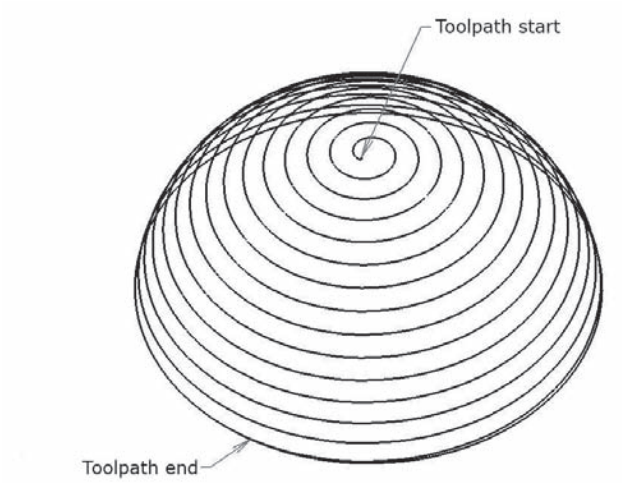

Fig. 3. *Toolpath strategy*

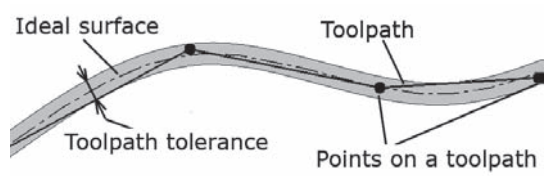

Fig. 4. *Toolpath tolerance*

rates (1,500 mm/min and 4,000 mm/min)
Spindle speed: 28,000 min^{-1}
Cutting depth: Ap = 0.1 mm
Cutting stepover: Ae = 0.008 mm (Figs. 5 and 6)

DIFFERENCES BETWEEN TOOLPATHS

The only attribute by which the toolpaths were distinctly different was the way the points were arranged along the toolpath. Algorithms that are used for toolpath point calculation differ from one CAM program to another. Even though the toolpaths look the same they don't have the same point arrangement along the toolpath. For our test we have used four different toolpaths:

Toolpath 1: Stochastically arranged points

Toolpath 1 had stochastically and unevenly arranged points along the toolpath. Because the calculating algorithm was not optimized the NC

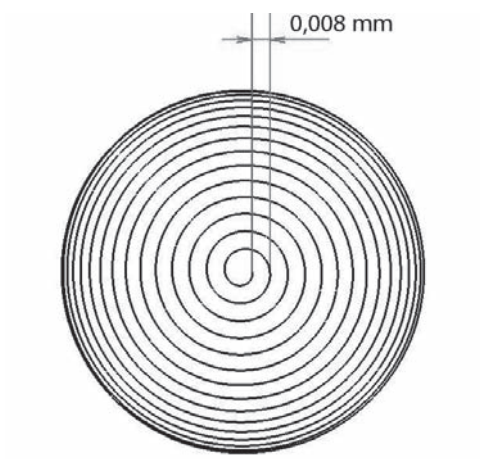

Fig. 5. *Toolpath stepover from top view*

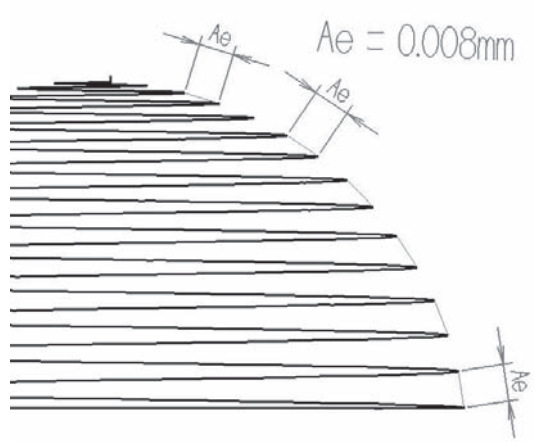

Fig.6. *Toolpath stepover from side view*

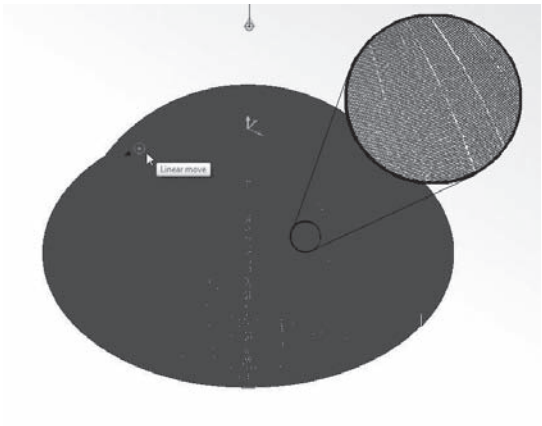

Fig. 7. *NC program simulation of toolpath 1*

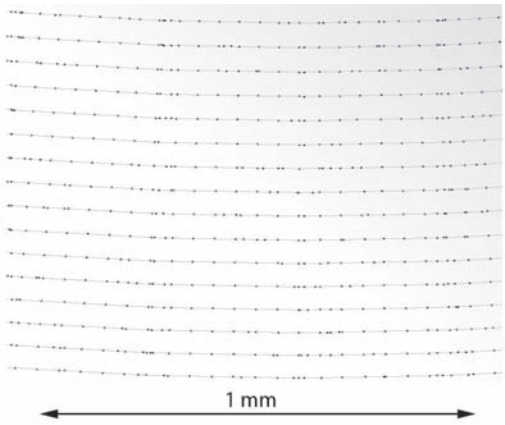

Fig. 8. *Section of toolpath 1*

program consisted of 10-times more points than any other tested toolpath (Fig. 7).

The toolpath section (Fig. 8) demonstrates that the distances between the adjacent toolpath points can vary between 0.002 mm and 0.05 mm.

Fig. 9 shows enlarged section of the toolpath. It can be noticed that there are 5 points on a section, which is only about 0.01 mm long.

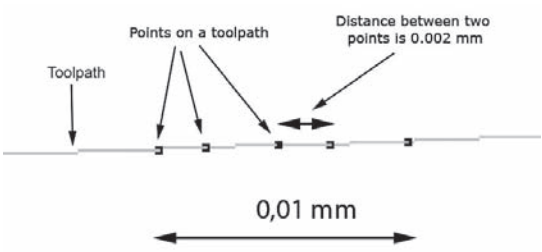

Fig. 9. *Section of the toolpath 1*

Fig. 10. *NC program simulation of toolpath 2*

Toolpath 2: Evenly arranged points that don't show a pattern along Z-axis

This toolpath point's arrangement displays no recognizable pattern along Z-axis (Fig. 10). The distances between the adjacent toolpath points are relatively constant and vary between 0.25 mm and 0.35 mm (Fig. 11). When comparing Figure 10 to Figure 7 it can be clearly noticeable that toolpath 1 has much higher density of points then the toolpath 2.

Toolpath 3: Evenly arranged points that show a distinct pattern along Z-axis

This toolpath consisted of substantially smaller number of points than toolpaths 2 and 4 (see Tables 3, 4 and 5). In this was mainly the result of the CAM algorithm leaving out the points on the lover portions of the test part where the toolpath radius is larger. Some sections of the toolpath had

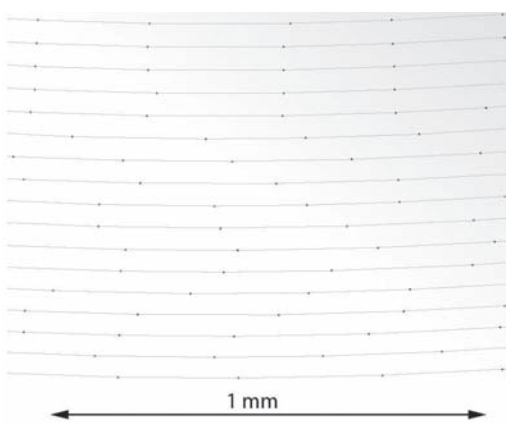

Fig. 11. *Enlarged section of toolpath 2*

Fig. 12. *NC program simulation of toolpath 3*

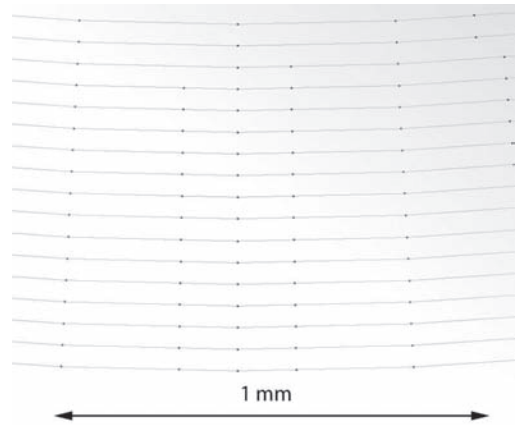

Fig. 13. *Enlarged section of toolpath 3*

smaller distances between adjacent points than other sections (Fig. 13). The toolpath simulation is shown on Figure 12.

Toolpath 4: Evenly arranged points that show a distinct sun-ray pattern along Z-axis

The points are evenly arranged along the toolpath and show a distinct sunray pattern along Z-axis (Figs. 14 and 15). This means that the distance between adjacent points on the toolpath is rising with the toolpath depth and radius of the surface.

3 TEST RESULTS

Each of the test parts has been machined with two programmed feed rates. Machining with the lower feed rate (f = 1500 mm/min) was used to produce finished surface, the higher feed rate was used to test machining time reduction. After running the tests we photographed the test parts under the optical microscope with 30x magnification. Each part was also checked by naked eye and photographed with a digital compact camera.

Toolpath 1

The results of test are summarized in Table 2. The first column represents measured parameters and the second column shows the results. Toolpath 1 machining time at 1,500 mm/min was 10% longer than theoretical machining time. The most probable two reasons for such a delay are the facts that toolpath consists of 10 times more points than other toolpaths and that in some sections we can find up to 5 points in only 0.01 mm length of the toolpath. The machine cannot process so many points with the programmed feed rate, which results in lowering the average feed rate. When we increased the feed rate to 4000 mm/min, the machining time

Fig. 14. *NC program simulation of toolpath 4*

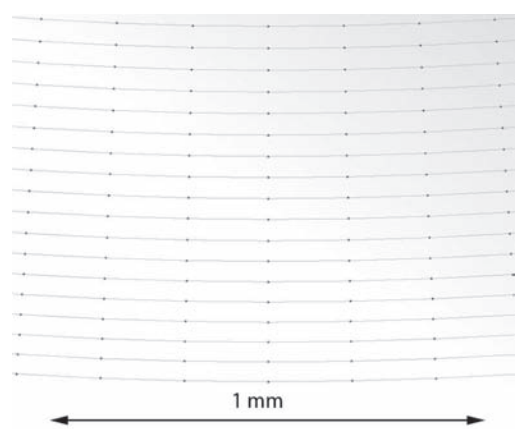

Fig. 15. *Enlarged section of toolpath 4*

Table 2. *Toolpath 1 test results*

Theoretical toolpath time (f = 1,500 mm/min)	571 s
Theoretical toolpath length	13,971 mm
Number of points	433,884
Toolpath density (average number of points on 1mm of toolpath)	31 points/mm
Measured toolpath time (f = 1,500 mm/min)	625 s
Measured toolpath time (f = 4,000 mm/min)	590 s
Minimum feed rate (f = 4,000 mm/min)	1,000 mm/min
Actual calculated feed rate (f = 1,500 mm/min)	1,341 mm/min
Actual calculated feed rate (f = 4,000 mm/min)	1,420 mm/min

decreased for only 6.5%. Minimum detected feed rate of 1000 mm/min at programmed 4000 mm/min shows that the toolpath had certain sections where the machine movement speed had to be largely reduced.

Figure 16 represents some issues regarding tool movement. In some sections of the toolpath the feed rate decreased rapidly which resulted in tool vibration and subsequently in gouges in the surface. Large gouge about 1 mm long and 0.5 mm wide can be seen in the upper left corner of Figure 16. As we can see on Figure 17 the gouges can be seen with naked eye. In the real world such part would be treated as a waste.

The other issue concerns faceted surface on the lover section of the part. The surface texture can be seen in Figure 17.

Toolpath 2

The results of the test are represented in Table 3. Toolpath 2 had 10 times less toolpath points than toolpath 1 even though theoretical machining time and toolpath length was the same as with toolpath 1.

Toolpath 2 machining time was 2.2% longer than theoretical. When we increased the feed rate to 4,000 mm/min, the machining time was shortened by 56%. Average feed rate at programmed 4,000 mm/min was 3,435 mm/min, which shows that the toolpath 2 is much more optimized for high feed rate than toolpath 1 (Table 3). Minimum detected feed rate of 2,500 mm/min at programmed 4,000 mm/min confirms that the toolpath did not have any sections where the machine movement speed had to be largely reduced.

The other reason of round and smooth finished surface was the fact that individual cuts overlay previous cuts and the toolpath did not show a sunray pattern along Z-axis (Figs. 18 and 19). The finished surface was therefore automatically better.

Figure 18 represents the finished surface photographed under the microscope with 30x magnification. Surface had no gouges; all the moves were smooth and did not produce any facets. The same result can also be observed on Figure 19, which shows the naked eye image of the part. Surface quality is very good. No facets or gouges can be seen on the surface.

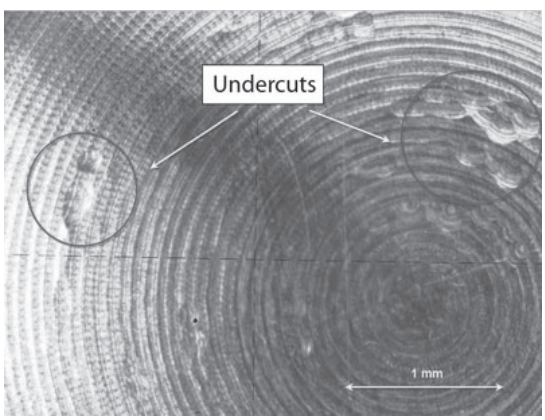

Fig. 16. *Finished part after toolpath1 (enlarged 30-times)*

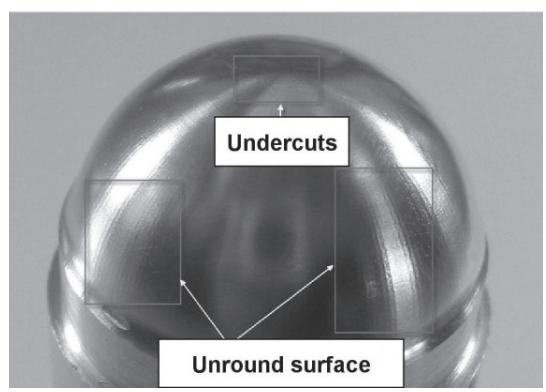

Fig. 17. *Finished part after toolpath1*

Table 3. *Toolpath 2 test results*

Theoretical toolpath time (f = 1,500 mm/min)	571 s
Theoretical toolpath length	13,971 mm
Number of points	47,634
Toolpath density (average number of points on 1mm of toolpath)	3.4 points/mm
Measured toolpath time (f = 1,500 mm/min)	559 s
Measured toolpath time (f = 4,000 mm/min)	244 s
Minimum feed rate (f = 4,000 mm/min)	2,500 mm/min
Actual calculated feed rate (f = 1,500 mm/min)	1,499 mm/min
Actual calculated feed rate (f = 4,000 mm/min)	3,435 mm/min

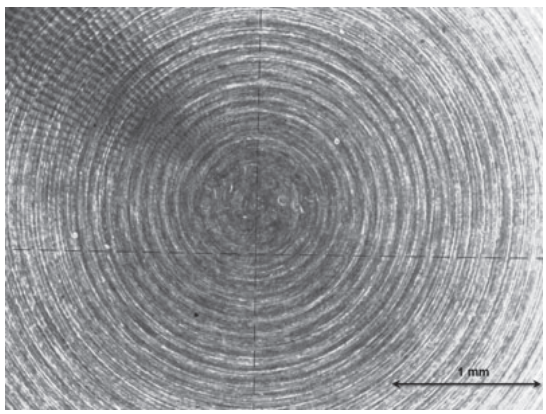

Fig. 18. *Part after toolpath 2 (enlarged 30-times)*

Fig. 19. *Finished part after toolpath2*

Toolpath 3

The results of the test are represented in Table 4. Toolpath 3 had smaller density of points then toolpath 2 but the actual average feed rate was lower than feed rate on toolpath 2. Toolpath 3 machining time was 5% longer than theoretical machining time. Compared to toolpath 2 this toolpath had certain areas where the points were more densely packed than others (Fig.13). When we increased the feed rate to 4,000 mm/min the machining time shortened by 20%. This toolpath had smaller density of points (number of points on 1 mm of toolpath) compared to toolpath 2 but the time gain from increasing the feed rate was smaller.

This shows that the toolpath was not as much optimized for high feed rates as toolpath 2 (Table 4). Minimum detected feed rate of 1000 mm/min at programmed 4000 mm/min shows that the toolpath had certain sections where the machine movement speed had to be largely reduced.

Figures 20 and 21 clearly reveal that the finished surface included facets. They are result of the large distance between adjacent points on the toolpath. On some sections (Fig. 21) they can be as large as 0.6 mm. The influence of large distances between adjacent points could be minimized if the points would not show pattern along Z-axis (like toolpath 2).

Table 4. *Toolpath 3 test results*

Theoretical toolpath time (f = 1,500 mm/min)	393 s
Theoretical toolpath length	9,823 mm
Number of points	27,243
Toolpath density (average number of points on 1mm of toolpath)	2.8 points/mm
Measured toolpath time (f = 1,500 mm/min)	414 s
Measured toolpath time (f = 4,000 mm/min)	330 s
Minimum feed rate (f = 4,000 mm/min)	1,000 mm/min
Actual calculated feed rate (f = 1,500 mm/min)	1,423 mm/min
Actual calculated feed rate (f = 4,000 mm/min)	1,786 mm/min

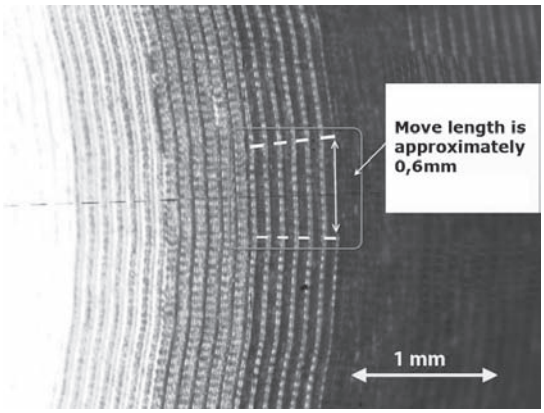

Fig. 20. *Part after toolpath 3 (enlarged 30-times)*

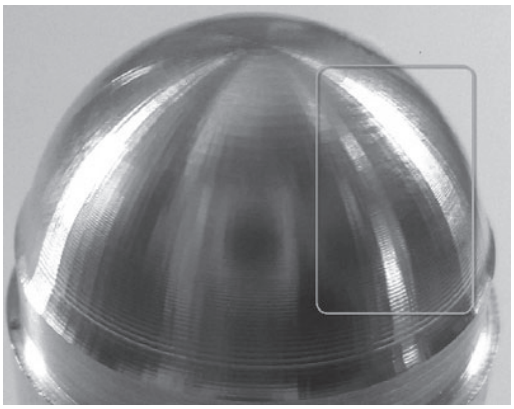

Fig. 21. *Finished part after toolpath3*

The facets are clearly seen even with naked eye (Fig. 21). In real world such part would most probably be considered as scrap part.

Toolpath 4

The results of the test are summarized in Table 5. Even though the toolpath density was higher than the toolpath density of toolpaths 2 and 3 the machining time was only 2% longer than theoretical machining time. When we increased the feed rate to 4,000 mm/min, the machining time was decreased by 60%. Minimum detected feed rate of 2,000 mm/min at programmed 4,000 mm/min confirms that the toolpath did not have any sections where the machine movement speed had to be largely reduced.

The average recorded feed rate was 3,603 mm/min, which shows that the toolpath was well optimized for high feed rate cutting.

Figure 22 represent the finished surface photographed under the microscope with 30x magnification. They demonstrate that the surface

Table 5. *Toolpath 4 test results*

Theoretical toolpath time (f = 1,500 mm/min)	623 s
Theoretical toolpath length	15,196 mm
Number of points	74,040
Toolpath density (average number of points on 1mm of toolpath)	4.9 points/mm
Measured toolpath time (f = 1,500 mm/min)	636 s
Measured toolpath time (f = 4,000 mm/min)	253 s
Minimum feed rate (f = 4,000 mm/min)	2,000 mm/min
Actual calculated feed rate (f = 1,500 mm/min)	1,433 mm/min
Actual calculated feed rate (f = 4,000 mm/min)	3,603 mm/min

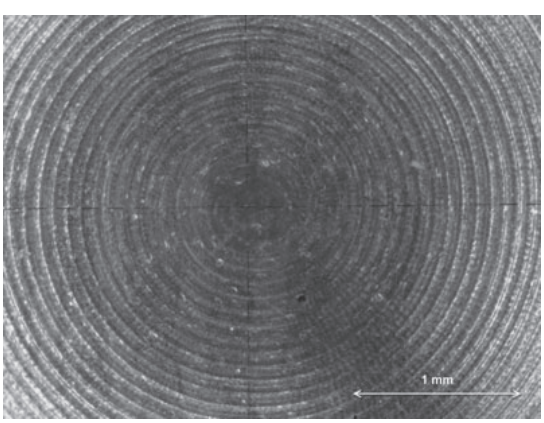

Fig. 22. *Part after toolpath 4 (enlarged 30-times)*

Fig. 23. *Finished part after toolpath 4*

did not include any gouges; the moves were smooth and short enough that they did not produce facets.

Figure 23 shows that the quality of surface is as predicted. There are no special marks or facets seen on the surface.

4 CONCLUDING REMARKS

Test results clearly show that point arrangement along the toolpath has a distinct influence on a surface quality of finished part and machining time.

1. Influence of the toolpath points arrangement on the surface quality

When comparing Figures 17, 19, 21 and 23 it can be clearly seen that surface quality differs from one toolpath to another. When we look at the parts 2 and 4 we can see that the surface is smooth and round, while the surface on the parts 1 and 3 has gouges and facets. The results clearly demonstrate that the toolpath tolerance is not the only parameter that influences the quality of the finished surface.

Results (Figs. 8, 11, 13, 15 and Tables 2, 3, 4 and 5) show that the toolpaths that had most evenly arranged points (toolpaths 2 and 4) showed the best results on the surface quality.

The toolpath density is important factor for getting good surface finish quality. If the density is very low this means that the toolpath tolerance was not correctly set. On the other side very high average density of points does not guarantee a good surface quality. This is clearly presented by comparing toolpath 3 and toolpath 4. Toolpath 4 had almost 2 times lower average point density than toolpath 3 but the surface quality was much better. The reason for lower surface quality in toolpath 3 is the fact that the points were not evenly arranged.

2. Influence of point arrangement on the machining time

At relatively small feed rates the influence of point arrangement to the machining time is not very large. Even with toolpath 1, which had very low quality of point arrangement, the machining at 1500 mm/min, was only 10% longer than theoretical machining time.

The influence gets noticeable when the feed rate is increased. When the feed rate was increased to 4000 mm/min the toolpaths with more evenly arranged points (toolpaths 2 and 4) showed noticeable decrease of machining time. On the other side toolpaths 1 and 3 did not demonstrate almost any decrease of machining time.

5 REFERENCES

[1] Young-Keun, C., Banerjee, A. Tool path generation and tolerance analysis for free-form surfaces. *International Journal of Machine Tools & Manufacture*, 47, 2007, p. 689-696.

[2] Suresh, K., Yang, D. Constant scallop-height machining of free-form surfaces. *Journal of Engineering for Industry*, 116, 1994, p. 253-259.

[3] Farin, G. *Curves and surfaces for CAGD*. San Diego, CA: Academic Press, 2002.

[4] Loney, G.C., Ozsoy, T.M. Machining of free form surface. *Computer Aided Design*, 19, 1987, p. 85-89.

[5] Kopač, J., Pogačnik, M. Theory and practice of achieving quality surface in turn milling. *Int. j. mach. tools manuf.*, 37/5, 1997, p. 709-715.

[6] Krajnik, P., Kopač, J. Modern machining of die and mold tools. *J. mater. process. technol*, 157/158, 2004, p. 543-552.

[7] Roblek, T., Kopač, J. G-code optimization enables HSC machining at low performance CNC machine tools. Conference proceedings. Celje: Tecos, 2003, p. 331-336.

[8] Zghal, B., Haddar, M, Numerical model for dynamic analysis of tool and workpiece in turning. *Advances in Production Engineering & Management*. vol. 2, no. 2, June 2007, p. 55-62.

[9] Čuš, F., Župerl U. Adaptive self-learning controller design for federate maximization of machining process. *Advances in Production Engineering & Management*, vol. 2, no. 1, March 2007, p. 18-27.

Strojniški vestnik - Journal of Mechanical Engineering 54(2008)4, 288-296
UDC 621.778
Paper received: 8.4.2008
Paper accepted: 15.5.2008

Impact of Young's Modulus Degradation on Springback Calculation in Steel Sheet Drawing

Marko Vrh[1,2] - Miroslav Halilovič[1] - Boris Štok[1,*]
[1]University of Ljubljana, Faculty of Mechanical Engineering, Slovenia
[2]Kovinoplastika Lož, Slovenia

The aim of the paper is to demonstrate, based on the results of respective numerical simulations of a drawing process, how springback of a steel sheet drawn part is affected by stiffness degradation, which results from the material damage evolved during the forming process. For the purpose of the presented paper the GTN (Gurson-Tvergaard-Needleman) damage constitutive model coupled with Mori-Tanaka approach has been implemented in ABAQUS/Explicit via VUMAT user material subroutine, while integration of the constitutive model is performed with a numerical scheme developed recently by the authors. Parameters of the constitutive model are identified, for authenticity of the paper, from the measurement data obtained from classical tensile tests of cold rolled stainless steel EN 1.4301, as well as from the measured stiffness degradation, as a function of the plastic strain. From a comparative analysis of numerical results of the springback behaviour, investigated on the Demeri springback cup test under assumption of different constitutive models, it can be concluded, that stiffness degradation should be incorporated in simulations of sheet metal forming. Its influence on a predicted final shape of a steel sheet drawn part is namely too significant to be neglected.

Keywords: drawing processes, steel sheet, springback, material damage, elastic properties, stiffness degradation

0 INTRODUCTION

A great concern in sheet metal forming design is devoted to aa appropriate prediction of the final shape of a formed part, or actually to springback, which plays a key role in a formation of this shape. Springback, a phenomenon that is related to the elastic strain recovery after removal of forming loads, is physically governed by the stress state achieved at the end of the forming process and by the elastic response of a formed part. Researchers dealing with springback prediction are mostly focused on the accurate prediction of the final stress state after forming. In this context many improvements were proposed from a numerical point of view, resulting in a development of finite elements that are capable to cover stress behaviour in a sheet more precisely [1] to [5]. Another wide attention and intense research, related to springback, was paid to the mathematical modelling of constitutive laws of respective materials, in which a special attention was paid on Bauschinger effect [6] and [7], strain dependent hardening [8] and plastic anisotropy [9]. Despite all that and though it was reported several times that effective Young's modulus drops with the increase of plastic strain [10] to [14], the elastic response of the formed part associated with the forming tools removal is in the most of computational analyses still performed according to Hooke's law using initial elastic properties. In fact, Young's modulus degradation can be noticed with several experimental techniques, like unloading of the prestrained specimen [10], ultrasonic testing [11], acoustic technique [12] and nano–indentation testing [13]. Experimental evidence, as well as theoretical results obtained from consideration of corresponding mathematical models, shows that the mechanism causing the degradation of stiffness of material is appearance of cavities and cracks in materials [12] and [14].

1 EXPERIMENTAL OBSERVATIONS AND MEASUREMENTS

Though in this paper the importance of considering stiffness degradation in the calculation of the final shape of a drawn part will be

*Corr. Author's Address: University of Ljubljana, Faculty of Mechanical Engineering, Aškerčeva 6, SI-1000 Ljubljana, Slovenia, boris.stok@fs.uni-lj.si

demonstrated comparatively by numerical means, i.e. by simulating springback under assumption of different constitutive models, the research will be performed by respecting macroscopic material behaviour and associated material data to its greatest extent. Thus, for the investigated stainless steel EN 1.4031 the yield curve and Young's modulus degradation have been measured on a sheet specimen. In addition, also microstructure of the stretched sheet has been observed in order to better understand physical background of the stiffness degradation.

Before proceeding we find necessary to explain the term "effective" which will be used regularly in a description of some quantities associated with material response. In the context followed in this research "effective" means that respective response is considered macroscopically, possibly hiding the actual reasons for evidenced behaviour. Thus, in a homogeneous material stiffness is directly correlated to Young's modulus of the material, and it is actually from the stiffness measurements that magnitude of the elastic modulus can be uniquely evaluated. The situation is not so straightforward when we consider a porous or damaged material. Namely, experimentally we can only evaluate stiffness of the considered material structure as a whole, i.e. including all possible inclusions and voids. In this case we will refer to effective Young's modulus which will definitely depend not only on the intrinsic material properties of the matrix, but in particular on the properties specifying departure from a homogeneous solid material.

1.1 Yield Curve

The effective yield curve of stainless steel EN 1.4031 has been obtained upon measurements from a standard tensile test that was performed on the Tira 2300 tensile test machine. The experimental results were fitted according to Ludwig's law which was found to be appropriate to fit experimental data (Fig. 1).

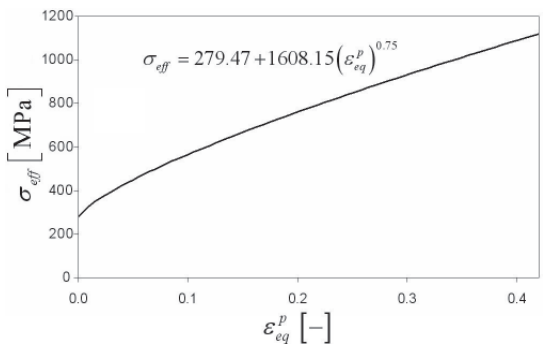

Fig. 1. *Effective yield curve*

1.2 Effective Young's Modulus Degradation

To measure effective Young's modulus degradation as a function of equivalent plastic strain, which is for uniaxial stress case $\varepsilon_{eq}^{p} = \ln\left(L / L_0\right)$, standard specimens were first plastically prestrained in the tensile test machine to a certain degree of equivalent plastic strain. After that the thickness and width of each specimen were precisely measured in order to evaluate the respective cross–sectional area. Each specimen was then clamped again in the tensile test machine, with a dynamometer measuring force range up to ±10 kN and accuracy class being 1 (ISO376–EN10002–3). The guaranteed accuracy class of the strain transducer, which was mounted on the specimen as shown in Figure 2, is 0.1, its nominal displacement range being ±2.5 mm.

From the measured force–displacement relationship registered by elastic loading and unloading of the plastically prestrained specimen the effective elastic modulus was calculated considering Hooke's law, using interpolation of the measurement data of length, cross–sectional area and force. In order to retrieve Young's modulus degradation as a function of equivalent plastic strain the described procedure is repeated for different plastic prestrains. As it can be clearly seen from the plotted graph in

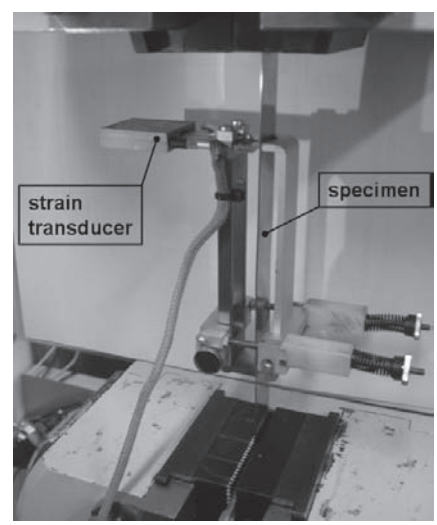

Fig. 2. *Measurement of the elastic elongation*

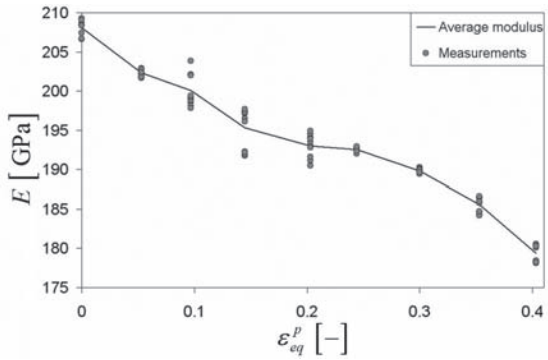

Fig. 3. *Effective Young's modulus degradation*

Figure 3, it is beyond all question that the evidenced degradation of the effective Young's modulus is directly correlated to the degree of plastic prestrain. The fact that in our experiment plastic prestraining was achieved under condition of uniaxial stress state certainly does not affect the general statement.

1.3 Observation of Microstructure

In order to gain a better insight into a cause of the proved stiffness degradation the plastically stretched material was inspected by electronic microscope JEOL KSM–5610. Small specimens of dimensions 10×10mm were cut out with plate shears from the prestrained steel specimens for that purpose. In the sequel we give some comments on findings of the observed microstructure.

First, we observe a specimen that was stretched until rupture, which happened at the magnitude of 0.55 of the equivalent plastic strain.

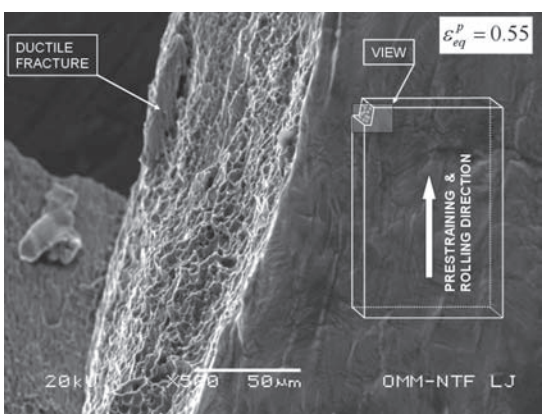

Fig. 4. *Fracture area (microscope view)*

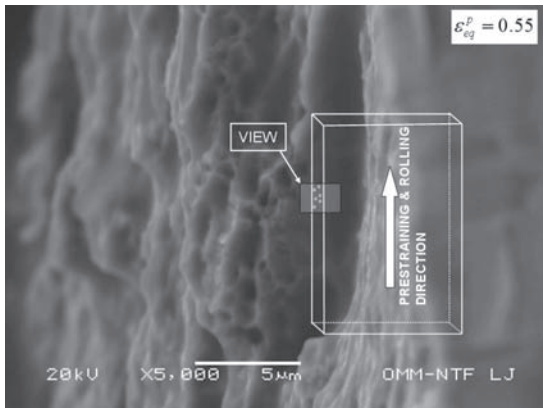

Fig. 5. *Revealed voids at the edge of specimen at* $\varepsilon_{eq}^{p} = 0.55$ *(microscope view)*

Figure 4 shows the detail of a fracture area and the respective material appearance along of it. The front (rolled) surface of the specimen does not give us much information about any damage in the material, even in the immediate vicinity of fracture. In the fracture area, however, this is observed to be surprisingly different. From inspection of this region it can be concluded that the main mechanism of occurred ductile damage in the investigated material is voids appearance. Since microstructure of a homogeneous stretched sheet metal must exhibit a certain level of continuation through its domain, one can assume, that microstructure in the inside of the deformed sheet metal should be similar to the microstructure in the fracture area.

Figure 5 shows the photography of the material internal structure at the cut edge of a same specimen as shown in Figure 4. By cutting a small piece of material was nipped off the surface because of a small defect in plate shears blade, thus

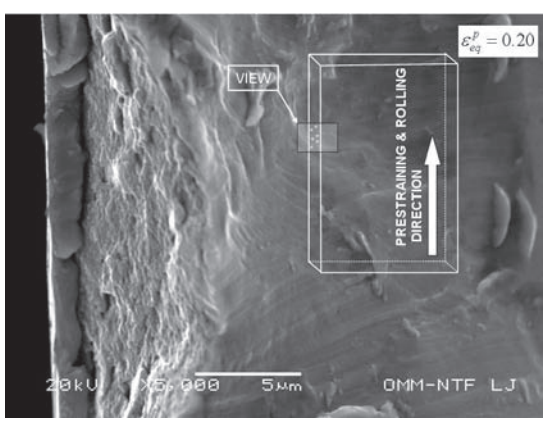

Fig. 6. *Revealed voids at the edge of specimen at* $\varepsilon_{eq}^{p} = 0.2$ *(microscope view)*

revealing fortunately the internal microstructure. From that surface, which is distinctively visible in Figure 5, damage in the form of voids may be easily perceived. Based on this evidence it can be concluded, that voids in material appear throughout the volume.

Let us now observe what is happening in the sheet metal before rupture. Again the microstructure at the cut edge of a specimen, this time prestrained to the magnitude of 0.20 of the equivalent plastic strain, was observed, where cutting again nips off a small piece of material and thus reveals the internal microstructure. Appearance of voids in microstructure can be seen in considerable smaller amount. From comparison of Figures 5 and 6 it can be concluded, that voids evolution in material depends on stretching. Their presence is obviously the main mechanism of ductile damage and the true reason of progressive stiffness degradation.

2 CONSTITUTIVE MODELLING AND NUMERICAL IMPLEMENTATION

For the purpose of this research we have adopted the isotropic GTN model which establishes the respective constitutive laws for the evolution of ductile damage in porous materials [15]. This model considers void nucleation due to plastic deformation and void growth due to hydrostatic stress, i.e. two essential elements of damage evolution besides void coalescence. In order to perform our investigation we have coupled the GTN model with a respective model considering stiffness degradation.

2.1 Plastic Potential

Plastic potential associated with the GTN model reads:

$$\Phi = \frac{\left(\sigma_{eq}\right)^2}{\left(\sigma_M\right)^2} + 2\, f\, q_1 \cosh\left(\frac{3 q_2\, \sigma_H}{2\sigma_M}\right) - \left(1 + q_3\, f^2\right) \quad (1).$$

Above, σ_{eq} is Mises equivalent stress, σ_M is yield stress of the matrix material, $\sigma_H = \sigma_{kk}/3$ is hydrostatic stress, q_1, q_2 and q_3 are parameters of the damage model and f is void volume fraction or porosity in the material. Here, it should be reminded that due to porosity in material the effective yield stress σ_{eff}, which is obtained experimentally, does not equal the yield stress of the matrix material.

2.2 Evolution of Porosity

The law governing the porosity evolution considers two mechanisms, void growth and void nucleation, respectively:

$$\mathrm{d}f = \mathrm{d}f_{growth} + \mathrm{d}f_{nucleation} \quad (2).$$

The first term on the right hand side can be formulated by considering mass conservation:

$$\mathrm{d}f_{growth} = (1 - f)\, \mathrm{d}\varepsilon_{kk}^p \quad (3),$$

whereas the nucleation of voids due to microcracking and decohesion of particle–matrix interface is related to plastic deformation of the matrix material:

$$\mathrm{d}f_{nucleation} = A_n\, \mathrm{d}\bar{\varepsilon}_m^p$$
$$A_n = \frac{f_n}{s_n\sqrt{2\pi}} \exp\left[-\frac{1}{2}\left(\frac{\bar{\varepsilon}_m^p - \varepsilon_n}{s_n}\right)\right] \quad (4).$$

Above, A_n follows a normal distribution about the mean nucleation strain ε_n with a standard deviation s_n. Parameter f_n is maximum nucleated void volume fraction and $\bar{\varepsilon}_m^p$ is equivalent plastic strain of matrix material, obtained from the following equivalent plastic work expression:

$$(1 - f)\sigma_M \mathrm{d}\bar{\varepsilon}_m^p = \sigma_{ij} \mathrm{d}\varepsilon_{ij}^p \quad (5).$$

In this study decrease of strength of material due to extensive void coalescence is omitted.

2.3 Stiffness Degradation

For the characterization of the stiffness degradation due to damage Eshelby's equivalence principle and his solution of the elastic field of an ellipsoidal inclusion in an infinite elastic medium [16] can be used. As it was verified several times for different materials [17] to [19] Eshelby's principle is best combined with Mori–Tanaka's concept of average stress in a matrix [20] and [21]. Combination of the GTN model with Eshelby and Mori–Tanaka approach builds an appropriate constitutive model for a simulation of the measured material response. Here, linear and isotropic elastic law $\sigma_{ij} = C_{ijkl}\varepsilon_{kl}^e$ will be used, with degradation of stiffness taken into account. According to Mori-Tanaka approach effective Young's modulus $\bar{E}$ and effective Poisson's ratio $\bar{\nu}$ are related to porosity for material which contains spherical voids:

$$\bar{E} = \frac{2E_0(1-f)(7-5\nu_0)}{2(7-5\nu_0)+f(13-2\nu_0-15\nu_0^2)} \qquad (6)$$

$$\bar{\nu} = \frac{2\nu_0(7-5\nu_0)+f(3-2\nu_0-5\nu_0^2)}{2(7-5\nu_0)+f(13-2\nu_0-15\nu_0^2)} \qquad (7),$$

where E_0 and ν_0 are Young's modulus and effective Poisson's ratio of undeformed material.

2.4 Numerical Implementation Procedure

The above presented constitutive model has been implemented in a general purpose finite element code ABAQUS via VUMAT subroutine. In the implementation a new explicit integration scheme, developed recently by the authors, is used, its task being to find an appropriate increment of the plastic multiplier $\Delta\lambda$ from given total strain increments $\Delta\varepsilon_{ij}$. This is achieved by expanding the consistency condition, which is practically a condition of fulfilled yield criterion, $\Phi = 0$, that must be respected through all the integration process during the evolution of plastic strains, into Taylor series, where higher order differentials are neglected. The numerical scheme is thus based, provided the values of state variables are known at the beginning of a considered increment, on imposing:

$$\Phi + \mathrm{d}\Phi = 0 \qquad (8)$$

to be fulfilled in a considered increment. When considering (1) this leads to:

$$\Phi + \frac{\partial\Phi}{\partial\sigma_{ij}}\Delta\sigma_{ij} + \frac{\partial\Phi}{\partial\sigma_M}\Delta\sigma_M + \frac{\partial\Phi}{\partial f}\Delta f = 0 \qquad (9).$$

With regard to the forward–Euler approach, which uses the differential form of the consistency condition, i.e. $\mathrm{d}\Phi = 0$, our approach considers the additional term Φ. Though this term should be zero, because it represents a function whose value should obey the consistency condition $\Phi = 0$, numerically this is usually not true. This small difference between the two explicit schemes is, according to our experience, the key reason for a considerable improvement of the stability of numerical integration.

The remaining equations of the GTN model are the evolution equations, here expressed in the incremental form:

$$\begin{aligned}
\Delta\sigma_{ij} &= C_{ijkl}\left(\Delta\varepsilon_{kl} - \Delta\varepsilon_{kl}^p\right)\\
\Delta\varepsilon_{ij}^p &= \frac{\partial\Phi}{\partial\sigma_{ij}}\Delta\lambda\\
\Delta\bar{\varepsilon}_m^p &= \frac{\sigma_{ij}\dfrac{\partial\Phi}{\partial\sigma_{ij}}}{(1-f)\sigma_M}\Delta\lambda\\
\Delta\sigma_M &= \frac{\partial\sigma_M}{\partial\bar{\varepsilon}_m^p}\Delta\bar{\varepsilon}_m^p = \frac{\partial\sigma_M}{\partial\bar{\varepsilon}_m^p}\frac{\sigma_{ij}\dfrac{\partial\Phi}{\partial\sigma_{ij}}}{(1-f)\sigma_M}\Delta\lambda\\
\Delta f &= \left((1-f)\frac{\partial\Phi}{\partial\sigma_{ii}} + A_n\frac{\sigma_{ij}\dfrac{\partial\Phi}{\partial\sigma_{ij}}}{(1-f)\sigma_M}\right)\Delta\lambda
\end{aligned} \qquad (10).$$

Considering the above evolution equations in (9) yields the increment of plastic multiplier:

$$\Delta\lambda = \frac{\Phi + \dfrac{\partial\Phi}{\partial\sigma_{ij}}C_{ijkl}\Delta\varepsilon_{kl}}{\dfrac{\partial\Phi}{\partial\sigma_{ij}}C_{ijkl}\dfrac{\partial\Phi}{\partial\sigma_{kl}} - \dfrac{\partial\Phi}{\partial\sigma_M}\dfrac{\partial\sigma_M}{\partial\bar{\varepsilon}_m^p}\dfrac{\sigma_{ij}\dfrac{\partial\Phi}{\partial\sigma_{ij}}}{(1-f)\sigma_M} - \dfrac{\partial\Phi}{\partial f}\left((1-f)\dfrac{\partial\Phi}{\partial\sigma_{ii}} + A_n\dfrac{\sigma_{ij}\dfrac{\partial\Phi}{\partial\sigma_{ij}}}{(1-f)\sigma_M}\right)} \qquad (11),$$

where the corresponding derivatives are defined as:

$$\begin{aligned}
\frac{\partial\Phi}{\partial\sigma_{ij}} &= \frac{1}{(\sigma_M)^2}\left(3\sigma_{ij} - \sigma_{kk}\delta_{ij}\right) + \frac{f\,q_1q_2}{\sigma_M}\sinh\left(\frac{q_2\sigma_{kk}}{2\sigma_M}\right)\delta_{ij}\\
\frac{\partial\Phi}{\partial\sigma_M} &= -2\frac{(\sigma_{eq})^2}{(\sigma_M)^3} - \frac{f\,q_1q_2\,\sigma_{kk}}{(\sigma_M)^2}\sinh\left(\frac{q_2\sigma_{kk}}{2\sigma_M}\right)\\
\frac{\partial\Phi}{\partial f} &= 2q_1\cosh\left(\frac{q_2\sigma_{kk}}{2\sigma_M}\right) - 2q_3\,f
\end{aligned} \qquad (12).$$

Let us remind that according to explicit approach all the state variables appearing in equations (10) to (12) are written at the beginning of the increment. When the increment of plastic multiplier $\Delta\lambda$ is calculated (11), the respective increments of the other state variables can be readily calculated using (10).

3 INVERSE IDENTIFICATION

3.1 Identification of the GTN Model Parameters

Since yield condition $\Phi = 0$ is fulfilled during plastic loading, the ratio σ/σ_M in the case of uniaxial loading remains almost independent of the magnitude of the yield stress of matrix material. Therefore, the GTN model parameters can be identified separately from the yield curve.

Parameters q_1, q_2 and q_3 are essentially an improvement of the basic Gurson's constitutive model upgrading thus the original plastic potential. Values of those parameters are similar for all metals [22], so we adopt them accordingly, taking $q_1 = 1.5$, $q_2 = 1$ and $q_3 = q_1^2 = 2.25$. The remaining three parameters describing void nucleation, f_n, ε_n and s_n, can be estimated from the observed porosity evolution. The latter may be thus deduced by using equation (6):

$$f = \frac{2(7-5\nu_0)\left(1-\frac{\bar{E}}{E_0}\right)}{2(7-5\nu_0)+\frac{\bar{E}}{E_0}(13-2\nu_0-15\nu_0^2)} \qquad (13),$$

where $\bar{E}$ is measured effective Young's modulus at different loading stages and $\nu_0 = 0.3$.

From observation of the measurements it can be concluded first, that the porosity evolution does not follow a normal distribution (Fig. 7), and second, that a linear trend of the porosity increase is reasonable to be assumed. In that case only one parameter is needed for the description of the evolution law instead of three:

$$\mathrm{d}f_{nucleation} = \bar{A}_n \, \mathrm{d}\bar{\varepsilon}_m^p \qquad (14).$$

Inverse identification of the parameter $\bar{A}_n$ is carried out using Gauss minimization method, in which the cost function, defined as a sum of squares of the differences between calculated and measured values of porosity, is iteratively minimized [23]. The inverse identification procedure gives as the final result $\bar{A}_n = 0.1458$.

3.2 Identification of the Yield Curve of Matrix Material

From the measured force *F*, elongation ΔL and initial cross–sectional area A_0 effective (true) stress σ_{eff}, total logarithmic strain ε and equivalent plastic strain ε_{eq}^p were calculated, assuming that total strain can be additively decomposed into elastic and plastic strain $\varepsilon_{ij} = \varepsilon_{ij}^e + \varepsilon_{ij}^p$. For the identification of the yield curve of matrix material a rather simple method, based on a numerical simulation of the performed experiment, was used. The identification method consists of the following steps. In a computer simulation of the tensile test two geometrically equal specimens, say A and B as depicted in Figure 8, but having different material properties or obeying different constitutive laws, are considered. The specimens are completely separated in the analysis, but in order to provide for both the conditions of the experiment they are exposed to the same loading conditions, i.e. to a prescribed edge displacement in each time increment.

Specimen A follows the Mises constitutive model with yield curve being expressed by effective yield stress σ_{eff}, which corresponds to a classical continuum mechanics approach. For specimen B, on the contrary, a damage mechanics approach is applied with the GTN model prescribed. But to use the latter model yield curve of matrix material σ_M has to be known. Considering that from the experiment we have only effective yield curve the procedure of identifying yield curve of matrix material follows this iterative path. Assuming at the beginning that $\sigma_M = \sigma_{eff}$ we expose both specimens to the prescribed loading conditions and trace the respective response, i.e. resultant axial force $F(\Delta L)$ and effective stress σ_{eff}, during loading. Because of the porosity, which evolves in accordance with the assumed GTN model, specimen B exhibits smaller effective stress and resultant force than specimen A. Also, since the effective yield curve of the model A is calculated

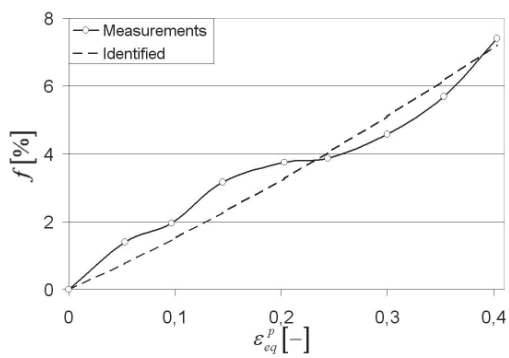

Fig. 7. *Growth of void volume fraction*

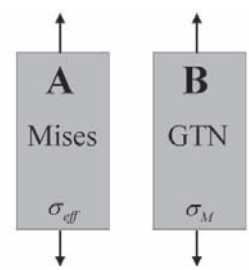

Fig. 8. *Schematic representation of models for identification of yield curve of matrix material*

directly from the measured dependence $F(\Delta L)$, the latter should intrinsically perfectly fit the response of specimen A. The task is now to equalize curve $F(\Delta L)$ of specimen B with the one of specimen A, the latter being actually identical to the measured one. This is done so that the yield curve of specimen B is correspondingly scaled for the simulation in the next iteration. The scaling should however take into account that difference between the two curves may depend on loading, therefore, in each increment scaling must be done by considering the actual forces. Accordingly, for a specific increment the yield curve of specimen B to be used in the next iteration should be scaled up for the same factor as it is evidenced between the calculated forces of the two specimens:

$$\sigma_M^{(i+1)} = \sigma_M^{(i)} \frac{F_{\mathrm{A}}^{(i)}}{F_{\mathrm{B}}^{(i)}} \qquad (15).$$

Since the yield curve of specimen B considered in the next iteration is higher, the resultant force should be closer to the resultant force of specimen A. The described procedure, which can be repeated until the difference between curves $F_{\mathrm{A}}(\Delta L)$ and $F_{\mathrm{B}}(\Delta L)$ becomes small enough, gives the yield curve of matrix material, which we were looking for. The procedure has proved to be very effective since its convergence is fast. The final result, which is depicted in Figure 9 and is obtained in only three iterations, is characterized by the maximum relative difference between curves $F_{\mathrm{A}}(\Delta L)$ and $F_{\mathrm{B}}(\Delta L)$ being smaller than $4 \cdot 10^{-4}$ in any point of the measured force.

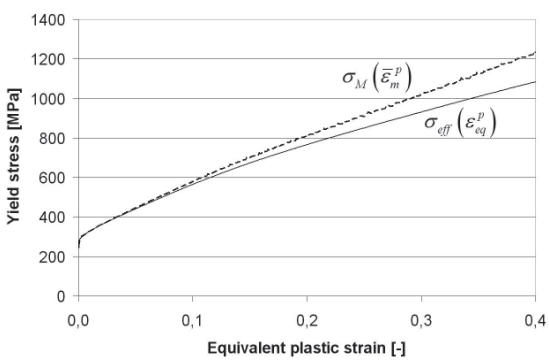

Fig. 9. *Effective yield stress and yield stress of matrix material*

4 SIMULATION OF DEMERI SPRINGBACK CUP TEST (ASTM, WK8010)

For the research of how Young's modulus degradation affects calculation of springback in steel sheet drawing the Demeri springback cup test may be considered [24]. The test consists of a ring sample taken from the sidewall of a cylindrical deep drawn cup. The stress state in the ring is characterized by residual hoop stresses that evolved during deep drawing process in the wall of the cup. When the ring is split, large ring opening displacement appears due to release of those stresses (Fig. 10). The evidenced displacement can be considered as a measure of the actual springback.

In the numerical simulation a steel circular blank of 200 mm diameter and nominally 0.88 mm thick is considered. Geometry of the tools is as follows: diameter of the die is 110 mm and diameter of the punch is 100 mm with 10 mm radii on the die and the punch. Nominal depth of the drawn cup is 56 mm. The forming rate in simulation is 1m/s and the holder force is constant, its magnitude being 600 kN. To obtain a ring the cup wall is cut 11 mm and 26 mm below the cup's upper edge. Two material models have been used in simulations to study the influence of stiffness degradation and damage in material, the classical isotropic Mises model with yield curve being effective stress σ_{eff} and the GTN damage model with the material data identified as described in the previous sections. In addition, also effect of degradation of elastic properties is considered.

In the FEM simulations 2776 four–node linear shell elements with reduced integration were used for the sheet blank, while the tool is assumed

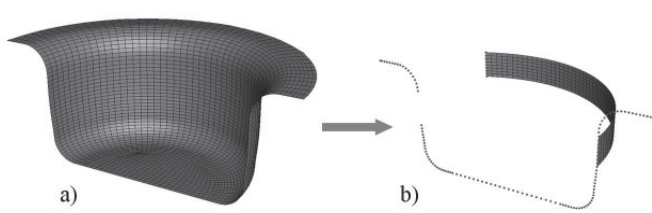

Fig. 10. *Numerical simulation of Demeri springback cup test. a) circular cup, b) splitted ring*

Table 1. *Ring opening – comparison of the models*

Used model	Ring opening [mm]
a) Mises model + initial elastic properties	156.2
b) GTN + initial elastic properties	165.0
c) GTN + degradation of elastic properties	177.2

to be rigid. The results of springback, which is defined with a ring opening displacement, are tabulated in Table 1. It is interesting to observe that even if in the considered Demeri cup test the maximum porosity in the ring reaches about 4%, the difference between the computed results is around 14%.

5 CONCLUDING REMARKS

From the comparison of numerical results of the springback behaviour, performed upon corresponding computer simulations of the considered sheet forming case and subsequent Demeri springback cup test, it can be concluded, that stiffness degradation in material has a significant influence on the final result of elastic strain recovery, and consequently on the final shape of the formed part. Therefore, the stiffness degradation in terms of Young's modulus degradation and damage occurrence cannot be neglected in calculations of springback. One way to take those effects into account is the approach, presented in this paper.

Acknowledgement

Authors would like to express their gratitude to Kovinoplastika Lož Ltd. and to prof. L. Kosec from Faculty of Natural Sciences and Technology, University of Ljubljana, who enabled experimental research, presented in the paper.

6 REFERENCES

[1] Wagoner, R.H., Li, M. Simulation of springback, Through–thickness integration. *International Journal of Plasticity*, 2007, 23/3, p. 345–360.

[2] Dong, W.P., Soo, I.O. A four–node shell element with enhanced bending performance for springback analysis. *Comput. Methods Appl. Mech. Eng.*, 2004, 193, p. 2105–2138.

[3] Guo, Y.Q., Gati, W., Naceur, H., Batoz, J.L. An efficient DKT rotation free shell element for springback simulation in sheet metal forming. *Computers and Structures*, 2002, 80, p. 2299–2312.

[4] Tabourot, L., Vacher, P., Coudert, T., Toussaint, F., Arrieux, R. Numerical determination of strain localisation during finite element simulation of deep–drawing operations. *Journal of Materials Processing Technology*, 2005, 159/2, p. 152–158.

[5] Chun, B. K., Kim, H. Y., Lee, J. K. Modeling the Bauschinger effect for sheet metals, part II: applications. *International Journal of Plasticity*, 2002, 18/5-6, p. 597–616.

[6] Yoshida, F., Uemori, T. A model of large–strain cyclic plasticity and its application to springback simulation. *International Journal of Mechanical Sciences*, 2003, 45/10, p. 1687–1702.

[7] Gau, J.T., Kinzel, G.L. A new model for springback prediction in which the Bauschinger effect is considered. *International Journal of Mechanical Sciences*, 2001, 43/8, p. 1813–1832.

[8] Geng, L., Shen, Y., Wagoner, R. H. Anisotropic hardening equations derived from reverse–bend testing. *International Journal of Plasticity*, 2002, 18/5–6, p. 743–767.

[9] Geng, L., Wagoner, R. H. Role of plastic anisotropy and its evolution on springback. *International Journal of Mechanical Sciences*, 2002, 44/1, p. 123–148.

[10] Morestin, F., Boivin, M. On the necessity of taking into account the variation in the Young modulus with plastic strain in elastic–plastic software. *Nuclear Engineering and Design*, 1996, 162(1), p. 107–116.

[11] Cleveland, R. M., Ghosh, A. K. Inelastic effects on springback in metals. *International Journal of Plasticity*, 2002, 18(5–6), p. 769–785.

[12] Yeh, H.Y., Cheng, J. H. NDE of metal damage: ultrasonics with a damage mechanics model. *International Journal of Solids and Structures*, 2003, 40(26), p. 7285–7298.

[13] Yang, M., Akiyama, Y., Sasaki, T. Evaluation of change in material properties due to plastic

deformation. *Journal of Materials Processing Technology*, 2004, 151(1–3), p. 232–236.

[14] Bonora, N., Gentile, D., Pirondi, A., Newaz, G. Ductile damage evolution under triaxial state of stress: theory and experiments. *International Journal of Plasticity*, 2005, 21(5), p. 981–1007.

[15] Gurson, A.L. Continuum Theory of Ductile Rupture by Void Nucleation and Growth: Part I—Yield Criteria and Flow Rules for Porous Ductile Materials. *Journal of Engineering Materials and Technology*, 1977, 99, p. 2–15.

[16] Eshelby, J.D. The determination of the elastic field of an ellipsoidal inclusion, and related problems. *Proc. Roy. Soc. London*, 1957, A241, p. 376–396.

[17] Carvalho, F.C.S., Labuz, J.F. Experiments on effective elastic modulus of two–dimensional solids with cracks and holes. *International Journal of Solids and Structures*, 1996, 33(28), p. 4119–4130.

[18] Pundale, S.H., Rogers, R.J., Nadkarni, G.R. Finite element modeling of elastic modulus in ductile irons: Effect of graphite morphology. *AFS Transactions*, 1998, 106, p. 99–105.

[19] Böhm, H. J., Eckschlager, A., Han, W. Multi–inclusion unit cell models for metal matrix composites with randomly oriented discontinuous reinforcements. *Computational Materials Science*, 2002, 25(1–2), p. 42–53.

[20] Mori, T., Tanaka, K. Average stress in matrix and average elastic energy of materials with misfitting inclusions. *Acta Metall*., 1973, 21, p. 571–574.

[21] Zhao, Y. H., Tandon, G.P., Weng, G.J. Elastic Moduli for a Class of Porous Materials. *Acta Mehanica*, 1989, 76, p. 105–130.

[22] Tvergaard, V. Influence of Voids on Shear Band Instabilities under Plane Strain Condition. *International Journal of Fracture Mechanics*, 1981, 17, p. 389–407.

[23] Koc, P., Štok, B. Computer–aided identification of the yield curve of a sheet metal after onset of necking. *Computational Materials Science*, 2004, 31(1–2), p.155–168.

[24] Foecke, T., Gnaeupel–Herold, T. Robustness of the sheet metal springback cup test. *Metallurgical and Materials Transactions A*, 2006, 37A, p. 3503–3510.

Instructions for Authors

From 2008 the Journal of Mechanical Engineering is to be published in English only, but with separate Slovene abstracts. The authors are entirely responsible for the correctness of the language. If a reviewer indicates that the language in the paper is poor, the editor will require the author to correct the text with the help of a native English speaker before the paper is reviewed again.

Papers can be submitted electronically to the journal's e-mail address (info@sv-jme.eu) or by post.

Papers submitted for publication should comprise the following:

- Title, Abstract, Keywords,
- Main body of text,
- Tables and Figures (graphs, drawings or photographs) with captions,
- List of References,
- Information about the authors, the corresponding author and a full set of addresses.

For papers from abroad (in the case that none of the authors is a Slovene) the editor will obtain a Slovenian translation of the Abstract.

Papers should be short, about 8 to 12 pages of A4 format, or at most, 7000 words. Longer papers will be accepted if there is a special reason, which should be stated by the author in the accompanying letter. Short papers should be limited to less than 3000 words.

THE FORMAT OF THE PAPER

The paper should be written in the following format:

- A Title, which adequately describes the content of the paper.
- An Abstract, which should not exceed 250 words. The Abstract should state the principal objectives and the scope of the investigation, the methodology employed, summarize the results and state the principal conclusions.
- An Introduction, which should provide a review of recent literature and sufficient background information to allow the results of the paper to be understood and evaluated.
- A Theory and the experimental methods used.
- An Experimental section, which should provide details of the experimental set-up and the methods used for obtaining the results.
- A Results section, which should clearly and concisely present the data using figures and tables where appropriate.
- A Discussion section, which should describe the relationships and generalisations shown by the results and discuss the significance of the results, making comparisons with previously published work.
- Because of the nature of some studies it may be appropriate to combine the Results and Discussion sections into a single section to improve the clarity and make it easier for the reader.
- Conclusions, which should present one or more conclusions that have been drawn from the results and subsequent discussion and do not duplicate the Abstract.
- References, which must be numbered consecutively in the text using square brackets [1] and collected together in a reference list at the end of the paper.

THE LAYOUT OF THE TEXT

Texts should be written in Microsoft Word format. The paper must be submitted in an electronic version, by e-mail or by post on a CD.

Do not use a LaTeX text editor, since this is not compatible with the publishing procedure of the Journal of Mechanical Engineering.

Equations should be on a separate line in the main body of the text and marked on the right-hand side of the page with numbers in round brackets.

Units and abbreviations

Only standard SI symbols and abbreviations should be used in the text, tables and figures. Symbols for physical quantities in the text should be written in italics (e.g., *v, T, n,* etc.). Symbols for units that consist of letters should be in plain text (e.g. m/s, K, min, mm, etc.).

All abbreviations should be spelt out in full on first appearance, e.g., variable time geometry (VTG).

The meaning of symbols and units belonging to symbols should be explained in each

case or quoted in special table at the end of the paper before the References.

Figures

Figures must be cited in consecutive numerical order in the text and referred to in both the text and the caption as Fig. 1, Fig. 2, etc. Pictures should be saved in a resolution good enough for printing, and in any common format, e.g., BMP, GIF or JPG. However, graphs and line drawings should be prepared as vector images, e.g., CDR, AI.

All Figures should be prepared in black and white, without borders and on a white background. All the figures should be sent separately in their original formats.

When labeling axes, physical quantities, e.g., *t, v, m,* etc., should be used whenever possible. Multi-curve graphs should have the individual curves marked with a symbol. The meaning of the symbol should be explained in the figure caption.

In the case that the author wishes, for whatever reason, to publish Figures in colour, the author must pay the resulting costs.

Tables

Tables must be cited in consecutive numerical order in the text and referred to in both the text and the caption as Table 1, Table 2, etc. In addition to the physical quantity, e.g., *t* (in italics), units (normal text), should be added in square brackets. Each column should have the title line. Tables should not duplicate information that is already noted anywhere in the paper.

Acknowledgement

An acknowledgement for cooperation or help can be included before the References. The author should state the name of the research (co)financer.

The list of references

All references should be collected at the end of the paper in the following styles for journals, proceedings and books, respectively:

[1] Wagner, A., Bajsić, I., Fajdiga, M. Measurement of the surface-temperature field in a fog lamp using resistance-based temperature detectors. *Strojniški vestnik – Journal of Mechanical Engineering*, February 2004, vol. 50, no. 2, p. 72-79.

[2] Boguslawski L. Influence of pressure fluctuations distribution on local heat transfer on flat surface impinged by turbulent free jet. *Proceedings of International Thermal Science Seminar II*, Bled, June 13.-16., 2004.

[3] Muhs, D., et al. *Roloff/Matek mechanical parts*, 16th ed. Wiesbaden: Vieweg Verlag, 2003. 791 p. (In German). ISBN 3-528-07028-5

ACCEPTANCE OF PAPERS AND COPYRIGHT

The Editorial Board reserves the right to decide whether a paper is acceptable for publication, obtain professional reviews for submitted papers, and if necessary, require changes to the content, length or language.

The corresponding author must, in the name of all authors, also enclose a written statement that the paper is original unpublished work, and not under consideration for publication elsewhere.

On publication, copyright of the paper shall pass to the Journal of Mechanical Engineering. The JME must be stated as a source in all later publications.

Submitted materials will not be returned to the author. Unpublished materials are not preserved and will not be sent anywhere without the author's consent.

The paper, prepared for publication, will be sent to the author in PDF format. The author should check for any necessary corrections, which should be the minimum required. With this the author confirms that the paper is ready for publication.

PUBLICATION FEE

For all papers the authors will be asked to pay a publication fee prior to the paper appearing in the journal. However, this fee only needs to be paid after the paper is accepted for publication by the Editorial Board. The fee is €180.00 (for all papers with a maximum of 6 pages), €220.00 (for all papers with a maximum of 10 pages) and €20.00 for each additional page. The publication fee includes 25 off-prints of each paper, which will be sent to the corresponding author.

Vsebina

Strojniški vestnik - Journal of Mechanical Engineering
letnik 54, (2008), številka 4
Ljubljana, april 2008
ISSN 0039-2480

Izhaja mesečno

Uvodnik
Gantar, G. SI 40

Povzetki razprav
Gantar, G., Sterzing, A.: Robustno načrtovanje preoblikovalnih postopkov SI 41
Fernandez, A., Mercado, D., Javierre, C., Muniesa, M.: Izboljšanje kakovosti velikih termoplastičnih izdelkov z nadzorovano brizgalno šobo SI 42
Petek, A., Podgornik, B., Kuzman, K., Čekada, M., Waldhauser, W., Vižintin, J.: Analiza zahtevnega tribološkega sistema enotočkovnega koračnega preoblikovanja pločevine SI 43
Kocańda, A., Czyżewski, P.: Eksperimentalna in numerična analiza bočnih sil v kovaškem orodju SI 44
Kopač, J., Kržič, P.: Vpliv CAM algoritmov na kakovost obdelane površine SI 45
Vrh, M., Halilovič, M., Štok, B.: Vpliv zmanjšanja Youngovega modula na izračun elastične povračljivosti pri vleku jeklene pločevine SI 46

Osebne vesti
Doktorata, magisteriji in diplome SI 47

Uvodnik

Malokdo se zaveda, kako pomembna je vloga tehnologov in orodjarjev, ki izdelajo namenska preoblikovalna orodja v razvojem postopku novega izdelka. Ti so strateško zelo pomemben del verige razvoja novih izdelkov v vseh industrijskih panogah iz naslednjih razlogov:

1. za izdelavo skoraj vsakega sestavnega dela v novih izdelkih, je potrebno izdelati eno ali več namenskih orodij,
2. značilnosti in kakovost namenskih orodij imajo odločujoč vpliv na lastnosti in stroške izdelkov,
3. razvoj in izdelava orodij v razvojni verigi nastopita v zadnji, pogosto kritični fazi, kjer vsaka napaka zato odločilno vpliva na čas za uvedbo novega izdelka.

Podjetja, ki se ukvarjajo z razvojem tehnologij in izdelavo orodij, so ena od gonilnih sil tehnološkega razvoja in imajo pomnoževalen učinek na ekonomske razmere v okolju (državi, regiji, podjetju), v katerem delujejo. V BDP-ju imajo ta podjetja sicer delež, ki je manjši od 1%, je pa od njihove kakovostne podpore odvisno 42% predelovalne industrije. Obstaja veliko primerov s področij medicine, mehatronskih sistemov, elektronike, kjer so novi izdelki razviti in uspešno preizkušeni s pomočjo prototipov. V redno proizvodnjo te nove izdelke lahko uvedejo le tisti, ki imajo podporo kakovostnega tehnološkega oddelka in orodjarskega servisa, ki razvijejo tehnologijo in orodja za njihovo proizvodnjo. Na primer - ni težko skonstruirati mobilni telefon, ki je še enkrat tanjši od obstoječih modelov, na trg pa ga lahko lansira le podjetje, ki bo sposobno osvojiti tudi tehnologije za proizvodnjo vseh mikro komponent, ki morajo biti vgrajene v takšen telefon. Podobno velja za najbolj privlačne stvaritve industrijskih oblikovalcev, ki jih praviloma s sprejemljivi stroški ni enostavno izdelati.

Ta tematski zvezek je namenjen nekaterim zanimivim prispevkom iz področij razvoja tehnologij in namenskih orodij različnih avtorjev. Prispevki so izbrani z mednarodne konference ICIT&MPT 2007, ki jo je organiziral Razvojni center orodjarstva Slovenije TECOS z namenom prenosa znanja v industrijsko okolje. Iz prvotne kratke oblike so razširjeni v celovito predstavitev.

Doc.dr. Gašper Gantar, direktor TECOS-a

Strojniški vestnik - Journal of Mechanical Engineering 54(2008)4, SI 41
UDK 621.9
Prejeto: 23.2.2008
Sprejeto: 15.5.2008

Robustno načrtovanje preoblikovalnih postopkov

Gašper Gantar*,[1] - Andreas Sterzing[2]
[1]TECOS - Razvojni center orodjarstva Slovenije, Celje
[2]Fraunhofer Institut für Werkzeugmaschinen und Umformtechnik, Chemnitz, Nemčija

Lastnosti vhodnega materiala (pločevine, palic itd.), ki se uporablja v preoblikovalnih postopkih, so spremenljive. Tudi ostali vhodni parametri preoblikovalnega sistema (torni pogoji, nastavitve stroja, temperatura itd.) med proizvodnjo znatno nihajo. Izboljševanje proizvodnih postopkov je bil vedno pomemben cilj v kovinsko-predelovalni industriji. Cilj je razviti stroškovno učinkovite in stabilne preoblikovalne postopke, kjer je izmet zmanjšan na najmanjšo vrednost. V prvem delu prispevka je opisan pristop, ki uporabniku omogoča napovedati, kako bo raztros vhodnih spremenljivk vplival na končne lastnosti izdelkov. V drugem delu prispevka je razviti pristop uporabljen za optimizacijo preoblikovalnega postopka z namenom zmanjšanja izmeta, pri čemer je upoštevan vpliv nenadzorovanega raztrosa vhodnih spremenljivk. Optimizacijski postopek sloni na uporabi numeričnih simulacij, metode odzivne površine in stohastične optimizacije. Uporabljen je lahko v zgodnji fazi tehnološke priprave proizvodnje. Predstavljen pristop je bil uspešno uporabljen pri razvoju preoblikovalnih tehnologij za različne obdelovance v industrijskem okolju.

Ključne besede: preoblikovalni postopki, robustnost postopkov, numerične simulacije, optimiranje

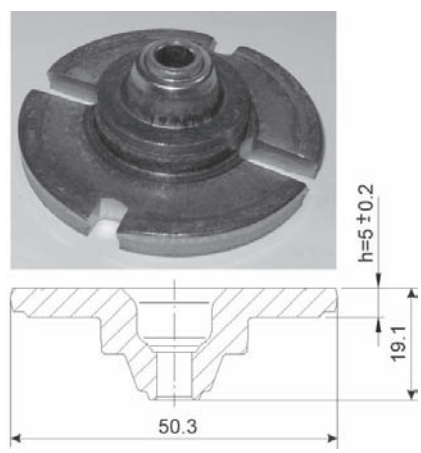

Sl. 1. *Magnetno jedro*

*Naslov odgovornega avtorja: TECOS - Razvojni center orodjarstva Slovenije, Kidričeva 25, 3000 Celje, gasper.gantar@tecos.si

Strojniški vestnik - Journal of Mechanical Engineering 54(2008)4, SI 42
UDK 678-1
Prejeto: 6.12.2007
Sprejeto: 15.5.2008

Izboljšanje kakovosti velikih termoplastičnih izdelkov z nadzorovano brizgalno šobo

Angel Fernandez* - Daniel Mercado - Carlos Javierre - Manuel Muniesa
Univerza v Zaragozi, Fakulteta za strojništvo, Španija

Nadzor nad reološkim vedenjem termoplastičnega materiala je kritičen pri zagotavljanju zanesljive proizvodnje brez napak kot so prelitje ali nepopolno zabrizganje. Te napake so še posebej kritične pri brizganju velikih izdelkov, če ne moremo zagotoviti stalnih postopkovnih parametrov. Nihanja v viskoznosti med proizvodnjo so odvisna predvsem od izbranega materiala in vnaprej programiranih temperaturnih parametrov. Razumevanje reološkega vedenja taline v brizgalni šobi je kritično pri zagotavljanju velikih serij velikih izdelkov brez napak. V tem prispevku je bila dejanska viskoznost pridobljena z nadzorovano brizgalno šobo in potem uporabljena kot vhodni podatek za MoldFlow analizo za predvidevanje napak. Simulacijski model je vključeval dve različne orodni votlini kadi za pralni stroj iz polipropilena, polnjenega s smukcem (kalcijev karbonat), vroče-kanalni sistem in strojno šobo. Za overitev analize se je brizgalo več serij s šobo pri dveh različnih tlakih in temperaturnim zaznavalom v gretem debelostenem valjnem kanalu ter s tipalom za pomik polža. Pred tem je bila šoba umerjena z testiranjem vpliva izgube pritiska s spremembo strižnega razmerja; dejanska viskoznost s spremembo tlaka; ter drugimi testi kot so viskozno gretje polimera. Napake na izdelku so bili opisane s statističnimi obdelavami zajetih podatkov med zapolnjevanjem in delovanjem naknadnega tlaka v orodju. Simulacije enakih eksperimentalnih parametrov za dobre in slabe izdelke so bile uporabljene za ovrednotenje rezultatov in karakterizacijo napak.

Ključne besede: šobe, poliolefini, viskoznost, brizganje polimerov, meritve tlaka, meritve temperature

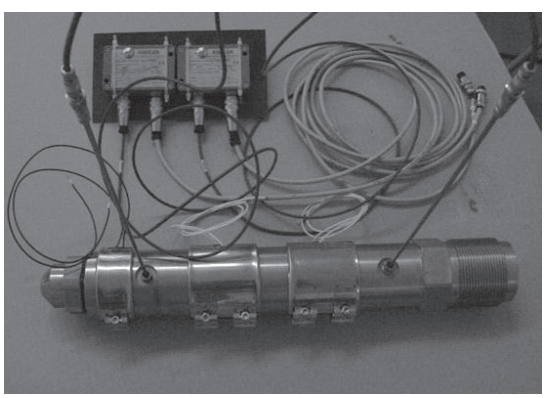

Sl. 1. *Šoba z zaznavali za napravo 3000T*

*Naslov odgovornega avtorja: Univerza v Zaragozi, Fakulteta za strojništvo, C.P.S Torres Quevedo, María de Luna, 3, 50018 Zaragoza, Španija, afernan@unizar.es

Strojniški vestnik - Journal of Mechanical Engineering 54(2008)4, SI 43
UDK 621.9
Prejeto: 7.2.2008
Sprejeto: 15.5.2008

Analiza zahtevnega tribološkega sistema enotočkovnega koračnega preoblikovanja pločevine

Aleš Petek*[,1] - Bojan Podgornik[1] - Karl Kuzman[1] - Miha Čekada[2] -
Wolfgang Waldhauser[3] - Jožef Vižintin[1]
[1]Univerza v Ljubljani, Fakulteta za strojništvo
[2]Institut "Jožef Stefan", Ljubljana
[3]Joanneum Research, Leoben Laser Centre, Avstrija

V sodobnem industrijskem okolju ima ekološki vidik izredno pomembno vlogo pri izbiri preoblikovalnega postopka pločevine. Če želimo izdelovati izdelke z najmanjšim vplivom na okolje, je potrebno skrajšati preoblikovalni postopek vključno z izdelavo namenskih orodji, kot tudi omejiti uporabo mazalnih sredstev. Večina pločevinsko preoblikovalnih opravil zahteva uporabo olj v katerih so vključeni dodatki, ki pa so zaradi različnih razlogov nevarni za okolje. Glede na omenjeno je v prispevku predstavljena analiza različnih načinov mazanja (suh stik, tekoče mazivo in trde prevleke) in preiskovanje triboloških lastnosti med enotočkovnim koračnim preoblikovanjem pločevine, ki je dandanes izredno privlačna tehnologija preoblikovanja pločevine in večinoma primerna za maloserijsko proizvodnjo.

Prvi del prispevka opisuje raziskave izvedene na napravi s trnom, kjer je predstavljeno merjenje in primerjava koeficientov trenja pri različnih načinih mazanja. V drugem delu prispevka pa je predstavljena analiza merjenja temperature preoblikovalnega orodja med koračnim oblikovanjem piramidastega preizkušanca glede na tri različne načine mazanja. V primeru enotočkovnega koračnega preoblikovanja pločevine se povišanje temperature orodja pojavi zaradi trenja v stičnem področju med orodjem in pločevino.

Ključne besede: preoblikovanje pločevine, koračno preoblikovanje, trenje, prevleke orodij

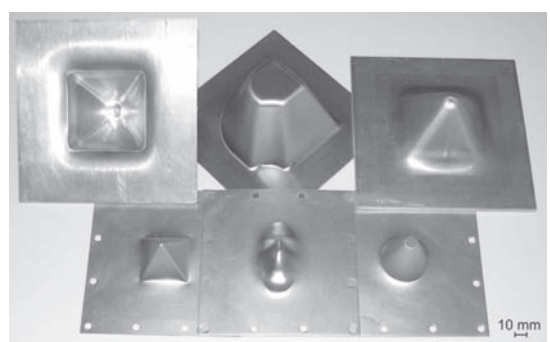

Sl. 1. *Izdelki izdelani s sistemom enotočkovnega koračnega preoblikovanja pločevine*

*Naslov odgovornega avtorja: Univerza v Ljubljani, Fakulteta za strojništvo, Aškerčeva 6, 1000 Ljubljana, ales.petek@fs.uni-lj.si

Strojniški vestnik - Journal of Mechanical Engineering 54(2008)4, SI 44
UDK 621.73
Prejeto: 16.11.2007
Sprejeto: 15.5.2008

Eksperimentalna in numerična analiza bočnih sil v kovaškem orodju

Andrzej Kocańda* - Piotr Czyżewski
Tehnična univerza Varšava, Fakulteta za proizvodno inženirstvo, Poljska

Čeprav so orodja za vroče kovanje obremenjena predvsem s silami, ki delujejo v smeri gibanja orodja/drsnika, v orodni votlini nastanejo tudi bočne sile glede na tok materiala v različnih smereh. Te sile so lahko razmeroma velike, še posebej v primerih kovanja nesimetričnih ali po prerezu neenakomernih izkovkov, kar povzroči zamik zgornjega in spodnjega dela orodja in s tem geometrijske napake na izkovku. V prispevku sta predstavljena dva načina za določevanje bočnih sil s pomočjo numeričnega in fizičnega modeliranja. Obravnavana sta dva industrijska postopka in sicer za izdelavo zapiralne ročice ter vzvoda ventila. Pridobljene so bile vrednosti in smeri bočnih silo od začetka do zaključka postopka deformacije. Na podlagi teh rezultatov je bilo mogoče uvesti spremembe v konstrukciji orodja in izbiri tehnoloških parametrov, z namenom zmanjšanja vpliva bočnih sil na geometrijske napake izkovkov. Kot primer sta prikazana načina, kako je mogoče zmanjšati bočne sile s spreminjanjem nagiba delilne ravnine (kovanje zapiralne ročice) in s spreminjanjem začetnega položaja surovca v orodju (kovanje vzvoda ventila).

Ključne besede: kovanje, kovaški utopi, geometrijske netočnosti, numerično modeliranje, fizikalno modeliranje

Sl. 1. *Zapiralna ročica*

*Naslov odgovornega avtorja: Tehnična univerza Varšava, Fakulteta za proizvodno inženirstvo, Oddelek za preoblikovanje, Narbutta 85, 02-524 Varšava, Poljska, akocanda@wip.pw.edu.pl

Strojniški vestnik - Journal of Mechanical Engineering 54(2008)4, SI 45
UDK 621.9
Prejeto: 7.1.2008
Sprejeto: 15.5.2008

Vpliv CAM algoritmov na kakovost obdelane površine

Janez Kopač* - Primož Kržič
Univerza v Ljubljani, Fakulteta za strojništvo

Prispevek predstavlja test štirih različnih NC programov, ki so bili izdelani s pomočjo štirih različnih CAM algoritmov in enakih nastavitvenih parametrov. Rezultat eksperimentalnega dela prinese sklep, da razporeditev točk vzdolž obdelovalne poti lahko pomembno vpliva na čas obdelave in kakovost obdelane površine.

Ključne besede: CAM sistemi, pot orodja, NC programi, kakovost površin, obdelovalni časi

Sl.2. *Frezalni Stroj Sodick MC430L*

*Naslov odgovornega avtorja: Univerza v Ljubljani, Fakulteta za strojništvo, Aškerčeva 6, 1000 Ljubljana, janez.kopac@fs.uni-lj.si

Strojniški vestnik - Journal of Mechanical Engineering 54(2008)4, SI 46
UDK 621.778
Prejeto: 8.4.2008
Sprejeto: 15.5.2008

Vpliv zmanjšanja Youngovega modula na izračun elastične povračljivosti pri vleku jeklene pločevine

Marko Vrh[1,2] - Miroslav Halilovič[1] - Boris Štok[1,*]
[1]Univerza v Ljubljani, Fakulteta za strojništvo
[2]Kovinoplastika Lož

Pričujoč prispevek prikazuje vpliv upoštevanja zmanjšanja togosti v materialu, ki je posledica razvoja poškodbe med preoblikovanjem, na rezultate računalniške simulacije elastične povračljivosti globoko vlečenega izdelka. Za ta namen je GTN (Gurson-Tvergaard-Needleman) poškodbeni model, ki smo ga ustrezno nadgradili z Mori-Tanaka modelom, s pomočjo podprograma VUMAT vnešen v programsko kodo ABAQUS/Explicit. Integracija konstitutivnega modela je izvedena z numerično shemo, ki je bila nedavno razvita s strani avtorjev. Zaradi avtentičnosti študije smo identificirali parametre konstitutivnega modela iz rezultatov meritev običajnega nateznega preizkusa ter meritev zmanjšanja elastičnega modula za nerjavno jeklo EN 1.4301. Na osnovi izvedene primerjalne analize numeričnih rezultatov elastične povračljivosti lahko sklepamo, da je potrebno zmanjšanje togosti materiala vključiti v simulacije preoblikovanja pločevine. Vpliv le-te na izračunano končno geometrijo preoblikovanega izdelka je namreč prevelik, da bi ga smeli zanemariti.

Ključne besede: postopki vlečenja, jeklena pločevina, elastična povračljivost, poškodbe materialov, elastične lastnosti, spremembe togosti

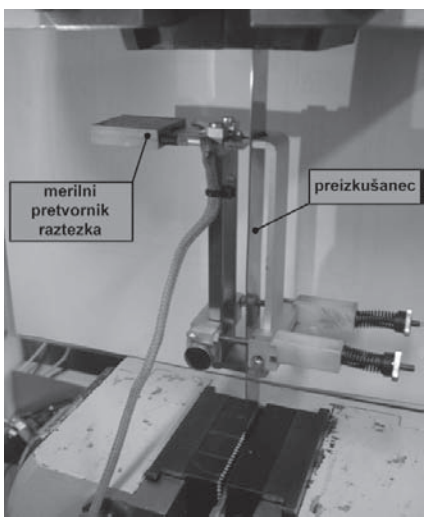

Sl. 2. *Merjenje elastičnega raztezka*

*Naslov odgovornega avtorja: Univerza v Ljubljani, Fakulteta za strojništvo, Aškerčeva 6, 1000 Ljubljana, boris.stok@fs.uni-lj.si

Osebne vesti

Doktorata, magisteriji in diplome

DOKTORATA

Na Fakulteti za strojništvo Univerze v Ljubljani sta z uspehom zagovarjala svoji doktorski disertaciji:

dne *7. januarja 2008*: **Alira Srdoč**, z naslovom: "Model vodenja kakovosti na osnovi baze podatkov in znanja" (mentorja: prof. dr. Alojz Sluga in akad. prof. dr. Ivan Bratko);

V predloženemu doktorskemu delu smo zasnovali nov pristop k vodenju kakovosti s poudarkom na znanju. Pristop smo poimenovali koncept globoke kakovosti (DQC). V okviru dela smo razvili tudi nov model vodenja kakovosti, ki temelji na zasnovanem konceptu DQC. V okviru raziskav smo preučili najbolj pomembne modele vodenja kakovosti in trende razvoja na tem področju. Identificirali smo baze podatkov in koncepte, ki se nanašajo na znanje, ki dandanes niso v zadostni meri upoštevani, ali niso dovolj sistematično vključeni v obstoječih modelih vodenja. Prav tako smo analizirali tipe znanja, ki so običajno prisotni v organizaciji in odgovarjajoče načine shranjevanja znanja. Prepoznali oz. identificirali smo razliko med tradicionalnim pristopom in novimi možnostmi. Posebno skrb smo posvetili pojasnitvi nekaterih temeljnih pojmov in ekspertnemu znanju - še posebno nememu in globokemu znanju o domeni, ki je odločujoče za kakovost in primerjalno prednost neke organizacije glede na konkurenco, in ga je težko ali pa celo nemogoče forrnalizirati s tradicionalnimi metodarni. Zato smo preiskali in analizirali obstoječe pristope zajemanja in formalizacije tovrstnega znanja v okviru upravljanja znanja in bolj formalnih pristopov v okviru umetne inteligence. V našem pristopu smo nato opredelili koncepte in mehanizrne, ki so potrebni za zajemanje in vključevanje tega znanja v sisteme vodenja kakovosti. Navedli smo tudi nekatere druge koncepte, ki jihje potrebno vključiti. Na tejosnovi je razvit 12-nivojski model vodenja kakovosti, ki je v delu tudi predstavljen. Opredeljeni so tudi potrebni koraki iq moŽlli scenariji za njegovo implementacijo. Nadalje smo opisali kaj se pričakuje na izhodu vsakega nivoja razvitega modela. Za nivoje, ki predstavljajo posarnezne dele organizacije, smo definirali tudi ciljne značilnosti. Model vsebuje: (1) del, ki se nanaša na razvoj standardov in kriterijev nagrad kakovosti v skladu z našim pristopom; in (2) del, ki se nanaša na Implementacijo tako opredeljenih standardov in kriterijev nagrad kakovosti. Tako glavne točke modela kot tudi potencial našega pristopa smo validirali na problemu ocenjevanja trajanje del popravila ladij v ladjedelnici. Pri tem je dan poudarek na specifičnih konceptih in transparentnih strukturah .za ocenjevanje in odločanje z uporabo strojnega učenja - ene najbolj poznanih tehnik umetne inteligence za zajem in prikaz znanja. S pozicioniranjem DQC koncepta napram obstoječim konceptom vodenja kakovosti in odgovarjajočim interesnim področjem smo podali tudi naš pogled na vodenje kakovosti v prihodnosti.

dne *26. marca 2008*: **Miha Ambrož**, z naslovom: “Računalniško podprto določanje kritičnih situacij v cestnem prometu” (mentor: prof. dr. Ivan Prebil);

Razvit je sistem za ana1izo prometnih situacij v cestnem prometu, ki zapolnjuje vrzel na področju orodij za interaktivne ana1ize dinamike vožnje. Sestavljen je iz programske aplikacije i3Drive za interaktivno simulacijo dinamike kolesnih vozil na poljubnih voznih ploskvah ter merilnega sistema za merjenje parametrov dinamike vožnje na vozilih in voznih ploskvah. i3Drive simulira vožnjo kolesnih vozil na osnovi sistema togih teles z interaktivnim prikazom v navideznem trirazsežnem prostoru, z uporabo prilagojenih krmilnih naprav in zapisom rezultatov v različne formate izhodnih datotek. Merilni sistem meri parametre dinamike vožnje. Možno ga je vgraditi v različna vozila in rezultate meritev uporabiti za verifikacijo simulacij ter za pridobivanje vhodnih podatkov.

S tem sta navedena kandidata dosegla akademsko stopnjo doktorja znanosti.

MAGISTERIJI

Na Fakulteti za strojništvo Univerze v Ljubljani so z uspehom zagovarjali svoja magistrska dela:

dne *22. januarja 2008*: **Stanislav Meglič**, z naslovom: "Načrtovanje in vodenje dobavnih verig podjetja" (mentor: prof. dr. Marko Starbek);

Načrtovanje in vodenje dobavnih verig podjetja pomeni prestopiti meje podjetja in v širši timski sestavi skupaj z dobaviteljem iskati t.i. globalni optimum. Pri tem je poudarek na virtualni podpori, skladiščnih sistemih, oblikovanju naročila, strukturnih in transportnih parametrih. Management oskrbnih verig zato sestavljajo orodja za vodenje skladišč, logističnih centrov in proizvodnje, kot sta sistem napredovalnih števil in kanban, ki od sodelujočih zahtevata izvrševanje pogodbenih obveznosti, popolno zaupanje, ažurno informiranje ter dosledno dobavljanje. Transportni parametri so v pogojih svobodnega tržnega gospodarstva odvisni le od ekonomskih in zakonodajnih dejavnikov, odločitve za načine transporta pa pragmatične in največkrat v škodo razvoju somodalnega transporta.

dne *22. januarja 2008*: **Aleš Silič**, z naslovom: "Integracija potisnega in vlečnega sistema proizvodnje" (mentor: prof. dr. Marko Starbek);

Na osnovi glavnih značilnosti proizvodnje opečnih izdelkov sem izmed obstoječih PPS sistemov, uporabil kombinacijo (hibrid) MRP/MRP 11 sistem (od oblikovanja do pakiranja in skladiščenja) in KANBAN sistem (od izkopa in dovoza surovine do oblikovanja vključno z engobiranjem) ter izdelal vlečno-potisni računalniško integriran model za obvladovanje celotnega sistema planiranja in krmiljenja proizvodnje opečne kritine, v katerega sem vključil tudi sistem odčitavanja črtnih kod, s katerim je omogočeno zajemanje podatkov ter s tem sledljivost procesnih izdelkov v posamezni fazi.

dne *4. marca 2008*: **Mitja Mahnič**, z naslovom: "Optimiranje parametrov za razvojno napovedovanje zdržljivosti pri povišanih hitrostih" (mentor: prof. dr. Matija Fajdiga);

V delu je predstavljen postopek za pridobivanje parametrov kompleksnih vrednotenj pri povišanih hitrostih obremenjevanja. Postopek, ki smo ga izpeljali, temelji na enostavni Taylorjevi teoriji za analitični popis trka. V ta namen smo izdelali preizkuševališče za Taylorjev test ter dobljene rezultate meritev uporabili kot osnovo za optimiranje parametrov kompleksnih vrednotenj. Optimiranje parametrov smo izvedli na analitičnem in numeričnem modelu ter s pomočjo genetskega in stigmergičnega algoritma določili vrednosti posameznih parametrov. Dobljene parametre smo nato uporabili pri simulaciji trka, s spremenjeno obliko preizkušanca in s spremenjenimi pogojih obremenjevanja. Rezultate smo nato ponovno primerjali z eksperimentalnimi vrednostmi ter jih kritično ocenili.

Na Fakulteti za strojništvo Univerze v Mariboru so z uspehom zagovarjali svoja magistrska dela:

dne *7. januarja 2008*: **Saša Ajd**, z naslovom: "Modeliranje onesnaženja podtalnice" (mentorja: prof. dr. Leopold Škerget in prof. dr. Matjaž Hriberšek);

Predmet raziskovalne naloge je bila računalniška simulacija onesnaženja vodonosnika Selniške dobrave kot posledice površinskega izlitja goriva. Kurilno olje je zmes številnih ogljikovodikov, izmed katerih je podrobneje obravnavan benzen, ki kljub majhnemu deležu v gorivu predstavlja veliko nevarnost za onesnaženje podtalnice vsled relativno dobre topnosti v vodi ter karcinogenega delovanja na zdravje ljudi. Kot izhodiščni podatki za simulacijo so služili pridobljeni empirični rezultati, sad večletnih terenskih raziskav Selniške dobrave. Za tok in prenos benzena v oljni ter vodni fazi na poti od površja do gladine podtalnice (vadozna cona) je bil uporabljen 1D fizikalno-matematični model, vsebovan v računalniškem programu HSSM. Tako dobljeni rezultati so bili osnova za 3D simulacijo prenosa raztopljenega kontaminanta v zasičeni plasti, na čigar hitrost razširjanja ter koncentracijo v vodi vplivajo hitrost podtalnice, sestavljena iz konveksne ter disperzivne komponente, biološka razgradnja ter adsorbcija kontaminanta na porozno snov. Orodje, ki je to omogočilo, se imenuje VISUAL MODFLOW, ver. 3.1. Cilj raziskovalne naloge je bil spremljanje časovno odvisnih koncentracijskih profilov benzena v referenčnih piezometrih na poti do vodnjakov ter v samih črpališčih pitne vode. Senzitivna analiza je pokazala, da imajo največji vpliv na rezultate simulacije parametri, kot so poroznost oz. koeficient hidravlične prevodnosti. Rezultati raziskave so v primeru povečanega črpanja pokazali možnost onesnaženja črpališč pitne vode, ki pa je ob upoštevanju sorpcije oz. biodegradacije malo verjetno.

dne *7. januarja 2008*: **Borut Križe**, z naslovom: "Raziskave neposrednega legiranja in rafinacije pri proizvodnji nodulatorjev in cepiv ter

vpliv spremenjene tehnologije na okolje" (mentor: prof. dr. Alojz Križman);

Današnja tehnologija proizvodnje nodulatorjev in del cepiv na indukcijskih pečeh je dodobra utečena. Je pa ta tehnologija v ekonomskem smislu neracionalna. Predvsem zaradi izračunanih prihrankov po enoti produkta in povečane storilnosti smo v podjetju začeli razmišljati o tehnologiji in razvoju tehnologije direktnega legiranja nodulatorjev. Da bi lahko ugotovili primernost tehnološkega postopka FeSiMgS smo naredili eksperimentalni poskus proizvodnje tega produkta po postopku direktnega legiranja na elektro obločni peči. Pri poskusu smo ugotavljali možnost izvedbe poskusa (tehnologijo) ter končne karakteristike produkta (kemična sestava, mikrostrukrura, sestava faz). Te karakteristike smo na koncu primerjali s karakteristikami FeSiMgS, ki je bil proizveden v indukcijski peči. Ugotovili smo, da so lastnosti FeSiMgS izdelanega v indukcijski peči in po direktnem postopku primerljive ter, da je možno z investicijo v postopek direktnega legiranja po tem postopku izdelati enakovreden nodulator FeSiMgS. Z vpeljavo postopka direktnega legiranja dosežemo poleg prihranka pri stroških proizvodnje FeSiMgS na enoto produkta še manjši vpliv na okolje.

dne *22. januarja 2008*: **Jasmin Kaljun**, z naslovom: "Ergonomski in estetski vidiki razvoja izdelkov" (mentor: prof. dr. Bojan Dolšak);

Ergonomija in estetika sta pri izdelkih široke potrošnje zelo pomembni. V pričujočem magistrskem delu so v obliki ergonomskih in estetskih priporočil predstavljeni rezultati raziskav ergonomskih in estetskih vidikov razvoja izdelkov. V ta namen je bilo potrebno pregledati in analizirati trenutno stanje na področju ergonomskega in estetskega oblikovanja, ter poiskati, pripraviti in urediti vire, iz katerih se je zajemalo znanje z obravnavanih področij. Zbrano znanje sem v naslednjem koraku uredil in ovrednotil, ter oblikoval ustrezna konstrukcijska oziroma oblikovalska priporočila, ki zbrana na enem mestu omogočajo lažji in učinkovitejši razvoj ergonomsko in estetsko ustreznejših izdelkov. Ob teoretičnem delu raziskav, katerih rezultat so že omenjena priporočila, predloženo magistrsko delo zajema še praktično analizo že izvedenih oblikovalskih projektov, katere namen je preveriti upoštevanje in praktično vrednost priporočil, zbranih v prvem delu magistrskega dela. Na koncu magistrskega dela so predstavljene smernice za nadaljnje raziskovalno delo na tem področju, predvsem v smeri uporabe naprednih računalniških tehnologij s poudarkom na metodah umetne inteligence.

dne *12. februarja 2008*: **Matjaž Kamnik**, z naslovom: "Uporaba strojnega vida v prilagodljivih obdelovalnih sistemih" (mentorja: prof. dr. Jože Balič in prof. dr. Miran Brezočnik);

Magistrsko delo obravnava področje sistemske integracije znanj in tehnologij strojnega vida, ki se kot rezultat pospešenega razvoja drugih tehnologij uspešno vključuje v tehnične rešitve na področju sodobnih avtomatiziranih tehnoloških sistemov, predvsem kot sistemi uporabljeni na področju vizualnega pregledovanja ali kot sistemi uporabljeni na področju robotskega vida. Sistem strojnega vida lahko, s sposobnostjo zajemanja slike tridimenzionalnega prostora ter procesiranja in analize podatkov vidnega polja, uspešno prispeva svoj delež k prilagodljivosti avtomatiziranih obdelovalnih sistemov. Hipoteza magistrskega dela temelji na ideji, da je mogoče z izvedbo praktične aplikacije sistema strojnega vida izboljšati prilagodljivost in produktivnost že relativno visoko avtomatiziranega obdelovalnega CNC centra, na podlagi obdelave, analize in merjenja značilnosti zajete digitalne slike. Magistrsko delo, na podlagi teoretičnih izhodišč, obravnava načrtovanje, postavitev in vrednotenje rezultatov realizacije sistema strojnega vida za prepoznavanje in lociranje proizvodov, kot realne delovne operacije znotraj avtomatiziranega obdelovalnega sistema.

dne *28. februarja 2008*: **Albin Leskovar**, z naslovom: "Analiza dinamike procesorsko vodene hidravlične stiskalnice v proizvodnji aluminija" (mentor: prof. dr. Edvard Kiker);

Pričujoče delo obravnava problematiko dinamičnega obnašanja hidravličnega sistema, ki se odraža v obliki velikih tlačnih sunkov. Pri tem so izvedene teoretične študije delovanja hidravličnih in regulacijskih elementov hidravlične stiskalnice v proizvodnji aluminija. Vzrok za nastanek tlačnih sunkov se kaže kot posledica sile lepljenja aluminija na površino delovne puše recipienta, kar ob sprostitvi povzroči prenos sunka mase recipienta na ohišje stroja. Zraven teoretične analize je opravljen simulacijski model in optimizacija parametrov različnih regulatorjev z namenom iskanja ustrezne regulacije. Zaradi nezmožnosti obstoječe

opreme za izvedbo optimizacije je na podlagi praktičnih testov narejena nadgradnja merilnega sistema in sprememba algoritma za krmiljenje pogonskih črpalk, s pomočjo katere je sunek zmanjšan za 50 %. Rezultat analize in izboljšave se kažejo v zmanjšanem vplivu na okolje in v večji produktivnosti stroja.

S tem so navedeni kandidati dosegli akademsko stopnjo magistra znanosti.

DIPLOMIRALI SO

Na Fakulteti za strojništvo Univerze v Ljubljani so pridobili naziv univerzitetni diplomirani inženir strojništva:

dne *27. marca 2008*: Jernej JERMAN, Tadej KERN, Rok SLOKAR.

Na Fakulteti za strojništvo Univerze v Mariboru sta pridobila naziv univerzitetni diplomirani inženir strojništva:

dne *27. marca 2008*: Janez JUG, Mitja KOSEC, Urban KRAJNC, Goran NIKOLIĆ, Martin PODGRAJŠEK, Igor ŠNUDERL.

*

Na Fakulteti za strojništvo Univerze v Ljubljani so pridobili naziv diplomirani inženir strojništva:

dne *13. marca 2008*: Primož BAJT, Matej KOLMAN, Aljaž MEZEG;

dne *14. marca 2008*: Marko KALAN, Saša KIRALY, Martin MIHELČIČ, Janez ROLIH;

dne *17. marca 2008*: Tadej DEBELAK, Janko KENE, Damir PELAK, Igor POLJANŠEK, Blaž ŠINKOVEC.

Na Fakulteti za strojništvo Univerze v Mariboru so pridobili naziv diplomirani inženir strojništva:

dne *27. marca 2008*: Damjan HROVAT, Oskar IRMAN, Matjaž KRIVEC, Goran KUHAR, Kristijan PLESNIK, Marko ROŽEJ, MIlan VUČKO;

dne *31. marca 2008*: Marjan FUJS, Miroslav KLEMENT.